AD-A126 676 THE DEVELOPMENT OF A TACTICAL DUAL-WAVELENGTH NEPHELOMETER(U) H S S INC BEDFORD MA D F HANSEN ET AL. 24 NOV 82 HSS-B-093 AFGL-TR-82-0374 F19628-81-C-0008 1/2

UNCLASSIFIED F/G 14/2 NL

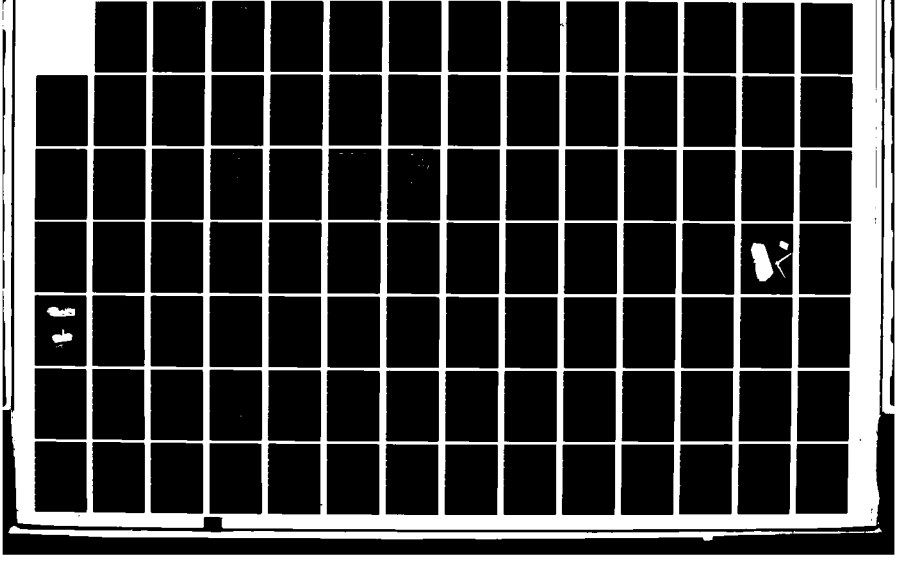

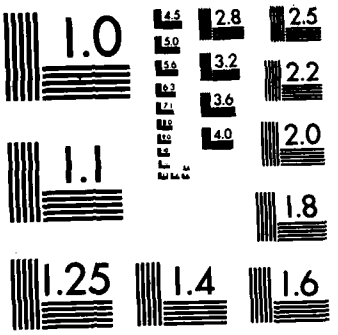

AFGL-TR-82-0374

THE DEVELOPMENT OF A TACTICAL DUAL-WAVELENGTH NEPHELOMETER

D. F. Hansen
H. S. Stewart

HSS Inc
2 Alfred Circle
Bedford, Mass. 01730

Final Report
27 February 1981 - 30 September 1982

24 November 1982

AIR FORCE GEOPHYSICS LABORATORY
AIR FORCE SYSTEMS COMMAND
UNITED STATES AIR FORCE
HANSCOM AFB, MASSACHUSETTS 01731

UNCLASSIFIED

SECURITY CLASSIFICATION OF THIS PAGE (When Data Entered)

REPORT DOCUMENTATION PAGE		READ INSTRUCTIONS BEFORE COMPLETING FORM
1. REPORT NUMBER AFGL-TR-82-0374	2. GOVT ACCESSION NO. A126676	RECIPIENT'S CATALOG NUMBER
4. TITLE (and Subtitle) THE DEVELOPMENT OF A TACTICAL DUAL-WAVELENGTH NEPHELOMETER		5. TYPE OF REPORT & PERIOD COVERED Final, 27 Feb 1981 - 30 Sept 1982
		6. PERFORMING ORG. REPORT NUMBER HSS-B-093
7. AUTHOR(s) D. F. Hansen H. S. Stewart		8. CONTRACT OR GRANT NUMBER(s) F19628-81-C-0008
9. PERFORMING ORGANIZATION NAME AND ADDRESS HSS Inc 2 Alfred Circle Bedford, Ma 01730		10. PROGRAM ELEMENT, PROJECT, TASK AREA & WORK UNIT NUMBERS 63707F 268801AD
11. CONTROLLING OFFICE NAME AND ADDRESS AFGL(LYR) Hanscom AFB Ma 01731 Monitor: Frederick Brousaides/ LYS		12. REPORT DATE 24 November 1982 13. NUMBER OF PAGES 187
14. MONITORING AGENCY NAME & ADDRESS(if different from Controlling Office) DCASMA, Boston 495 Summer St. Boston, Ma. 02210		15. SECURITY CLASS. (of this report) UNCLASSIFIED 15a. DECLASSIFICATION/DOWNGRADING SCHEDULE

16. DISTRIBUTION STATEMENT (of this Report)

Approved for public release; distribution unlimited.

17. DISTRIBUTION STATEMENT (of the abstract entered in Block 20, if different from Report)

18. SUPPLEMENTARY NOTES

19. KEY WORDS (Continue on reverse side if necessary and identify by block number)

Infrared nephelometer
Infrared transmission
visibility
seeability
aerosol scattering

20. ABSTRACT (Continue on reverse side if necessary and identify by block number)

A prototype dual-wavelength nephelometer operating at 0.55μm and 2.5μm was designed and fabricated. Limited testing was conducted in an environmental test chamber. The ultimate goal is to utilize these nephelometric measurements to infer atmospheric attenuation in the 8-12μm region; preliminary attempts using available models and some published field-test data were made to develop algorithms for this purpose. However, the general unavailability of adequate atmospheric data bases containing

DD FORM 1 JAN 73 1473 EDITION OF 1 NOV 65 IS OBSOLETE

UNCLASSIFIED

SECURITY CLASSIFICATION OF THIS PAGE (When Data Entered)

20 (Cont)

extinction and scattering coefficients at the wavelengths of interest prevents definitive conclusions to be made. In addition, until field tests of the nephelometer are made, a complete evaluation of the nephelometer itself cannot be forthcoming.

PREFACE

This report documents the development, calibration and testing of a two-channel,short-wave,infrared nephelometer (SWIRN). The primary function of the SWIRN is to provide measurements of the atmospheric aerosol scattering coefficient at two short wavelengths which can be used to accurately predict the aerosol scattering coefficient in the 8 to 12 μm atmospheric window. The instrument is intended for use on remote piloted vehicles (RPV s).

Development of the SWIRN was one part of a larger Air Force program named PRESSURS, an acronym for Pre-Strike Surveillance and Reconnaissance System . Mr. Fred Brousaides of AFGL was the technical monitor for the HSS Inc contract. Through his liaison efforts with the other parts of the program, Mr. Brousaides was instrumental in aiding HSS Inc in arriving at many key decisions during the design and fabrication phases of the SWIRN development program. Mr. Brousaides should also be acknowledged for many other contributions to the SWIRN development program, in particular, his participation and direction of the week-long calibration and test program at CALSPAN.

The successful completion of this instrument development program can be attributable to the HSS Inc personnel who made important contributions to the program: V. Logiudice, A. H. Pierson, W. Shubert, M. P. Shuler, A. H. Tuttle and J. M. Young.

Mr. Marion Shuler was responsible for calculating fog extinction coefficients used in the analysis of CALSPAN data. The calculations were performed using Mr. Eric Shettle's AFGL program "MIE 3; Mie Scattering Analysis". We gratefully acknowledge the assistance provided to Mr. Shuler by Mr. Shettle during the calculation process.

The arduous task of typing the manuscript was performed by Patricia Henckler whose patience and perseverance we gratefully acknowledge.

CONTENTS

Section	Title	Page
	PREFACE	3
	TABLE OF CONTENTS	4
	LIST OF ILLUSTRATIONS	7
	LIST OF TABLES	10
1.	BACKGROUND	11
2.	OPERATIONAL CONTRAINTS AND CONSIDERATIONS	15
3.	MEASUREMENT CONSIDERATIONS	17
3.1	General Approach	17
3.2	Measurement Performance Requirement	18
3.3	Wavelength Selection	22
3.4	Transmitter Light Source	23
3.5	Detector Selection	25
4.	DESIGN CONSIDERATIONS	37
4.1	Sample Rate	37
4.2	Signal Analysis	42
4.3	Noise Analysis	47
4.4	Instrument Layout	50
4.5	Optical Systems	53
4.6	Electronic Systems	56
4.6.1	Transmitter System	56
4.6.2	Receiver Systems	58
5.	R&D TEST AND ACCEPTANCE PLAN	61
6.	TEST AND CALIBRATION	62
6.1	Background	62
6.2	Test Program Objectives	62

CONTENTS

Section	Title	Page
6.3	Field Tests at Hanscom AFB	63
6.4	Test and Calibration at CALSPAN	64
6.5	Instrument Calibration	67
6.5.1	Data Base	67
6.5.2	Visible Channel	67
6.5.3	Infrared Channel	72
6.5.4	Calibration Equations	75
7.	SPECIFICATIONS	77
7.1	Introduction	77
7.2	General Specifications	78
7.3	Performance Characteristics	81
8.	EVALUATION OF THE SWIRN CONCEPT	85
8.1	Introduction	85
8.2	Correlation Equations from AFGL Aerosol Models	88
8.3	Modification of Correlation Relations Using Clay-Lenham Data	98
8.4	Tests of Empirical Correlation Equations Using CALSPAN Data.	104
8.5	Relationship Between Nephelometer Measurements and Aerosol Extinction Coefficients.	117
8.5.1	Aerosol Albedo	117
8.5.2	Aerosol Scattering Phase Function	119
9.	CONCLUSIONS AND RECOMMENDATIONS	131
9.1	Measurement Performance	131
9.2	Physical Features	133
9.3	Correlation Relationships	134

CONTENTS

Section	Title	Page
	REFERENCES	135
APPENDIX A	R&D TEST AND ACCEPTANCE PLAN, HSS-B-086, 10 DEC1981.	136
APPENDIX B	ARVIN CALSPAN DOCUMENTATION OF EXTINCTION AND PARTICLE SIZE MEASUREMENTS FOR CHAMBER TESTS OF MAY 1982.	155

LIST OF ILLUSTRATIONS

Fig. No.	Legend	Page
3.1	Lock-On Range for 8-12μm as a Function of Threshold Transmittance and Total Extinction Coefficient (from Reference 3).	20
3.2	Composite Plot of Spectral Characteristics of SWIRN Light Source.	27
3.3	Predicted SWIRN Signal-to-noise Characteristics using a Silicon Photovoltaic Detector Operated at 0.55 μm.	29
3.4	Predicted SWIRN Signal-to-noise Characteristics Using a Silicon Photovoltaic Detector Operated at 0.88 μm.	30
3.5	Predicted SWIRN Signal-to-noise Characteristics Using a Silicon Photovoltaic Detector Operated at 1.06 μm.	31
3.6	Predicted SWIRN Signal-to-noise Characteristics Using a Germanium Detector Operated at 1.06 μm.	32
3.7	Predicted SWIRN Signal-to-noise Characteristics Using a PbS Detector Operated at 2.5 μm.	33
3.8	Predicted SWIRN Signal-to-noise Characteristics Using a PbSe Detector Operated at 3.5 μm.	34
4.1	Schematic Diagram of the Optical System of One Channel of the SWIR Nephelometer.	42
4.2	Layout Drawing of the SWIR Nephelometer.	51
4.3	Photograph of the SWIR Nephelometer.	52
4.4	Photographs of the SWIR Nephelometer:(a) with access covers removed, (b) with reference standard calibrator installed.	54
4.5	Interconnecting Diagram, Two Wavelength Infrared Nephelometer. (SWIRN).	57
6.1	Visible Channel Calibrator Curve; Haze Episodes 6, 10, and 13.	68
6.2	Visible Channel Calibrator Curve; Haze Episodes 1 and 14.	69

LIST OF ILLUSTRATIONS

Fig. No.	Legend	Page
6.3	Visible Channel Calibration Curve; Fog Episodes 3, 7, 8, 9, 11, and 12.	70
6.4	Visible Channel Calibration Curve; Fog Episode 5.	71
6.5	Infrared Channel Calibration Curve; Haze Episodes.	73
6.6	Infrared Channel Calibration Curve; Fog Episodes.	74
8.1	Relationships between R_{10} and R_2 for the AFGL Aerosol Models.	91
8.2	Comparison of Aerosol Number Distributions: Deirmendjian Land Model and Shettle-Fenn Rural Model.	95
8.3	Comparison of Aerosol Number Distributions: Deirmendjian Maritime Model and Shettle-Fenn Maritime Model.	96
8.4	Comparison of Aerosol Number Distributions; Deirmendjian High Model and Shettle-Fenn Tropospheric Model.	97
8.5	Relationships between R_{10} and R_2 for the Clay-Lenham Measurements of Fog Extinction Coefficients.	102
8.6	Relationship between R_2 and $\gamma(.53\ \mu m)$ for Clay and Lenham Fog Data.	103
8.7	Comparison of Calculated Extinction Coefficients Vs Measured (Clay-Lenham) 10μm Extinction Coefficients.	106
8.8	Comparison of Predicted 10μm Extinction Coefficients (from improved relations) Vs Measured (Clay-Lenham) 10 μm Extinction Coefficients.	107
8.9	Comparison of Predicted and Measured Extinction Coefficients at 10 μm for the CALSPAN Test Data.	112
8.10	Comparison of Calculated and Measured Values of Extinction Coefficients: (a) for $\lambda = 0.55\ \mu m$, (b) for $\lambda = 2.2\ \mu m$.	115
8.11	(a) Comparison of Calculated and Measured Values of Extinction Coefficient at 10 μm; (b) Comparison of Predicted and Measured Values of Extinction Coefficient at 10 μm.	116

LIST OF ILLUSTRATIONS

Fig. No.	Legend	Page
8.12	Aerosol Albedo for Single Particle Scattering Used in Shettle-Fenn Aerosol Models.	120
8.13	Relationships between R_2 and Ratios of Albedo at Two Sets of Wavelengths.	122
8.14	Aerosol Scattering Phase Function at λ = 0.45 μm Vs Extinction Coefficient Ratio R_2 at Six Forward Scattering Angles for Four Deirmendjian Aerosol Models.	124
8.15	Aerosol Scattering Phase Function at λ = 0.7 μm Vs Extinction Coefficient Ratio R_2 at Six Forward Scattering Angles for Four Deirmendjian Aerosol Models.	125
8.16	Aerosol Scattering Phase Function at λ = 1.94 μm Vs Extinction Coefficient Ratio R_2 at Six Forward Scattering Angles for Four Deirmendjian Aerosol Models.	126
8.17	Aerosol Scattering Phase Function at λ = 10 μm Vs Extinction Coefficient Ratio R_2 at Six Forward Scattering Angles for Four Deirmendjian Aerosol Models.	127

LIST OF TABLES

Table No.	Title	Page
2.1	Constraints Imposed on the Design of the Prototype SWIRN.	16
3.1	Characteristics of the Targets, Atmosphere and FLIR System Used in Design Analysis of the SWIRN Instrument.	19
3.2	Characteristics of Light Source Employed in the SWIR Nephelometer.	26
3.3	Characteristics of the Detectors Employed in the SWIR Nephelometer.	36
6.1	Summary of Fog and Haze Tests Conducted at the CALSPAN Environmental Test Facility.	65
8.1	Extinction Coefficients at Three Wavelengths and Their Ratios for AFGL Aerosol Models.	89
8.2	Empirical Relationships Derived from the Shettle-Fenn Atmospheric Aerosol Models.	92
8.3	Test of the Derived Empirical Relations Using Deirmendjian's Calculated Values of Extinction Coefficient.	94
8.4	Test of the Correlation Relations Using the Data of Clay and Lenham.	99
8.5	Complete Set of Empirical Correlations Derived from the Shettle-Fenn Aerosol Models Including Improved Relations Based on the Clay-Lenham Measurements.	105
8.6	CALSPAN Data Used to Test Empirical Correlation Relations in Table 8.5.	109
8.7	Comparison of Computed Extinction Coefficients to the Measured Extinction Coefficients.	114
8.8	Albedo Values for Fog Droplets Used in the Shettle-Fenn Aerosol Models.	121
8.9	Aerosol Extinction Coefficients at Two Wavelenghts and their Ratio for Four Deirmendjian Aerosol Models.	129

1. BACKGROUND

Air to ground munitions systems require that an aircrew acquire a target before the weapons can be employed. For some systems the aircrew is required to make visual acquisition. In other cases imaging infrared systems must acquire and lock-on to the target. For either type system an advance knowledge of the target acquisition range (TAR) and of the system lock-on-range (LOR) is of fundamental importance. The present program is concerned with the development of a prototype airborne instrument to enable forecasters to determine, in advance of an air strike, the target acquisition range and the lock-on-range for infrared imaging systems. A separate program being conducted by HSS Inc (Reference 1) is concerned with development of a prototype instrument the measurements from which will enable forecasters to determine the visual target acquisition range.

A pre-strike surveillance/reconnaissance concept under consideration by the Air Force would utilize remote piloted vehicles (RPV s) to gather data for use by forecasters in assessing atmospheric conditions at target locales. Small, lightweight, low-power-consuming instruments are needed to perform meteorological and meteorological-related measurements from the RPV s. The prototype instrument being developed by HSS Inc under this program is intended to measure atmospheric aerosol scattering in the infrared spectral region.

Atmospheric aerosols represent the greatest uncertainty in predicting electro-optical system performance through the atmosphere; therefore, forehand knowledge on the extent of their presence in a target area is a requirement which cannot be overemphasized. A comment by L. M. Biberman (Reference 2) well describes the serious difficulty of predicting electro-optical system performance without detailed knowledge of aerosol conditions in the target locale. He states, "For this reason, (i.e. uncertainty in aerosol conditions), we cannot believe absolute performance predictions in less than clear weather for any forward-looking infrared (FLIR)

device". He goes on to say, "In past studies we have shown that these aerosol uncertainties may exceed by two orders of magnitude the uncertainties due to the molecular effects of the atmosphere".

Of particular interest to the Air Force is the ability to forecast the target acquisition range and the system lock-on-range for infrared imaging systems operating in the atmospheric window between 8 μm to 12 μm. Three physical mechanisms contribute to the attenuation of optical radiations in this wavelength region; they are: water vapor molecular absorption, water vapor continuum absorption and aerosol extinction. For most situations the water vapor effects on atmospheric transmission are well predicted by computer codes such as the AFGL LOWTRAN 5, based on inputs from simple, meteorological measurements. This is not true for aerosol extinction, as has been recognized by many investigators including Biberman.

Aerosol extinction is composed of two components, scattering and absorption. In the visible aerosol scattering generally exceeds the aerosol absorption; thus, it may only be necessary to measure the scattering coefficient to determine aerosol extinction. In the infrared, however, aerosol scattering and absorption are generally of the same order of magnitude.

The physical constraints on instruments to be carried by RPV's (i.e. small size, light weight, low power consumption) are such that an instrument with the capability of performing aerosol scattering measurements in the 8 μm to 12 μm spectral region is considered to be beyond the present state of the art in nephelometry.

An alternative approach has been taken in the case of the present infrared nephelometer concept. That approach is to perform aerosol scattering measurements at two wavelengths, one in the visible, the other in the near infrared and to utilize these two measurements and reliable models to predict the atmospheric aerosol extinction in the 8 μm to 12 μm region. This approach rests on the premise that reliable models can be

found, by either empirical or theoretical techniques --- or a combination, thereof, that will permit the determination of atmospheric aerosol extinction in the 8 μm to 12 μm spectral region from measurements at two shorter wavelengths.

Phase one of this program was devoted to the design and fabrication of the two channel nephelometer called the SWIRN (i.e. Short Wavelength Infrared Nephelometer). The second phase of the program was to have been a limited field measurement program. The field program was to consist of simultaneous measurements with the SWIRN and many other instruments (e.g. multi-wavelength infrared transmissometers, visible light transmissometers and nephelometers, particle measuring instruments and standard meteorological instrumentation). The program was to be conducted over an extended period of time to obtain measurements for a wide variety of environmental conditions.

The field program was to have been conducted in cooperation with the Atmospheric Optics Branch (OPA) of AFGL. OPA has a fully instrumented trailer for performing atmospheric optical measurements of the type required to calibrate, test and evaluate the SWIRN. Unfortunately the OPA trailer was committed to a series of test programs beginning around the time that the SWIRN was completed. A brief field program was conducted at Hanscom AFB with the OPA instrumented trailer and the SWIRN, but no environmental episodes occurred which limited either IR transmittance or visibility.

Because of the OPA trailer schedule it was necessary for the LYR-Group at AFGL, technical monitors of the contract, and HSS Inc to find an alternative to the original field test plan. The test program which was substituted took place in the CALSPAN Environmental Test Chamber at Ashford, N.Y.

The present Air Force concept for the deployment of an operational SWIRN instrument centers around RPV s as the carrier vehicle. A secondary means of deploying the instrument could be by an expendable drop-package wherein the instrument is housed with several meteorological instruments.

The size, weight, and cost of a SWIR Nephelometer is such that, in its present configuration, it is an unlikely candidate for use in an expendable drop sonde package. Two factors could ultimately change that status: (1) an extensive engineering effort could reduce the size, weight and cost of the instrument, and (2) the importance of the information to be gained from the SWIRN measurements might outweigh cost considerations in determining the deployment technique to be used.

2. OPERATIONAL CONSTRAINTS AND CONSIDERATIONS

Many of the operational constraints which would influence the design of the SWIRN were undefined at the outset of the program (and many have yet to be defined). The lack of information on these constraints results primarily from the fact that the deployment vehicle (i.e. the particular type of RPV) has yet to be selected. Limitations on size, weight and configuration will ultimately and unavoidably be imposed on the SWIRN by the particular RPV which is chosen. Location of the SWIRN aboard the RPV will influence the aerodynamic features and sampling configuration of the SWIRN. The speed and altitude ranges of the RPV combined with the flight profile tactics will impact sampling rates, measurement accuracy and electronic bandwidths (i.e. the electronic time constant).

The electrical power demand of the SWIRN will be modest; hence, it is unlikely to be influenced by any usage constraint on RPV power. The type of power available (400 cycle or 28 VDC) and the stability of that power will ultimately be of concern.

The SWIRN, in turn, will impact the data handling systems aboard the RPV. The telemetry system, for example, must be capable of handling the data rate and measurement precision of the SWIRN.

In the absence of knowledge of many of the physical and operational constraints which would be imposed on the SWIRN by the RPV characteristics and tactics, a "best estimate" list of constraints was compiled. That list of constraints is given in Table 2.1.

Near the conclusion of the SWIRN program a list of tentative specifications on accuracy of meteorological measurements by RPV-borne instruments was promulgated by the PRESSURS Program office. The differences in measurement accuracy between the current performance requirement and those given in Table 2.1 are discussed later in this report.

Table 2.1. Constraints Imposed on the Design of the Prototype SWIRN.

OPERATIONAL CONSTRAINTS	
A. RPV Deployment Mode	
Altitude Range	0 to 10,000 ft
RPV Speed	100 to 200 mph
Flight Pattern	to cover all altitudes from 100 ft to 10,000 ft.
B. Drop-Sonde Mode	
Altitude Range.	0 to 10,000 ft
Speed	1000 ft/min
PHYSICAL CONSTRAINTS	
Size and Weight	Minimal
Aerodynamic Configuration	Uncertain
Ambient Temperature Range	Uncertain
Internal Instrument Temp.Range	-35 °C to + 50 °C
Power Source	28 V DC
Output Signal (Analog)	0 to 10 V
PERFORMANCE REQUIREMENTS	
Target Lock-On-Range (LOR) (Predictive Capability at 8 μm to 12 μm)	(1) Determine if the LOR > 10 km or ≤ 10 km. (2) If LOR ≤ 10 km then determine LOR to ± 20 %

3. MEASUREMENT CONSIDERATIONS

3.1 General Approach

An instrument capable of measuring the atmospheric aerosol-extinction coefficient in the 8 μm to 12 μm spectral region, which is also compatible with the size, weight and power constraints of an RPV as host vehicle is generally believed to be beyond the present state of the art. For that reason the Air Force adopted the alternate approach of a two-channel nephelometer (one channel in the visible and one in the near infrared) whose measurements of the aerosol scattering coefficient can be used to derive the aerosol extinction coefficient in the 8 μm to 12 μm spectral region by applying tested and reliable extrapolation techniques.

The objective of the original HSS Inc program was limited to the design, fabrication and field test of the two-channel SWIR Nephelometer. Field testing of the instrument was to consist primarily of evaluating the performance of the instrument at the two measurement wavelengths, in a variety of environments. There was no provision in the program to explore the extension of the measurements to the 8 μm to 12 μm region. The alternative test program which was substituted for the original test program did provide for a limited investigation of techniques for extending the SWIRN measurements to predictions of the 8 μm to 12 μm atmosphere aerosol extinction coefficient.

During the initial design analysis phase of the program several combinations of detectors and operating wavelengths were explored for two purposes: (1) to optimize the predicted instrument performance, i.e. to maximize the signal to noise ratio, and (2) to achieve the maximum possible wavelength separation while simultaneously achieving the desired measurement accuracy and complying as well with the constraints imposed by the physical limitations of an RPV. These analyses led finally to the selection of an optimum combination of wavelengths, light source and detectors.

3.2 Measurement Performance Requirement

The range of measurement of the aerosol scattering coefficients which must be measured by the SWIR Nephelometer is an important design consideration. In order to establish the measurement range required of the SWIRN channels, some relationship with the measurement requirements at 8 μm to 12 μm must first be established and then translated into predicted requirements for visible and near-infrared wavelengths.

The measurement requirement for the 8 μm to 12 μm wavelength region was established by means of the data provided in Reference 3 and the assumptions made about the characteristics of the target, atmospheric conditions, and capabilities of an appropriate FLIR system. We have delineated these assumptions in Table 3.1.

Reference 3 is Volume 1 of an Electro-Optical Handbook prepared to assist forecasters in providing weather support for precision guided munitions. Figure 34 of that document was used to establish the atmospheric attenuation due to water vapor molecular-band-absorption (0.09 km^{-1}) and water vapor continuum absorption (0.28 km^{-1}) in the 8 μm to 12 μm spectral region for the atmospheric conditions specified in Table 3.1. Thus, the total extinction coefficient attributable solely to water vapor in that spectral region is 0.37 km^{-1}.

From Figure 36 of Reference 3, reproduced here as Figure 3.1 we may determine the maximum value of atmospheric extinction coefficients that the FLIR can operate in and still provide the necessary lock-on-range.

The ordinate of Figure 3.1 is the total extinction coefficient; i.e. the sum of the aerosol extinction coefficient and the total extinction coefficient due to water vapor. The abscissa is the threshold transmittance of the atmosphere defined as

$$\tau = \Delta T^{*}_{RT} / \Delta T^{*}_{o} \qquad (3.1)$$

where: ΔT^{*}_{RT} = Minimum detectable radiative temperature contrast

ΔT^{*}_{o} = Inherent difference between target and background radiative temperature.

Table 3.1. Characteristics of the Targets, Atmosphere and FLIR System Used in Design Analysis of the SWIRN Instrument.

TARGET CHARACTERISTICS	
Target Size	Large (e.g. Tank)
Temperature Contrast Range	$1\,^{\circ}C \leq \Delta T_o^* \leq 10\,^{\circ}C$
ATMOSPHERIC CONDITIONS	
Average Air Temperature	$\bar{T} = 20\,^{\circ}C$
Dew Point Temperature	$T_d = 20\,^{\circ}C$
Aerosol Vertical Distribution	Uniform
FLIR SYSTEM CAPABILITY	
Minimum Detectable Radiative Temperature Contrast (Of Sensor)	$\Delta T_{RT}^* = .01\,^{\circ}C$

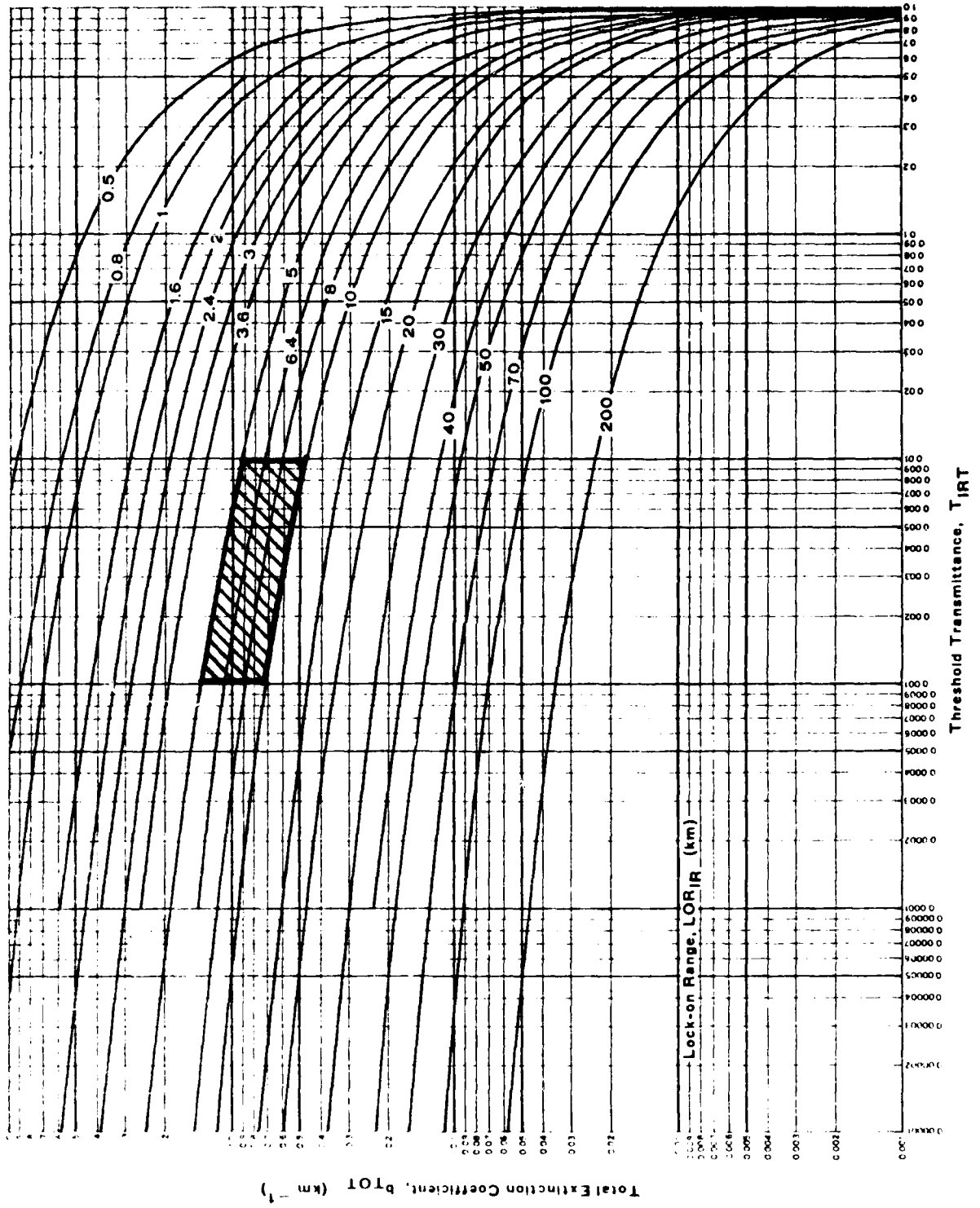

Figure 3.1. Lock-On Range for 8-12 μm as a Function of Threshold Transmittance and Total Extinction Coefficient (from Reference 3).

From the target characteristics and FLIR system capability defined in Table 3.1 we find a range of appropriate values for the threshold transmittance values of the atmosphere.

$$0.001 \leq \tau \leq 0.01 \tag{3.2}$$

Finally, the 8 μm to 12 μm IR lock-on-range, based on environmental parameters is derived from the equation

$$LOR_{IR} = -\ln \tau / b_{TOT} \tag{3.3}$$

where τ is the sensor's threshold transmittance and b_{TOT} is the total extinction coefficient. The above equation is represented by the curves in Figure 3.1

Based on conversations with the contract technical monitor concerning Air Force requirements for FLIR lock-on-range, we have taken a spread of values for the maximum LOR.

$$5 \text{ km} \leq LOR \leq 10 \text{ km} \tag{3.4}$$

The spread of values for LOR and τ defines a region on the Figure 3.1 plot depicted by the cross-hatched area. The minimum total extinction coefficient defined by this area is $b_{TOT} = 0.47 \text{ km}^{-1}$; i.e. the combination of $\tau = 0.01$ and LOR = 10 km.

The limiting aerosol extinction coefficient can now be determined by subtracting the contribution due to water vapor from the total extinction coefficient

$$b_{aerosols} = b_{TOT} - b_{H_2O} \tag{3.5}$$

The result is that the limiting aerosol extinction coefficient is

$$b_{aerosol} = 0.47 - 0.37 = 0.10 \text{ km}^{-1}$$

This limiting value of the aerosol extinction coefficient, at 8 μm to 12 μm, is the minimum value which needs be determined (to an accuracy of $\pm$ 20 percent) using the two SWIRN measurements at shorter wavelengths.

Currently there is large uncertainty in the determination of the 8 μm to 12 μm aerosol extinction coefficient by extrapolation of measurements made at shorter wavelengths. (Reference 2). We have made the conservative assumption, based on the atmospheric aerosol models of Shettle, and Fenn (Reference 4) that the aerosol extinction coefficients in the visible and near infrared will never be less than that in the 8 μm to 12 μm region for any haze situation. With this assumption we are able to set a lower limit to the aerosol scattering coefficients which must be measured by the SWIRN. The lower limit on aerosol scattering coefficients in the visible and near infrared wavelengths which must be measured by the SWIRN is, therefore, 0.1 km^{-1}. The measurement accuracy which we impose is the same as that required of the extinction coefficient in the 8 μm-12 μm region, i.e. $\pm$ 20 percent.

3.3 Wavelength Selection

The choice of operating wavelengths for the SWIR Nephelometer was influenced first of all by the requirement to separate the two channels by the maximum possible spread in wavelength---consistent with the other constraints on the instrument package. This requirement was imposed on the instrument design at the design review meeting (Reference 5) by several members of AFGL based on the AFGL knowledge and experience in modeling of atmospheric aerosols.

It was also decided at the design review meeting that one of the channels should be located in the center of the visible spectral region (i.e. at 0.55 μm). This choice was partly influenced by the obvious compatibility with the use of measurements at that wavelength to measure visual range.

The selection of the second, i.e. near-infrared, wavelength was influenced by two factors: (1) the need to achieve an accuracy of $\pm$ 20 percent in the measurement of an aerosol scattering coefficient whose minimum value is 0.1 km^{-1}, and (2) the constraints imposed by minimizing size, weight and power consumption of the instrument. The second of these factors, along with operational considerations eliminated the possibility of utilizing cryogenically cooled detectors. The choice of the near-infrared wavelength was thus limited to wavelengths short of about 5 μm.

A further obvious restriction on the wavelength range of the second channel was that the spectral coverage should coincide with an atmospheric window (i.e. a spectral region of high transmittance). This requirement is imposed by the necessity to perform measurements in a region where data from other measuring techniques, such as transmissometers, are available for calibration and evaluation of the SWIRN.

Two spectral regions were investigated as primary candidates for the near-infrared channel. These regions coincided with the atmospheric windows at 3.4 to 4.2 μm and from 2.0 to 2.5 μm. The latter spectral region was finally selected based on the outcome of a detailed signal-to-noise analysis which is discussed in a later section of this report.

3.4 Transmitter Light Source

A set of criteria were established for the light source, ---more properly the radiant energy source, of the SWIR Nephelometer. Candidate sources were compared against these criteria until the most suitable source type was selected. The selection criteria were:

(a) the source must have minimum power consumption

(b) it must have high radiant energy output in the visible and near-infrared spectral regions

(c) it must have a long lifetime

(d) it must be small, compact, and readily adaptable to a lenticular projection system

The first step in the selection process was to determine the class of sources having the most desirable features. The source classes which were evaluated were: (1) tungsten lamps, (2) miniature blackbody cavities, (3) glow bars, (4) ceramic rods and hollowed-out heating elements. The only category of sources which could justifiably meet the four selection criteria was tungsten lamps. The remainder failed to meet one or more of the criteria.

Once the type of source was determined the next step was to find a tungsten lamp which fulfilled the selection criteria in an optimum way. The myriad of lamps commercially available was rapidly narrowed to a few candidate lamps by means of another set of selection criteria:

(a) The lamp must operate at a high filament temperature (to produce a large amount of visible radiant energy as well as near infrared).

(b) It must have a quartz envelope (to transmit near-infrared radiation).

(c) It must have a lifetime greater than 1 year (to minimize time-consuming replacement and re-calibration costs).

(d) It must be a miniature lamp (therefore small, compact and consume a minimum of power).

(e) It must be a quartz-halogen cycle type of lamp (to best fulfill criteria c and d above).

(f) It must be a low voltage lamp (to assure a heavy, rugged filament capable of withstanding vibration and shock).

(e) It must have a small compact filament (so that it can be optically projected as a solid element).

Miniature tungsten lamps, with quartz envelopes and having halogen cycle gas fill, made by all leading lamps manufacturers, were investigated. Sifting through the possible lamps finally led to one lamp which most embodied all the desirable features --- the General Electric Type 1974D. The characteristics of this lamp are detailed in Table 3.2 .

The emissivity of tungsten is both temperature and wavelength dependent. Figure 3.2 shows the emissivity of a tungsten filament operating at 2500°K. This emissivity data was supplied to HSS Inc by the General Electric Co. for a lamp similar to the Type 1974D. (It was not available for the 1974D lamp.) Also shown in Figure 3.2 are curves for: (a) the transmission of a fused quartz lamp envelope (from Reference 6), and the radiant power output of a blackbody operating at 2500°K.

3.5 Detector Selection

The dominant design goal for the SWIR Nephelometer was to separate the two measurement channels by the maximum wavelength spread --- consistent with the physical constraints placed on the size, weight and power consumption of the instrument. There were many compelling arguments for locating one of the channels in the middle of the visible spectral region. The second channel thus had to be located at a wavelength as far as possible into the near infrared coincident with an atmospheric window.

The atmospheric window constraint (plus the requirement for a non-cryogenically cooled detector) limited the choice of near-infrared operating wavelengths to two specific regions: (a) 2.0 to 2.5 μm, and (b) 3.4 to 4.2 μm). The optimum detectors for these spectral regions (i.e. the detector with the lowest noise-equivalent-power, NEP, are: (a) lead sulphide, PbS, detectors for the shorter wavelength region, and (b) lead selenide, PbSe, for the longer wavelengths. In either case it was considered essential to thermoelectrically cool the detector to achieve the lowest possible NEP.

Table 3.2. Characteristics of Light Source Employed in the SWIRN Nephelometer.

Feature or Parameter	Ident. or Value
Lamp Manufacturer:	G.E.
Lamp Type:	Miniature
No:	1974D
Design Voltage:	6 volts
Power Requirement:	20 watts
Luminous Output:	10 candella
Average Lab. Life:	10,000 hr.
Filament Type:	C-6
Color Temperature:	2500°K
Bulb:	
Type	T-3
Material	Qtz.
Fill Gas	Halogen Cycle
Diameter	9.5 mm
Light Center Length	7.25 mm
Overall Length	28.85 mm
Operating Temp. (Min.)	250° C
Base:	
Type	Wire Terminal
Operating Temp. (Max.)	350° C

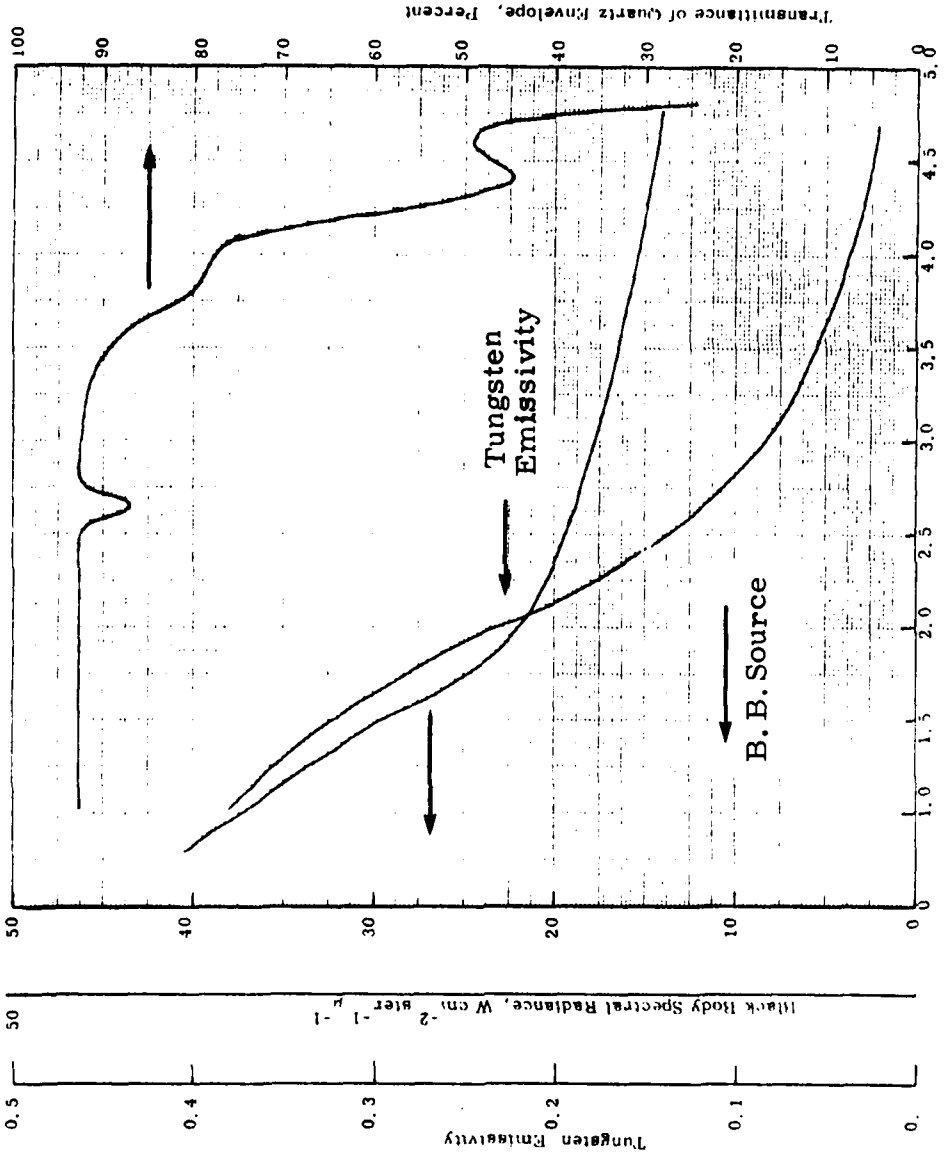

Figure 3.2. Comparative plot of spectral characteristics of SWIRN light source.

The characteristics of the light source obviously have an influence on selection of the optimum wavelength region for the near-infrared channel. Referring to Figure 3.2 it is apparent that the 1974D lamp will emit approximately eight times the radiant power at 2.25 μm than at 3.8 μm (the central wavelengths of the two candidate spectral regions). These numbers are arrived at by taking the product of the envelope transmittance, the blackbody spectral radiance and the tungsten emissivity. The shorter wavelength region was thus highly favored by the spectral features of the tungsten lamp.

In spite of the lamp characteristics which favor the shorter wavelength window, the actual selection was based on signal-to-noise analysis which included not only the lamp and possible detectors but also the geometry of the instrument plus the imaging and transmission properties of all the optical elements. Details of that analysis are described in a later section.

The results of that signal-to-noise analysis are presented in Figure 3.3 through 3.8. The signal-to-noise analysis was part of the design analysis which was conducted prior to the design analysis review meeting with AFGL staff members. Thus the Figures 3.3 to 3.8 show the results for several combinations of detectors and wavelength regions which were candidates prior to the design review meeting.

All signal-to-noise ratios shown in the figures are based on an electronic output time constant of $\tau = 0.5$ seconds. The independent variable in the plots is the background radiance which could be present in the field-of-view of the receiver system. The signal-to-noise ratio varies inversely as the square root of background radiance --- once the NEP due to the background radiance dominates the inherent NEP of the detector.

Figure 3.3 provides the S/N characteristics of the detector and wavelength combination chosen for the visible channel. The predicted measuring performance is marginally acceptable for 10 km lock-on ranges.

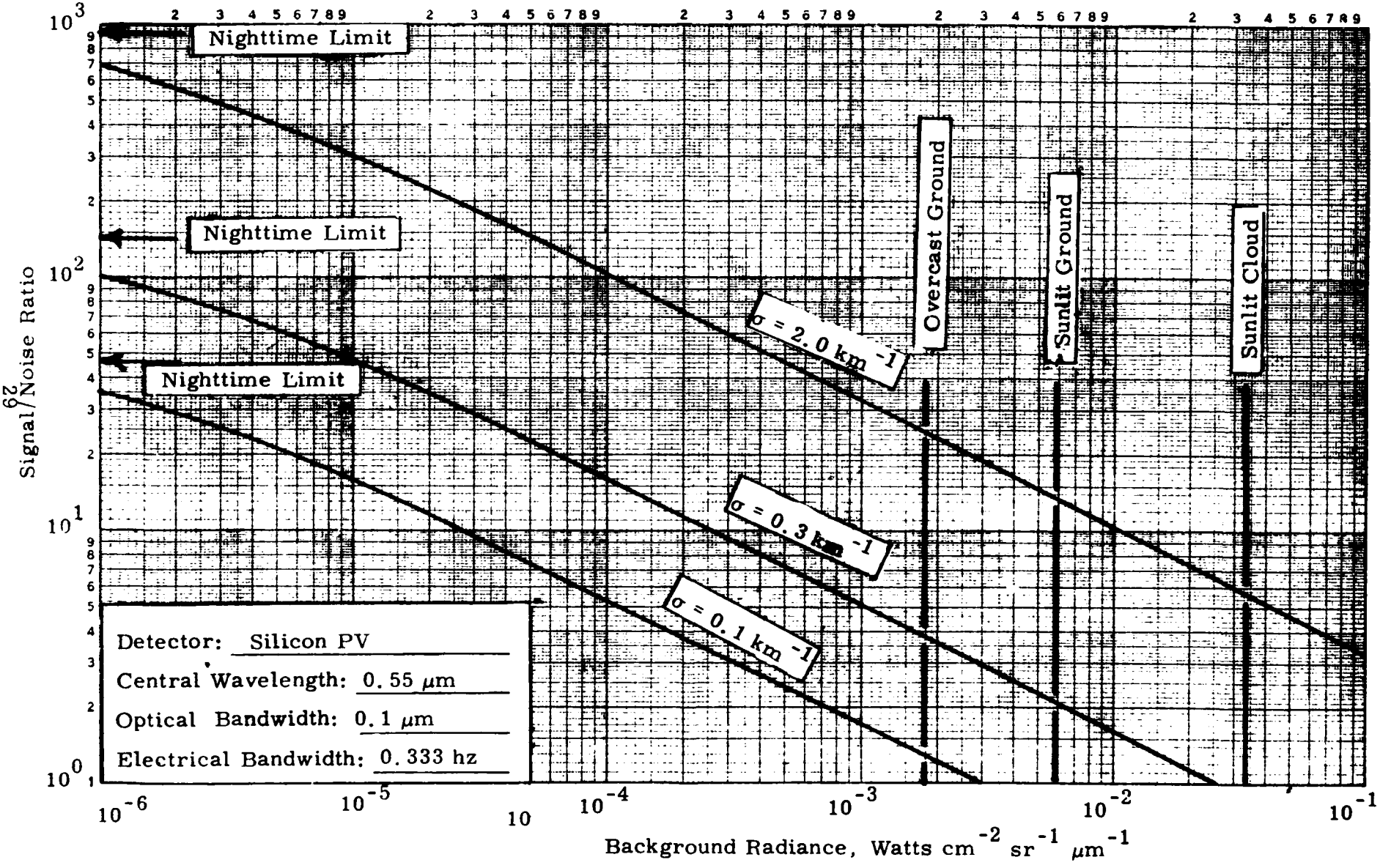

Figure 3.3. Predicted SWIRN Signal-to-noise Characteristics using a Silicon Photovoltaic Detector Operated at 0.55 μm.

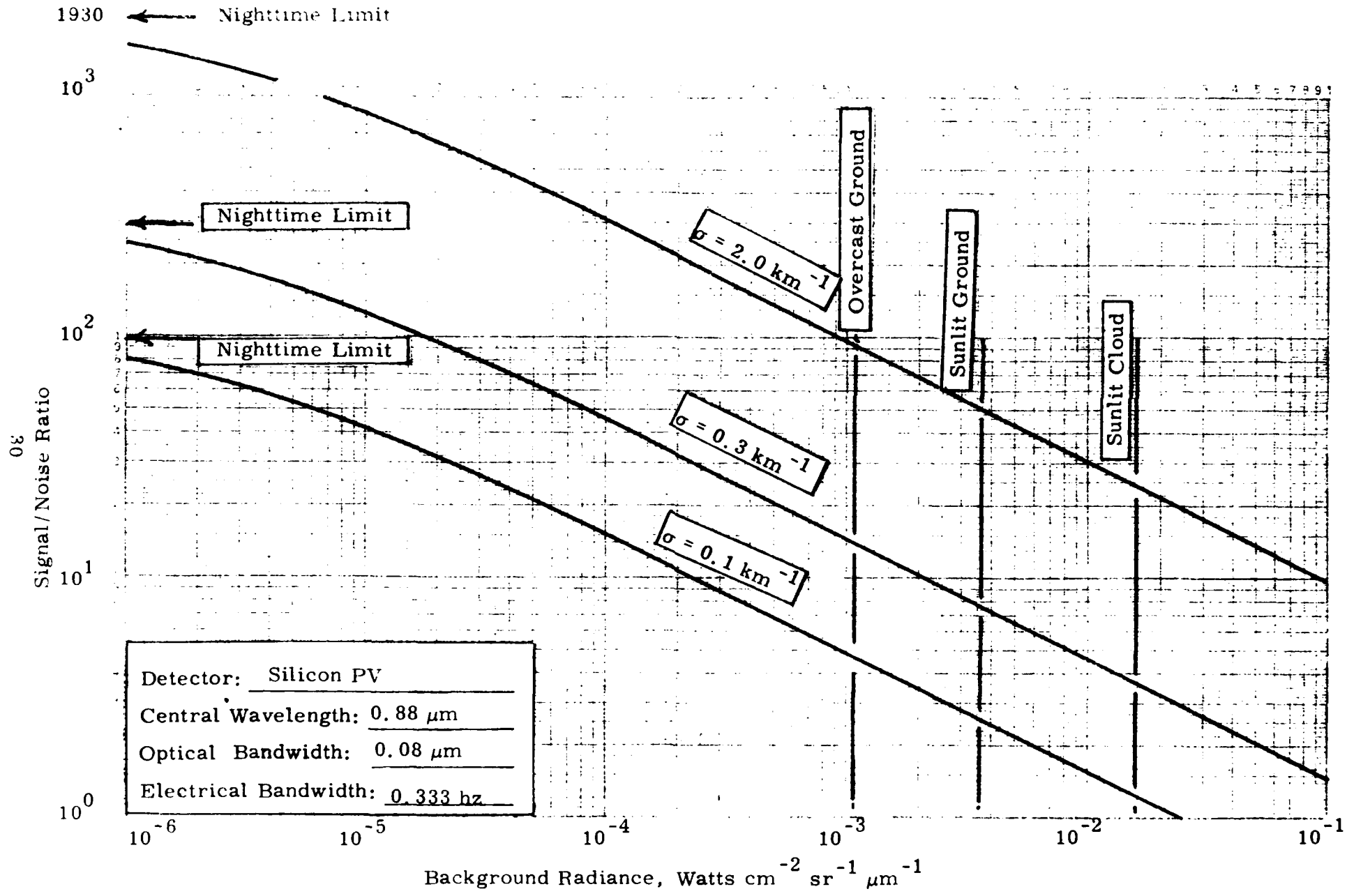

Figure 3.4. Predicted SWIRN Signal-to-noise Characteristics Using a Silicon Photovoltaic

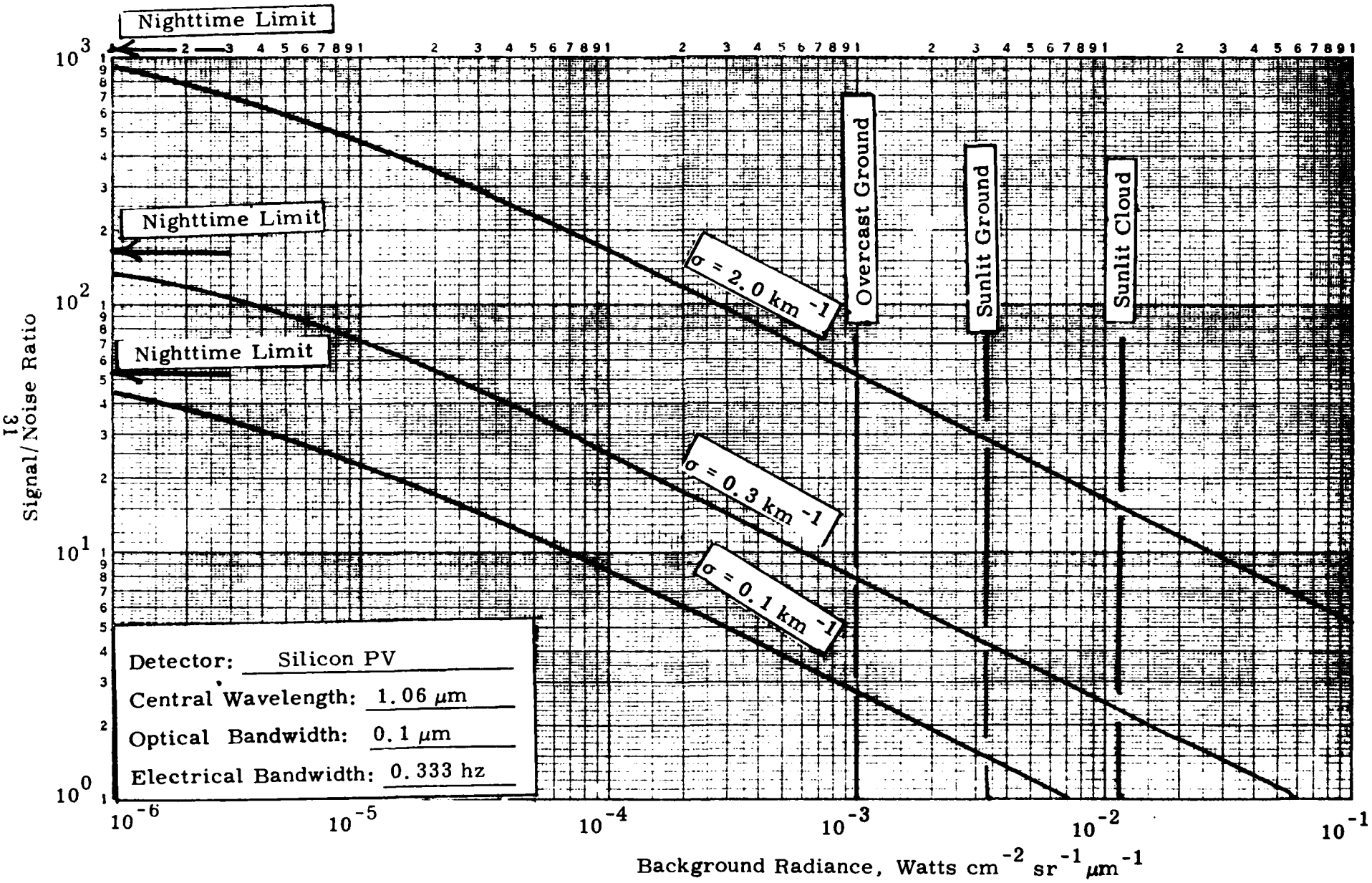

Figure 3.5. Predicted SWIRN Signal-to-noise Characteristics Using a Silicon Photovoltaic Detector Operated at 1.06 μm.

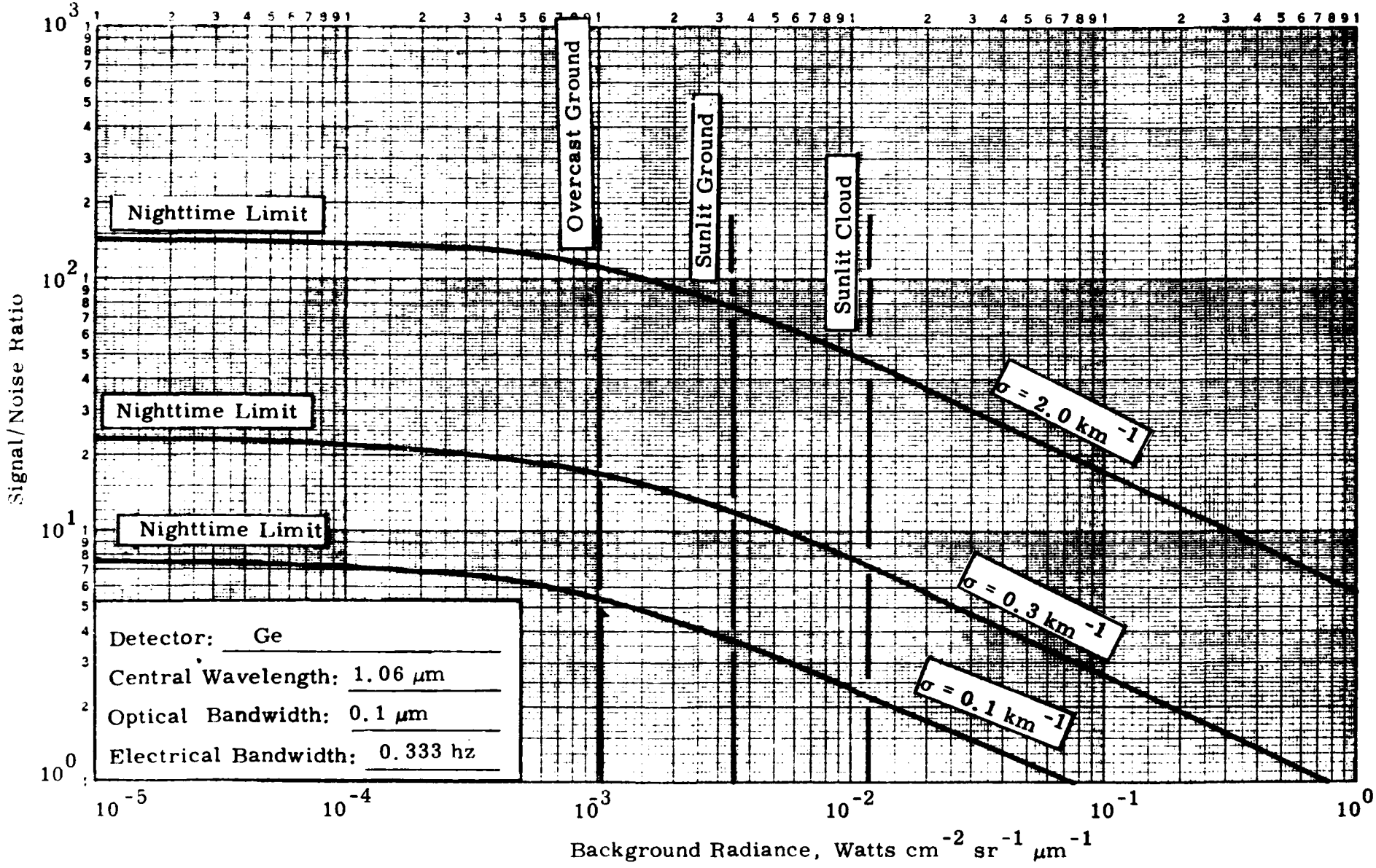

Figure 3.6 Predicted SWIRN Signal-to-noise Characteristics Using a Germanium Detector

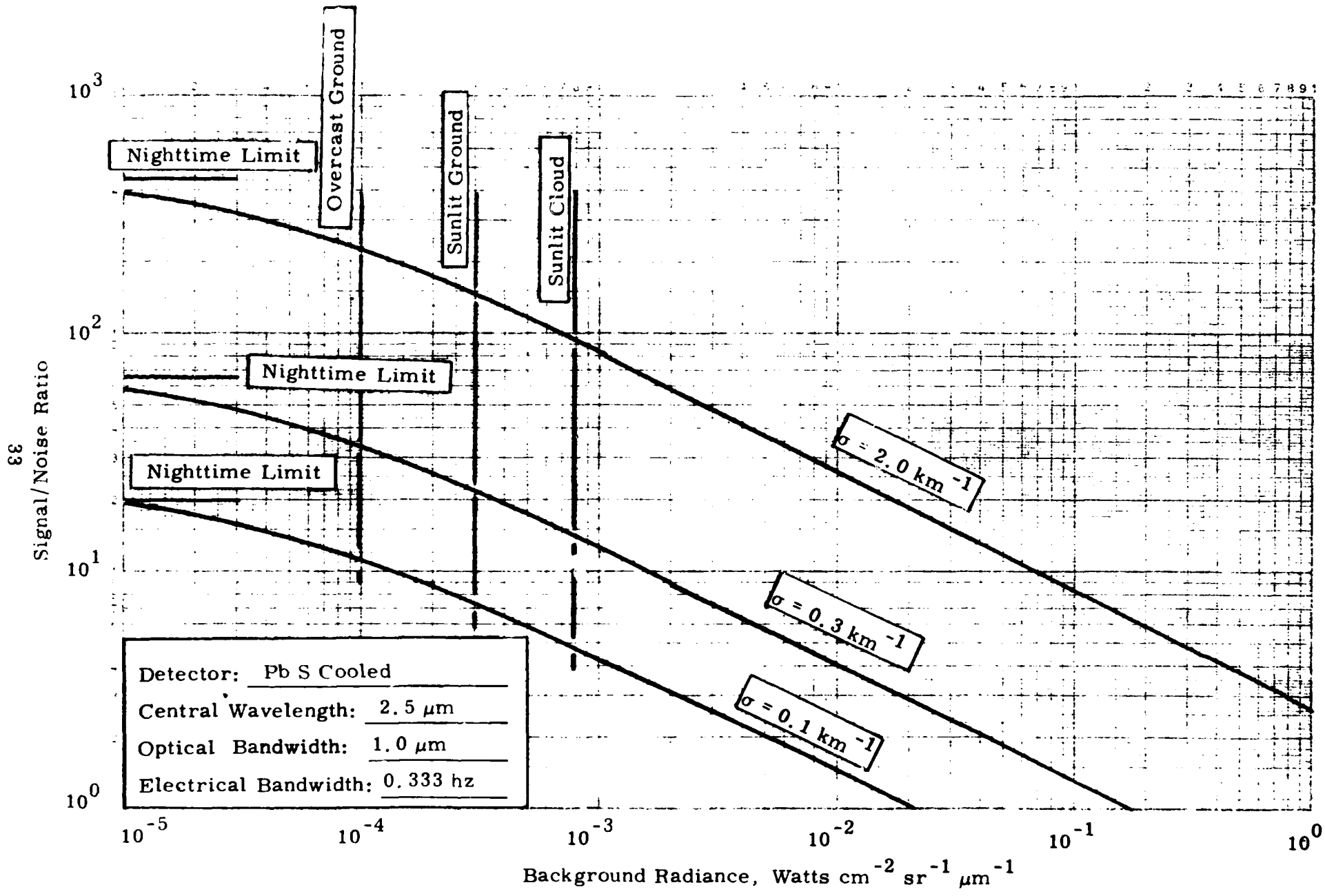

Figure 3.7. Predicted SWIRN Signal-to-noise Characteristics Using a Pb S Detector Operated at 2.5 μm.

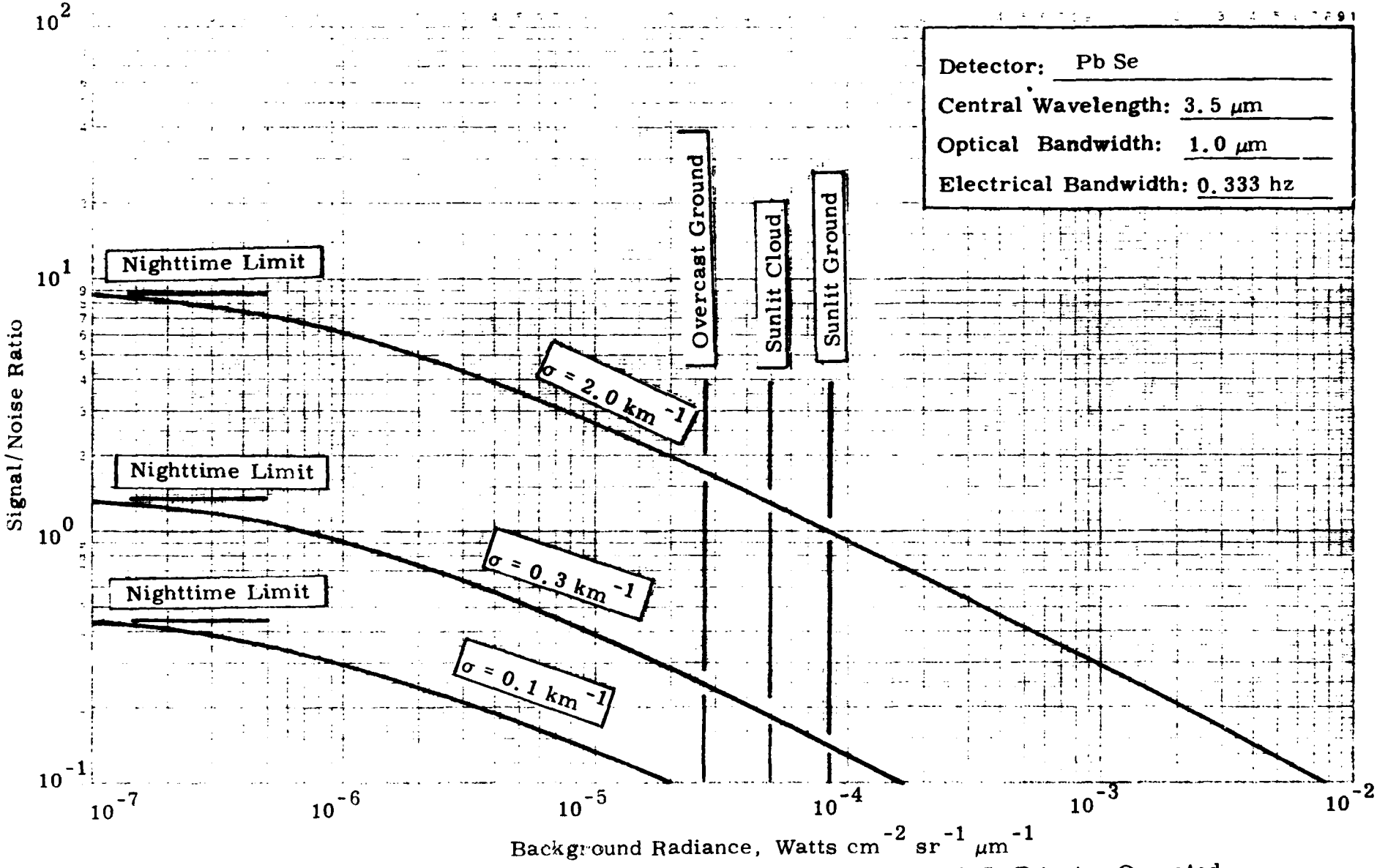

Figure 3.8. Predicted SWIRN Signal-to-noise Characteristics Using a Pb Se Detector Operated at 3.5 μm.

It would, of course, improve if the electronic time constant were increased.

Figures 3.4, 3.5 and 3.6 provide S/N characteristics for Channel 1 candidate detector/wavelength combinations which were eliminated in the selection process which took place at the design review meeting.

The two candidate detector/wavelength combinations for the second channel are shown in Figures 3.7 and 3.8. The signal-to-noise analysis indicates less than acceptable performance for the PbSe detector operating at 3.5 μm (see Figure 3.8). The PbS detector operating at 2.5 μm is predicted to have adequate performance for a scattering coefficient of $\sigma = 0.1\ km^{-1}$. On the basis of these analyses the PbS detector was chosen for Channel 2. Table 3.3 provides the pertinent detector characteristics for both wavelength channels of the SWIR Nephelometer.

The wavelength coverage of Channel 2 was permitted to extend from 2.0 to 3.0 μm even though the atmospheric window in that region extends only from 2.0 to 2.5 μm. The additional coverage increased the signal/noise ratio and did not degrade the measurement for two reasons: (1) aerosol absorption in single scattering processes is negligible in this region, and (2) scattering from aerosols in the wavelengths from 2.5 to 3.0 μm will not differ significantly from that in the 2.0 to 2.5 μm region.

Table 3.3. Characteristics of the Detectors Employed in the SWIR Nephelometer.

Feature or Parameters	Ident. or Value	
	Channel 1	Channel 2
Detector: Mfg:	EG&G	Opto-Electronics
Type:	Silicon P.V.	Pb S
Model:	HUV-1000B	OTC-22 S-82TC
Element: Area:	5.1 mm^2	4.0 mm^2
Temperature:	Ambient	228° K
Cooler: Type:	N.A.	2-stage T.E.
Model:	-	PN 11454-8
Spectral: Max. Response	0.9 μm	2.7 μm
SWIRN Central λ	0.55 μm	2.5 μm
SWIRN Bandpass	0.08 μm	2.0-3.0 μm (1)
Responsivity: peak λ	1.2×10^8 v/w	6.5×10^5 v/w
SWIRN Central λ	6.7×10^7 v/w	6.2×10^5 v/w
D*(Detectivity)	2.6×10^{12}	3.0×10^{11}
(Mfg. Conditions)	(.9, 20, 1)	(2.7, 600, 1)
NEP (Mfg. Conditions)	8.7×10^{-14} w/$\sqrt{Hz}$	6.7×10^{-13} w/$\sqrt{Hz}$
NEP (SWIRN)	1.5×10^{-13} w/$\sqrt{Hz}$	1.2×10^{-12} w/$\sqrt{Hz}$
Conditions	(0.55, 533, .33)	(25, 533, .33)

Note (1) The shortwavelength cut-off is determined by the germanium lens of the receiver; the long wavelength cut-off is determined by the spectral response of the detector.

4. DESIGN CONSIDERATIONS

4.1 Sample Rate

In the discussion which follows the term sample rate implies more than the rate at which the SWIRN output signals are interrogated by the telemetry or recording system of the RPV. As used here the term implies: (1) a minimum integration to assure that a representative aerosol distribution has been sampled, and (2) a maximum integration time permitted by the operational flight profile of the RPV. The integration time is characterized by the time constant of the output circuits of the receiver amplifiers. Thus, we infer that meaningful sample rates are determined by the time constant of the instrument.

Three factors dictate the permissible time constant that can be employed in the SWIRN: (1) the need to measure the scattering coefficient of a truly representative sample of the ambient aerosol distribution, (2) the need to achieve a measuring accuracy of $\pm$ 20 percent for scattering coefficients as small as $\sigma = 0.1\ km^{-1}$, and (3) the need to minimize the error due to sensor lag when the RPV is conducting measurements of the vertical profile of the scattering coefficient.

The above three factors have been treated at some length in the final report on the Airborne Visibility Meter (Reference 1). The reader is referred to that report for more detail than is provided in the following discussion.

Representative Sample Volume - The geometric sample volume of the SWIRN was deliberately made small to maximize the S/N ratio, and to be compatible with the physical constraints imposed on the instrument. To make a valid measurement of the aerosol scattering coefficient requires that a volume of air sufficiently large to include a representative distribution of aerosol sizes be sampled.

A large integrated sample volume is swept out by the small geometric sample volume of the SWIRN and AVM

nephelometers because of the motion of the RPV. Here we take the integration time to be roughly equivalent to the time constant of the instrument.

A worst case situation will be assumed: a maritime haze environment with 99 percent relative humidity. From Mie-scattering calculations we can establish the range of aerosol sizes which contribute 90 percent of the total scattering coefficient. These calculations have been documented in the final report on the design of a polar nephelometer (Reference 7). From Figures E16 and E17 of that report we see that if all aerosol sizes up to 10 μm are included in the sample, and all larger sizes excluded then the truncated sample population will still account for at least 90 percent of the total scattering coefficient at both 0.55 μm and 2.5 μm. The Shettle and Fenn maritime aerosol model (Reference 4, see Figure 6) indicates that there are 0.02 aerosol particles per cubic centimeter in the radius range from 9.5 μm to 10.5 μm of a maritime atmosphere when the relative humidity is 99 percent.

To assure a truly representative sample we conservatively demand that 25 particles of 10 μm size be present in the integrated sample volume. The integrated sample volume must then be at least 1250 cm^3 (i.e. 25/.02). From Reference 1 (Figure 4.1) we find that an integrated sample volume of 1 liter can be achieved with a time constant τ = 0.5 seconds if the RPV velocity exceeds 50 mph. Since all RPV's under consideration by AFGL will maneauver at speeds considerably in excess of 50 mph there would appear to be no problem in measuring a representative aerosol sample with the SWIRN.

Measurement Accuracy: The basic premise underlying the SWIRN development program is that the measurements at shorter wavelengths can be used to predict the atmospheric aerosol attenuation coefficient in the 8 to 12 μm atmospheric window. It is a requirement that the predictive capability be capable of determining an 8 to 12 μm lock-on range of 10 km to an accuracy of $\pm$ 20 percent. We have shown that as a worst case situation this requirement translates to a measurement accuracy of $\pm$ 20 percent for each SWIRN channel when the scattering coefficient is $\sigma = 0.1\ km^{-1}$ at all wavelengths (this environmental situation is approached by a maritime aerosol distribution). This measurement requirement implies a S/N = 5:1 capability for each SWIRN channel when $\sigma = 0.1\ km^{-1}$. From Figure 3.3 we observe that the visible channel falls short of this requirement when the time constant is $\tau = 0.5$ seconds, whereas the 2.5 μm channel (Figure 3.8) meets this requirement with the same time constant. (One reason for this behavior is the low background radiance at 2.5 μm as compared to that at 0.55 μm). A longer time constant could improve the performance of the visible channel, but too long a time constant could introduce errors due to sensor lag time.

Errors Due to Sensor Lag Time - Tentative deployment plans for the RPV suggest ascent and descent rates of between 5000 to 10,000 feet per minute when performing vertical profile measurements of atmospheric parameters. At these rapid ascent and descent rates all sensors will lag behind in their measurements if the parameter they measure is changing at a rate that the time constant of the instrument cannot follow. An error is thus introduced into the measurement due to sensor lag time.

In Reference 1 it was established that to monitor essentially any probable atmospheric aerosol vertical profile distribution a 2 second time constant was the maximum permissible value for an RPV with an ascent/ descent rate of 5000 ft/ minute.

If the SWIRN is required to determine cloud base heights as is the AVM then more stringent requirements are placed on the time constant of the instrument. Tentative requirements of the PRESSURS program specify that the cloud base height be measured to an accuracy of $\pm$ 100 feet for cloud bases up to 1000 ft, and to an accuracy of $\pm$ 10 per cent for cloud bases above 1000 ft. For RPV ascent ratio of 5000 ft/min it has been established (Reference 1) that a time constant no longer than $\tau = 0.5$ seconds be used if the required $\pm$ 100 ft accuracy is to be achieved. In this instance S/N ratio is not a consideration since the cloud droplets provide ample signal.

The two measurement objectives, i.e. aerosol scattering coefficient and cloud base height, place conflicting demands on the SWIRN time constant. A possible solution to this dilemma may be to provide each channel with two outputs; a short time constant for cloud base height measurements and a longer time constant for aerosol scattering coefficient measurements.

Most, but not all, of the flux collected by the receiver will come from the region defined by the intersection of the collimated light bundle projected by the transmitter and the focal zone of the receiver system. The focal zone of the receiver is the shaded region shown in Figure 4.1 which has the appearance of two cones with a common base.

The maximum flux is collected by the receiver system when the sensing element of the detector is imaged into the center of the sample volume as shown in Figure 4.1; the base of the cones in the focal zone is actually the image of the detector projected into the sample volume. The focal zone is defined by four rays as shown in the figure. Rays a and a' terminate at the edges of the detector but cross the optical axis of the receiver lens beyond the detector, which implies that in object space they must cross the optical axis at a distance nearer to the lens than is the object. Similarly, rays b and b' also terminate on the edges of the sensing element, but cross the optical axis in front of the sensor; hence, they must cross the optical axis beyond the object in object space. All other rays terminating at the sensor must be included within the locus of rays defined by the four rays a, b, a' and b' which, in turn, define the focal zone.

The focal zone thus defines a region in which the full lens acts to collect light from every scatterer in the illuminated part of the zone. There are regions around the focal zone where light can be scattered to the lens and reach the detector, but only a fraction of the lens can observe this light. Most of the light which can reach the detector will be that which originates within the focal zone. For signal analysis purposes, therefore, we need consider only the focal zone radiation. The small amount of light which will be contributed by the regions peripheral to the focal zone will be an added bonus.

4.2 Signal Analysis

The geometry of one channel of the SWIRN nephelometer is depicted in Figure 4.1. Light from the tungsten source is projected by a lens through the region encompassing the sample volume. A receiver system, composed of a photovoltaic detector and objective lens, collects light which is scattered by aerosols at a nominal scattering angle θ from the sample volume, which volume is defined by the intersection of the ray bundles of the transmitter and receiver optics.

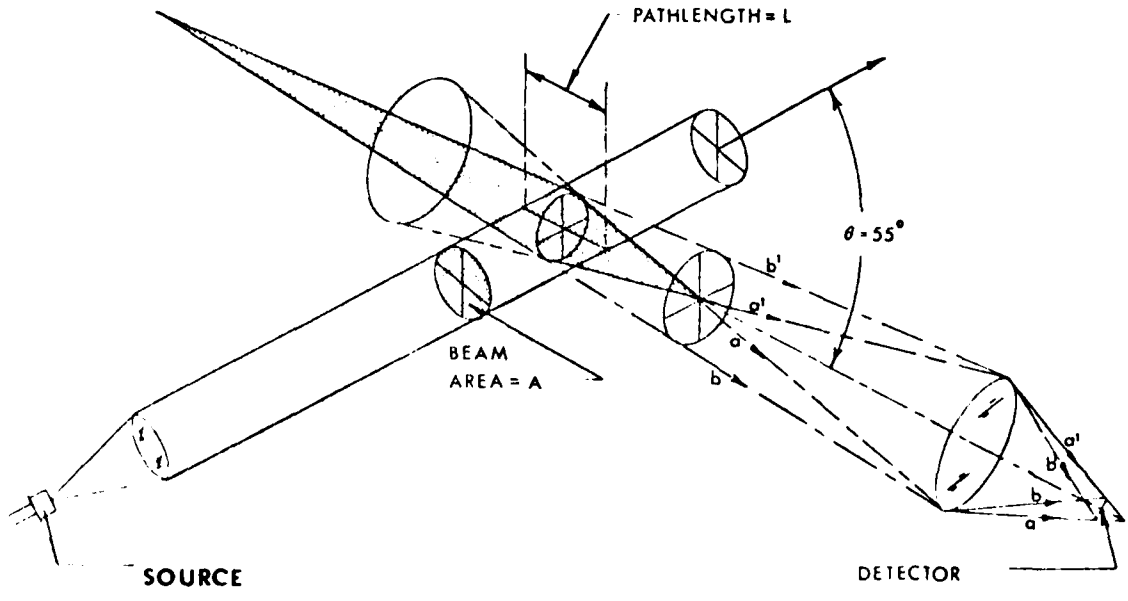

Figure 4.1. Schematic diagram of the optical system of one channel of the SWIR Nephelometer.

When the light source is a tungsten lamp, the optimum flux transfer situation occurs if the lamp filament is imaged such that the maximum diameter of its focal zone (i.e. the image of the filament) intersects the maximum diameter of the receiver focal zone (i.e. the image of the sensor element). This is one of the two principles upon which the original SWIRN concept was based (this and a second principle described later dictate the optimal overall geometry for fixed angle nephelometers. (The beneficial use of this combination of principles appears to have been first recognized by HSS Inc).

For a tungsten lamp source, the flux, F_t, collected from the source by the transmitter lens is

$$F_t = \frac{\pi \epsilon_\lambda N_\lambda \Delta\lambda \; T_t(\lambda) \; A_s}{1 + 4 (f/n)_t^2} \quad \text{Watts} \qquad (4.1)$$

where: A_s = Effective area of the source, cm^2

N_λ = Spectral radiance of the lamp filament, Watts $cm^{-2}\ sr^{-1}\ \mathring{A}^{-1}$

$\Delta\lambda$ = Effective wavelength bandwidth of the instrument, $\mathring{A}$; (actually defined by a wavelength isolation filter in the receiver optics)

ϵ_λ = Average spectral emissivity of tungsten in the spectral region defined by $\Delta\lambda$

$T_t(\lambda)$ = Transmittance of the projection optics in the wavelength interval $\Delta\lambda$

$(f/n)_t$ = Relative aperture of the transmitter optics

The constant irradiance H throughout the focal zone of the transmitter lens is determined by the ratio of the total flux collected and imaged by the transmitter lens to the effective area of the filament image; that is,

$$H = F_t/A_1, \text{ Watts cm}^{-2} \qquad (4.2)$$

The scattering cross section per unit volume of scatter (i.e. the scattering coefficient, σ) has the units cm^2/cm^3 or cm^{-1}. The product of σ and the irradiance H is the total flux σH scattered from the beam per unit pathlength in the beam. The flux F_1 scattered per unit volume per unit solid angle in the direction θ is determined by the phase function for scattering Φ, $ster^{-1}$, i.e.

$$F_1 = \Phi\sigma H \text{ Watts cm}^{-3} \text{ ster}^{-1} \qquad (4.3)$$

The radiance (brightness), B_1, of the sample volume as observed from the receiver lens is obtained by multiplying Equation 4.3 by that length L of the focal zone of the receiver system which is illuminated by the transmitter beam

$$B_1 = \Phi\sigma HL \text{ Watts cm}^{-2} \text{ sr}^{-1} \qquad (4.4)$$

Finally, the scattered flux, F, collected from the sample volume by the receiver lens is given by the expression

$$F = \frac{\pi B_1 A_1 T_r(\lambda)}{1 + 4 (f/n)_r^2} \text{ Watts} \qquad (4.5)$$

where: $(f/n)_r$ = relative aperture of the receiver lens (in object space)

A_1 = cross-sectional area of scattering volume as seen from the receiver lens, cm^2

$T_r(\lambda)$ = Transmittance of the receiver optics in the wavelength interval $\Delta\lambda$

Combining Equations 4.1 through 4.5 gives the complete expression for flux received at the detector

$$F = \frac{\pi^2 \Phi \sigma L \epsilon_\lambda N_\lambda \Delta\lambda T_t(\lambda) T_r(\lambda) A_s}{[1 + 4(f/n)_t^2][1 + 4(f/n)_r^2]} \quad (4.6)$$

HSS Inc appears to have been the first to recognize that Equation 4.6 can be written in the following form:

$$F = \Phi\sigma \epsilon_\lambda N_\lambda \Delta\lambda E_t (L/A_1) E_r \quad (4.7)$$

where:

$$E_t = \pi A_s T_t [1 + 4(f/n)_t^2]^{-1} \quad (4.8)$$

is the throughput of the transmitter optical system and

$$E_r = \pi A_1 T_r [1 + 4(f/n)_r^2]^{-1} \quad (4.9)$$

is the throughput of the receiver optical system.

Equation 4.7 is the basic design trade-off equation for fixed angle nephelometers where both the source and detector are imaged into the sample volume (which as we have seen is one of the optimal conditions for maximizing flux onto the detector).

The design trade-off equation permits an interpretation to be enunciated, which appears to have previously gone unnoticed. That interpretation is as follows: Once the source radiance $\epsilon_\lambda N_\lambda$ and detector bandwidth $\Delta\lambda$ have been chosen and the throughputs E_t and E_r of the transmitter and receiver have been maximized for the geometry permitted by the physical constraints on the instrument, there remains a further means of maximizing flux on the detector; namely, the ratio (L/A_1).

To a firxt approximation $A_1 \simeq L^2$; t' us, we see that

$$F \sim \frac{1}{L} \quad (4.10)$$

enabling the statement to be made that the flux on the detector is inversely related to the linear size of the sample volume. The smaller the sample volume the greater the amount of flux received by the detector.

The analysis outlined above is the basis for making the sample volume of the SWIRN as small as possible consistent with the requirement to measure scattering from representative samples of air. The SWIRN sample volume chosen for design purposes is 2 cm^3. The numerical value of the pathlength L is thus L = 1.27 cm and the cross-sectional area of the sample as viewed from the detector lens is A_1 = 1.61.

A mechanical chopper wheel is used to square-wave modulate the light from the tungsten lamp. The received signal is synchronously detected in order to suppress noise due to background radiation. It is thus necessary to utilize the rms signal flux on the detector in S/N calculations. The rms signal flux is obtained by dividing Equation 4.7 by 2, giving

$$F_{rms} = \frac{1}{\sqrt{2}} \sigma_\lambda N_\lambda \Delta\lambda E_t (L/A_1) E_r \qquad (4.11)$$

A central scattering angle of 55 degrees was chosen for each SWIR Nephelometer channel. This angle was a compromise between two conflicting requirements: (1) the need to make the instrument as small as possible-- thus demanding a large angle, and (2) the need to maximize S/N --- which translates to a shallow forward scatter angle. For maximum accuracy forward-scatter visibility meters must measure the angular scattering coefficient within the range of scattering angles from 30 to 60 degrees (Ref. 1). In this range of angles the phase function for scattering of visible light has been shown to be almost constant for a large range of atmospheric environments. Similar measurements were not available for 2.5 μm radiation when the SWIRN was designed. It was assumed that a field test program would provide sufficient data to validate the choice of a 55 degree scattering angle at 2.5 μm as has been done by many investigators for the visible region.

In calculating the S/N ratios which are shown in Figures 3.3 through 3.8 a phase function value of $\phi = 0.08$ has been assumed for both wavelength channels.

4.3 Noise Analysis

There are three potential sources of noise which were of concern in the design of the SWIRN: (1) Photon noise due to background radiation in the field-of-view of the instrument, (2) detector noise i.e. the NEP of the detector, and (3) amplifier noise. It will be assumed that by use of high quality electronic components combined with good design practice the third noise source, i.e. amplifier noise, can be neglected in comparison with the other two noise sources.

The NEP of the detectors chosen for the SWIRN are given in Table 3.3. The NEP due to photon noise can be calculated from the relation (See Reference 8, p 11-40)

$$\text{NEP (Photons)} = \frac{4.46 \times 10^{-10}}{\eta} \left[\frac{F_b}{\lambda}\right]^{1/2} \sqrt{\Delta f} \qquad (4.12)$$

where: F_b = Flux at detector due to background radiation in the field-of-view of the receiver, Watts.

η = Quantum efficiency of the detector.

λ = Wavelength of the photons, microns

Δf = Electronic frequency bandwidth, Hz

The flux at the detector F_b due to radiation from the terrain, or clouds, within the field-of-view of the receiver is given by

$$F_b = \frac{\pi \, A_d \, B_\lambda \Delta\lambda \, T_r(\lambda)}{1 + 4\,(f/n)_r^{\,2}} \qquad (4.13)$$

where: B_λ = Average spectral radiance of background features Watts cm^{-2} sr^{-1} μ^{-1}

$\Delta\lambda$ = Optical bandwidth of receiver, microns

$T_r(\lambda)$ = Transmittance of receiver optics

$(f/n)_r$ = Relative aperture of receiver optics in image space.

Substituting appropriate values of receiver parameters into Equations 4.12 and 4.13, and combining the two equations, we have

$$\text{NEP (photons)} = 6.88 \times 10^{-11} [B_\lambda]^{1/2} \text{ Watts} \qquad (4.14)$$

The signal-to-noise ratio (S/N) of the AVM may be derived from the expression

$$S/N = \frac{\text{RMS Signal Flux}}{\left\{[\text{NEP(Detector)}]^2 + [\text{NEP (Photons)}]^2\right\}^{1/2}} \qquad (4.15)$$

or

$$S/N = \frac{F_{rms}}{\left\{7.56 \times 10^{-26} + 4.73 \times 10^{-21} B_\lambda\right\}^{1/2}} \qquad (4.16)$$

Using the design parameters of the SWIRN, graphs of S/N ratio vs background spectral radiance were made for three environmental situations using Equation 4.16; the results are shown in Figures 3.3 through 3.8. The three environments expressed in terms of their scattering coefficients σ are taken from the following environmental situations:

(a) $\sigma = 2\ km^{-1}$: Extremely heavy Rural Aerosol Haze, bordering on thin clouds or thin fog.

(b) $\sigma = 0.3\ km^{-1}$: The mean value of σ for a Slant Visual Range of 10 km in a Rural Aerosol Haze.

(c) $\sigma = 0.1\ km^{-1}$: The least value of σ which the SWIRN need measure in either wavelength channel.

The worst background situation which the SWIRN could encounter is a sunlit cloud. The preferred orientation of the SWIRN aboard an RPV will be such that the receiver stares in the downward direction, invariably, therefore, at terrain. On rare occasions, however, the RPV may stare down at the top of sunlit clouds. This worst case situation, CASE C,with the sun directly overhead, is included in Figures 3.3 to 3.8.

More typical background situations are described by Cases A and B. Case A is an overcast situation with the RPV under the overcast, the ground albedo is 0.5, and the diffuse cloud transmittance is 30 per cent. The spectral radiance B_λ of the background is calculated from the relation

$$B_\lambda = \frac{\omega H_\lambda T_c(\lambda) \cos Z}{\pi}, \text{ Watts cm}^{-2} \text{ sr}^{-1} \mu^{-1} \qquad (4.17)$$

where:

ω = albedo of the background

H_λ = Incident solar irradiance on top of the cloud at normal incidence to direction to the sun, Watts $\text{cm}^{-2} \mu^{-1}$

$T_c(\lambda)$ = Diffuse Transmittance of the Overcast

Z = Zenith angle of the sun

Case B is a typical situation when there is no cloud cover. The spectral radiance of the background can be found from the relation

$$B_\lambda = \frac{\omega H_\lambda \cos Z}{\pi} \qquad (4.18)$$

where the symbols are as previously described. The values of H_λ were taken from Reference 8 in all cases treated here.

4.4 Instrument Layout

A layout drawing of the SWIR Nephelometer is presented in Figure 4.2. The housing of the instrument serves to provide the structural rigidity required to support all internal optical and electronic components and to preserve the alignment of the optical system. To minimize design and construction costs the instrument was fabricated from aluminum plate (typically 1/4" thick). Side doors were provided in the housing for ease in servicing of the instrument.

The transmitter optical unit is an integral assembly containing the transmitter lens, chopper wheel motor, the 1 amp source, and a 1:1 concave mirror for increasing the radiant power output by a factor of two. The transmitter unit was fixed-mounted to the base of the instrument with no adjustments for steering of the light beam.

The instrument is divided into two compartments, one which houses the transmitter system, the other which houses the receiver system. This feature is intended to provide RFI shielding of the receiver electronics from external influences, and to provide the square-wave modulated radiation from the source from becoming a problem.

The receiver optical unit consists of the two detectors, each with its receiver lens. An interference filter is used in the visible channel for for restricting the radiation reaching the detector to an optical passband of 0.08μm. Each receiver optical unit is provided with alignment and focus adjustments to center the image of the sample volume on the detector.

No dew-heaters were provided for each of the two windows of the instrument to prevent condensation of moisture from occurring. The windows were fabricated from infrared transmitting quartz to assure good transmission out to 3.0 μm.

A photograph of the completed instrument is shown in Figure 4.3. Cooling fins were installed on the transmitter section of the instrument to aid in dissipating the heat generated by the lamp, chopper motor driver and

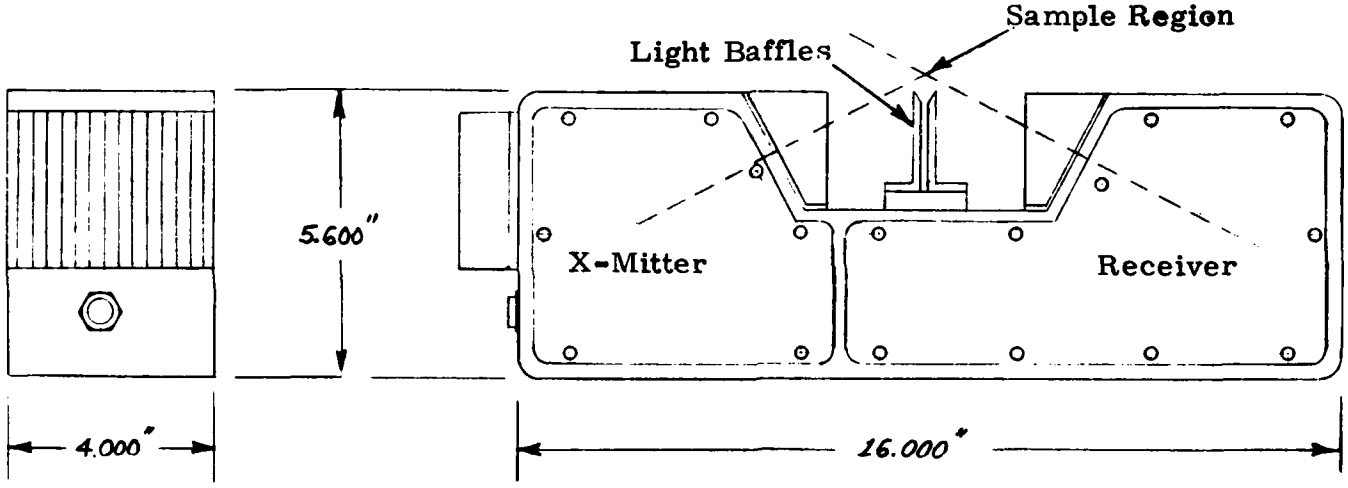

Figure 4.2. Layout drawing of the SWIR Nephelometer.

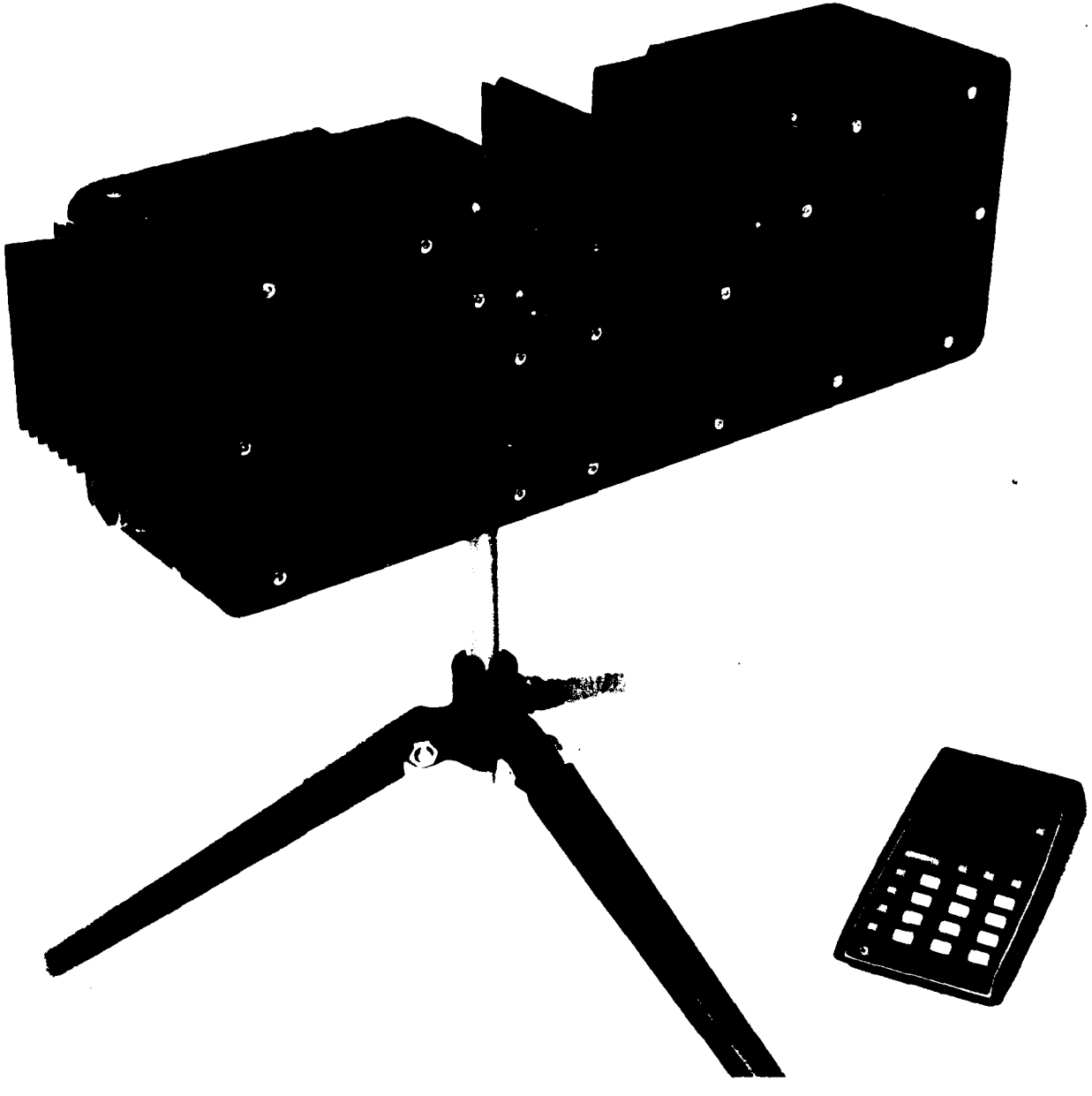

Figure 4.3 Photograph of the GWUP

DC/DC converters. In airborne use such fins would obviously not be required. Also, the body of an airborne instrument would be aerodynamically streamlined instead of having the box-like shape of the prototype instrument.

Figure 4.4 provides additional photographs of the instrument. Figure 4.4 (a) shows the instrument with its access covers removed. The transmitter optical assembly and one of the receiver systems can be seen. Figure 4.4 (b) shows the instrument with one of the two calibration reference standards installed. The reference standards are provided so that periodic checks on the calibration of the instrument can be made. The reference standards are essentially metal plaques with windows in them.

The 2.5 μm channel calibrator has infrared quartz window material; the visible channel employs thin glass. Sandwiched between two sheets of window material are sheets of Kodak flashed neutral density film. This film both scatters and attenuates, thus,providing a near-ideal reference standard medium. Stability tests of the Kodak neutral density material were conducted at HSS Inc. by subjecting the film to sunlight for many hours. There was no measurable change in its properties.

4.5 Optical Systems

The SWIR Nephelometer has one transmitter optical assembly and two receiver sub-assemblies.

In the case of the transmitter optical assembly the optical system must have good chromatic properties (transmission and image quality) over the wavelength range from 0.5 μm to 3.0 μm. A three-element all calcium-fluoride lens system was designed for the transmitter optical assembly.

The optics of the visible receiver channel are identical to

(a)

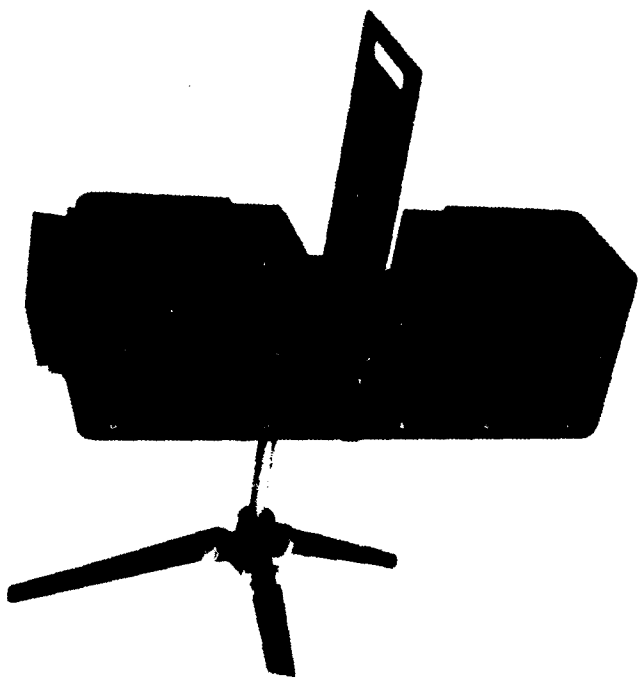

(b)

Figure 4.4. Photographs of the SWIRN Nephelometer: (a) with access covers removed, (b) with reference standard calibrator installed.

those of the AVM visibility meter (Reference 1). These optics are an off-the-shelf two-component pyrex condensor lens system. An interference filter is used to isolate the desired visible bandwidth. The filter is a four-cavity interference filter with a 0.08 μm bandwidth centered at 0.55 μm.

A two-element germanium lens-system was chosen as the optical system for the infrared channel. The choice of germanium was intended to serve two purposes: (1) for imaging the sample volume onto the Pb S detector; and (2) to serve as a high-pass infrared filter which transmits radiation at wavelengths above 2 μm (the upper end of the bandpass is then established by the cutoff in responsivity of the Pb S detector). Because germanium has such a high index of refraction (n = 4.0) the reflective loss R at each lens surface is severe,

$$R = \left(\frac{n-1}{n+1}\right)^2 = \left(\frac{3}{5}\right)^2 = .36 \qquad (4.19)$$

The transmission through two uncoated surfaces of germanium is

$$T = (1 - R)^2 = 0.41$$

Thus the transmission of two germanium lenses is only $(.41)^2$ or 17 per cent. To eliminate this unacceptable loss of energy the lenses were coated with anti-reflection coatings tailored to the wavelength region of the application.

As long as the anti-reflection coating can be peaked for a small wavelength region (a few μm) the cost of the coatings is modest and, in this particular case, was much less expensive than the alternative approach (three CaFl lenses and an infrared bandpass filter).

The two germanium lenses were sent to an evaporated-coating vendor to receive coatings which reduced the reflection loss at each surface to 2 per cent in the wavelength region from 2 to 3 μm.

Because of the wavelength region in which it is operated, the AVM visibility meter used pyrex windows to allow radiation to enter and exit the instrument. The SWIR nephelometer, on the other hand, has quartz windows to transmit the full spectrum of radiation used by the instrument. The choice of material was required to meet several qualifications: (1) it must be capable of withstanding the severe environments which the instrument will encounter; (2) have a low index of refraction, since evaporated coatings cannot be subjected to the harsh external environment; (3) be rugged, non-hygroscopic and have durable surfaces which are not easily scratched. CO-IR synthetic quartz (ESCO Corp) is the least expensive material that comes closest to satisfying all those requirements. The CO-IR quartz does not have the water absorption bands in the near-infrared that are present in most forms of synthetic quartz.

4.6 Electronic Systems

4.6.1 Transmitter System

The interconnecting wiring diagram of the SWIR nephelometer, Figure 4.5, indicates all the major electronic components of the transmitter and receiver electronic systems.

The chopper motor is a two-phase 6-pole Vernitech hysteresis synchronous motor operating at a speed of 8000 revolutions per minute. The motor driver board consists principally of a Burr-Brown precision quadrature oscillator chip (Type 4423) and 2 amplifiers to provide the 400 cycle power to drive the motor. The speed of the motor in RPM is governed by the relation

$$\text{Speed} = 120\, f/P \qquad (4.20)$$

where f is the drive frequency in Hz and P is the number of poles.

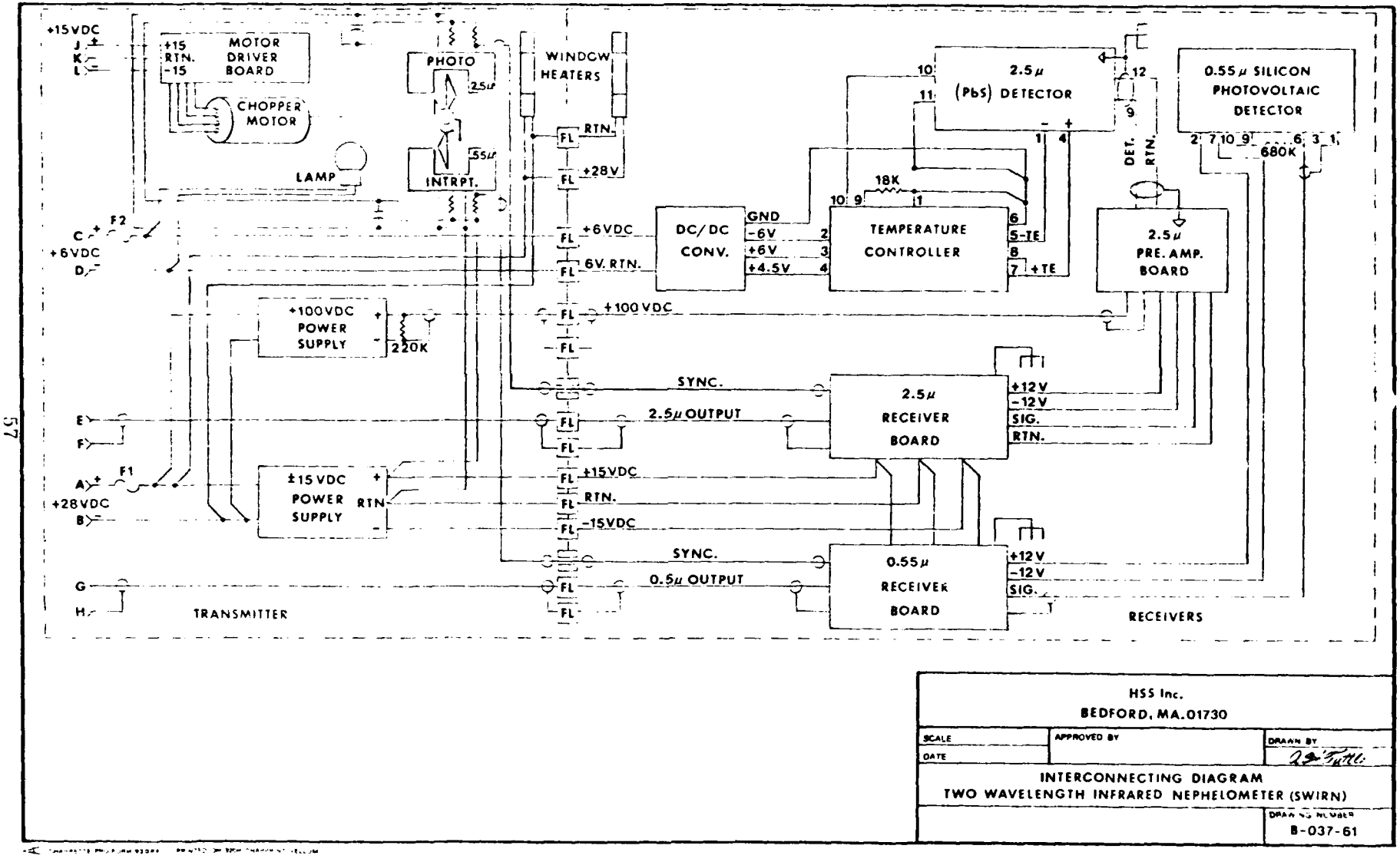

Figure 4.5. Interconnecting Diagram, Two Wavelength Infrared Nephelometer. (SWIRN).

The chopping frequency is determined by the speed of the motor and the number of chopper blades. In the case of the SWIRN, the chopper has four blades, so that the chopping frequency is

$$\frac{8000}{60} \times 4 = 533 \text{ Hz}$$

A slotted optical switch is located on the periphery of the chopper blade to provide the synchronous reference signal for the receiver amplifiers.

The electronic design plans for the instrument included a ± 15 V power supply which would power all components requiring those voltages, including the motor driver board. The first attempts to run the motor demonstrated that it was grossly under-powered. The motor was a customized motor which we eventually discovered required four times as much power to operate as originally quoted to us by the manufacturer. At the point in time that this discovery was made, the instrument was well along in construction and there was no room for a larger ± 15 V DC supply within the housing. Thus provision was made to supply power to the motor driver board from an external ± 15 VDC supply. The motor driver board also had to be redesigned to incorporate amplifiers with higher power ratings.

4.6.2 Receiver Systems

The transmitter and receiver compartments of the instrument are separated by an aluminum bulkhead. EMI filters are supplied to all power and signal leads passing through the bulkhead.

Each receiver system consists of the optical detector with integrated preamplifier, a 533 Hz center frequency bandpass filter, the synchronous rectifier including a phase splitter, and a low pass filter. Each filter stage provides signal gain. The output voltage range is 0 to 10 volts DC for input chopped optical signals of 0 to 6 nanowatts.

The detector-preamplifier of the visible channel is an EG&G HUV-1000B which uses a silicon photovoltaic diode. In its SWIRN configuration, the overall responsivity of the detector circuit is 500,000 volts per watt. The load resistor is selected to provide the maximum output signal for the internal amplifier without saturation of the amplifier due to the optical background (up to 20 microwatts). Maximizing the output signal also maximizes the signal to noise for the detector.

The detector-preamplifier of the 2.5μm channel is an Opto-electronics PbS detector Model OTL-22S-82TC detector having a basic responsivity of 620,000 volts per watt. The PbS detector has a miniature integral two-stage thermoelectric cooler contained within its housing to reduce the temperature of the sensor element to 228 °K. An auxiliary temperature control unit is required to power the cooler. A 100 volt, very low current power supply is also required to provide the bias voltage to the PbS detector.

Each detector channel has its own circuit board for the filters, amplifiers, synchronous rectifier and analog output circuit. The band pass filter is a four pole Butterworth design with 3 dB frequencies geometrically centered at 533 Hz. Its low frequency attenuation is designed to severely attenuate variations in the background signal which otherwise could swamp out the desired signal in this high gain receiver. The filter's high frequency attenuation eliminates noise at odd harmonics of the synchronous rectifier. This filter provides a signal voltage gain of 100.

The phase separator consists of a non-inverting amplifier and an inverting amplifier driven from the same signal. Each amplifier has a design voltage gain of 10. A potentiometer is used to adjust the gain of one amplifier to match that of the other amplifier.

The synchronous rectifier consists of an analog switch integrated circuit controlled by the optical switch signal from the transmitter. It alternately selects the outputs of the phase separator amplifiers for the input to the low pass filter. Since the two input signals are complementary, the net unidirectional (i.e. DC) signal at the synchronous rectifier output is due to the signal in phase with the switch control signal. This is the detected optical signal.

A low pass filter provides the "narrow band" filtering required by the receiver to increase the overall signal to noise to acceptable levels. This filter also provides the last stage of amplification of the signal with a low output impedance (less than one ohm). It consists of an op-amp and its associated components. It is a two pole Butterworth filter with a bandwidth of 6 Hz and has a voltage gain of 8.

5. R & D TEST AND ACCEPTANCE PLAN

The R&D Test and Acceptance Plan is presented in Appendix A in the form in which it was originally submitted to AFGL. (Reference 9). The actual program may have differed in some respects from the program put forth in the test plan. Such differences will be obvious when the results of the tests are presented in the later sections of the report.

Opinions of a negative nature nature are voiced in the test plan concerning the probability of finding an empirical correlation between the SWIRN measurements and the aerosol scattering coefficient in the 8 to 12 μm atmospheric window. These opinions were somewhat premature as will be discussed.

6. TEST AND CALIBRATION

6.1 Background

At the outset of the contract AFGL and HSS Inc had made plans to test the SWIRN at Otis AFB. Testing at Otis AFB was predicated on the presence there of the AFGL/OPA instrumented trailer. That trailer is equipped to make long-path IR atmospheric transmission measurements which are essential to the SWIRN test and evaluation program.

During the SWIRN development, other OPA commitments arose, and they decided not to operate the trailer at Otis AFB. This decision required AFGL technical monitors of the SWIRN contract and HSS Inc to consider alternative plans for the SWIRN test program.

The alternative test program for the SWIR Nephelometer which was approved by AFGL had two phases: (1) a one-month field test program during mid-1982 at Hanscom AFB which overlapped the presence of the OPA instrumented trailer, and (2) a week-long intensive test and calibration exercise at the CALSPAN Environmental Test Chamber at Ashford, New York.

6.2 Test Program Objectives

The primary objectives of the SWIRN test and evaluation program remained unchanged from the objective of the test program which was to be conducted at Otis AFB. Because the test and evaluation program was intended to address specific program objectives it is important that those objectives be carefully stated. The two primary objectives which were to be addressed are:

Objective 1: The ability to forecast the Target-Acquisition-Range (TAR) and System-Lock-On-Range (LOR) for 8 to 12 μm FLIR systems, based on pre-strike surveillance missions with instrumented RPV s, is an ongoing Air Force requirement. A severe limitation to the present-day Air Force capability to predict the TAR and LOR for 8 to 12 μm FLIR systems is the lack of a small airborne instrument to measure atmospheric aerosol extinction coefficients in that spectral region. The SWIRN development program is directed toward the ultimate fulfillment of this requirement.

Physical constraints were imposed on the SWIRN because the contemplated method for deployment is by Remote Piloted Vehicle (RPV). To be deployed on an RPV the instrument must be small in size, light in weight and have low power consumption. To perform the required aerosol scattering coefficient measurements in the 8 μm to 12 μm spectral region, given these constraints, is considered to be beyond the state-of-the-art in aerosol nephelometry.

An alternative approach has been taken by AFGL to the direct measurement of aerosol scattering in the 8 to 12 μm region. That approach we shall call the Indirect Method. It led to the development of the SWIR Nephelometer.

In the Indirect Method two widely separated short-wavelength measurements are to be used as inputs to a predictive model to determine the atmospheric extinction coefficient in the long-wavelength (8 to 12 μm) spectral region. The two wavelength bands adopted in the prototype SWIRN have central wavelengths located at 0.55 μm in the visible and 2.5 μm in the near infrared.

The Indirect Method rests on a premise, which had not been verified, that a predictive computer model, which has as inputs the SWIRN measurements and basic meteorological parameters, can determine atmospheric aerosol extinction properties at long IR wavelengths. The SWIRN test and evaluation program had as one of its objectives a preliminary evaluation of the Indirect Method.

Objective 2: The second objective of the test program relates specifically to the evaluation of the instrument as a nephelometer. Performance of the SWIRN must be tested and evaluated in an extreme range of environments, from heavy fog to very light hazes. Subjecting the instrument to an extreme range of attenuating conditions was also essential to the calibration of the prototype instrument.

Secondary objectives of the SWIRN tests relates to: (1) the long term stability of the instrument calibration (once established), (2) environmental and temperature effects on the instrument calibration and, (3) the degree and type of maintenance required to maintain optimum performance.

6.3 Field Tests at Hanscom Air Force Base

The SWIR Nephelometer was installed on a mount on top of the OPA instrumented trailer at Hanscom AFB, Ma. for a one-month period during March/April 1982. During that entire period not one low-visibility episode occurred, and as a result no measurements of atmospheric

attenuation were obtained. Toward late April the instrument was removed to prepare for its shipment to the CALSPAN Environmental Test Chamber.

6.4 Test and Calibration at CALSPAN

The CALSPAN test program was conducted during a five day period in the first week of May 1982 (3 May - 7 May). A total of fourteen tests were conducted to provide the wide range of haze and fog environments which are described in Table 6.1. An excellent characterization of the environments which were generated was provided by CALSPAN to AFGL and HSS Inc in their final report. The CALSPAN report in its entirety is included as Appendix B to this report.

The complement of instruments employed by CALSPAN for monitoring the atmospheric extinction coefficients and particle sizes was as follows:

(1) Long Path CALSPAN Visible Light Transmissometer: provided extinction coefficients over a path length of 18.3 meters in the test chamber in the spectral region from 0.4 to 0.6 μm.

(2) Short Path CALSPAN Visible Light Transmissometer: similar to the Long Path Transmissometer except the path is 2.67 meters.

(3) CALSPAN IR Transmissometer: measured extinction coefficient over a path length of 18.3 meters and at wavelengths of 2.22 μm and 9.73 μm using narrow bandwidth interference filters.

(4) MRI 2050 Integrating Nephelometers: measured the broadband visible light scattering coefficient in the range .08 to 8 km^{-1}.

(5) CALSPAN Fog Droplet Sampler: provided drop sizes in the range 3 to 100 μm by impaction on a gelatin covered slide.

(6) Royco Model 225 Particle Counter: measured aerosol size distribution in the range 0.3 - 10.0 μm.

Table 6.1 Summary of Fog and Haze Tests Conducted at the Calspan Environmental Test Facility.

Test Run	Date	Objective	Aerosol/Nuclei
1	3 May	Low Humidity Haze	Salty Dog (200 gm)
2	4 May	Large Droplet Fog	Ambient Nuclei
3	4 May	Large Droplet Fog	Ambient Nuclei
4	4 May	Medium Droplet Fog	Ambient Nuclei
5	4 May	Small Droplet Fog	Cigar Smoke
6	4 May	High Humidity Haze	Salty Dog (20 gm)
7	5 May	Large Droplet Fog	Ambient Nuclei
8	5 May	Large Droplet Fog	Ambient Nuclei
9	5 May	Small Droplet Fog	Cigar Smoke
10	5 May	High Humidity Haze	Salty Dog
11	6 May	Small-Med. Droplet Fog	Ambient Nuclei
12	6 May	Small Droplet Fog	Ambient Nuclei
13	6 May	High Humidity Haze	Salty Dog (50 gm)
14	7 May	Low Humidity Haze	Phosphorus

(7) Thermo-Systems Electric Aerosol Analyzer Model 3030: measured aerosol size distribution in the range .004 to 0.76 μm.

The only instrument for characterizing the infrared attenuation of the fog and haze environments was the CALSPAN IR Transmissometer. This instrument had measurement deficiencies in both fog and haze environments: (1) pressurization and exhalation of the test chamber during the process of creating fog disturbed the alignment of the optics which were rigidly attached to the walls of the cylindrical chamber, and (2) in haze situations the IR transmissometer, because of its short baseline, had no measurement capability --- except when the smoke employed to form aerosol nuclei was so dense that it created unnatural haze environments. These problems were realized in advance by HSS Inc and AFGL, but it was agreed to proceed with the CALSPAN tests despite the IR measurement limitations since there was no viable test alternative at that time.

A second major deficiency of the CALSPAN tests was not realized until HSS Inc was well into the reduction and analysis of data. This deficiency, discussed later in detail, was the small size of the aerosol particles used to simulate haze environments. The small aerosol size introduced no problems in the visible spectral region. The effects in the infrared spectral region were however quite serious.

Hazes were generated in the test chamber (9 meters high and 9 meters in diameter) by burning small quantities of pyrotechnic materials in various humidity situations. The two most common materials employed for generating aerosol nuclei were "Salty Dog" (mainly NaCl and KCl) and phosphorous. The blower and filter system of the test chamber was used to remove the haze particles, thus reducing the aerosol concentration and providing, as a function of time, a large range of haze environments.

Fogs were produced by spraying the inside wall of the chamber with copious amounts of water then pressurizing the chamber to approximately 30 millibars above ambient pressure. A controlled release of the pressure

(3 - 5 mb/min) generated the fog environment and a release rate of 1 mb/min was used to sustain the fog. Large droplet fogs were generated by filtering the air in the chamber overnight thus providing a minimum of nuclei for creation of fog droplets. Small droplet fogs were created by introducing many more nuclei for drop formation.

6.5 Instrument Calibration

6.5.1 Data Base

The haze and fog environmental episodes simulated in the CALSPAN Test Chamber provide the basis for the calibration of the two wavelength channels of the SWIR Nephelometer. Measurements performed by CALSPAN with their instrumentation defined the prevailing atmospheric attenuation coefficient in the chamber. These measurements when plotted against the output voltages of the SWIRN represent the calibration curves of the instrument.

6.5.2 Visible Channel

Calibration curves for the visible channel are shown in Figures 6.1 to 6.4. The calibration curves for the haze and fog episodes have been plotted separately:

Haze Episodes: The basic haze calibration curve for the visible channel is shown in Figure 6.1. The CALSPAN measurements represent a mixture of data from their visible light transmissometers and the MRI integrating nephelometer.

The simulated environments corresponding to these measurements are all high humidity hazes and,therefore,come closest to representing real environments. The data points for the two low humidity hazes (Episodes 1 and 14) do not fall on the same curve and are plotted separately (Figure 6.2). In the case of these two episodes copious amounts of smoke particles were generated by burning a relatively large amount of Salty Dog (Run 1) and phosphorous (Run 14). The reason that the data points do not fall on the Figure 6.1 calibration curve may be attributable to the size of the smoke

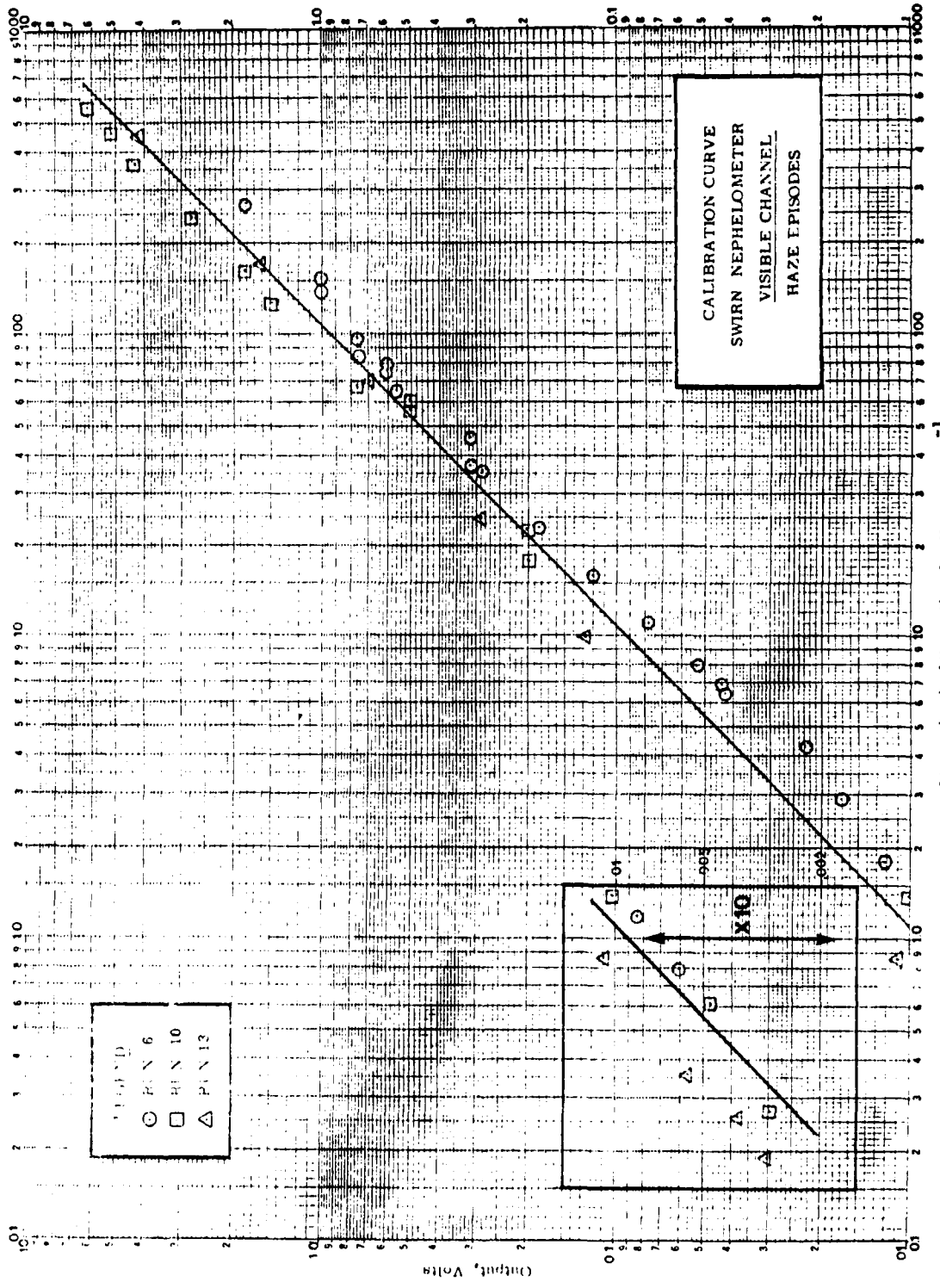

Figure 6.1. Visible channel calibration curve; Haze Episodes 6, 10 and 13.

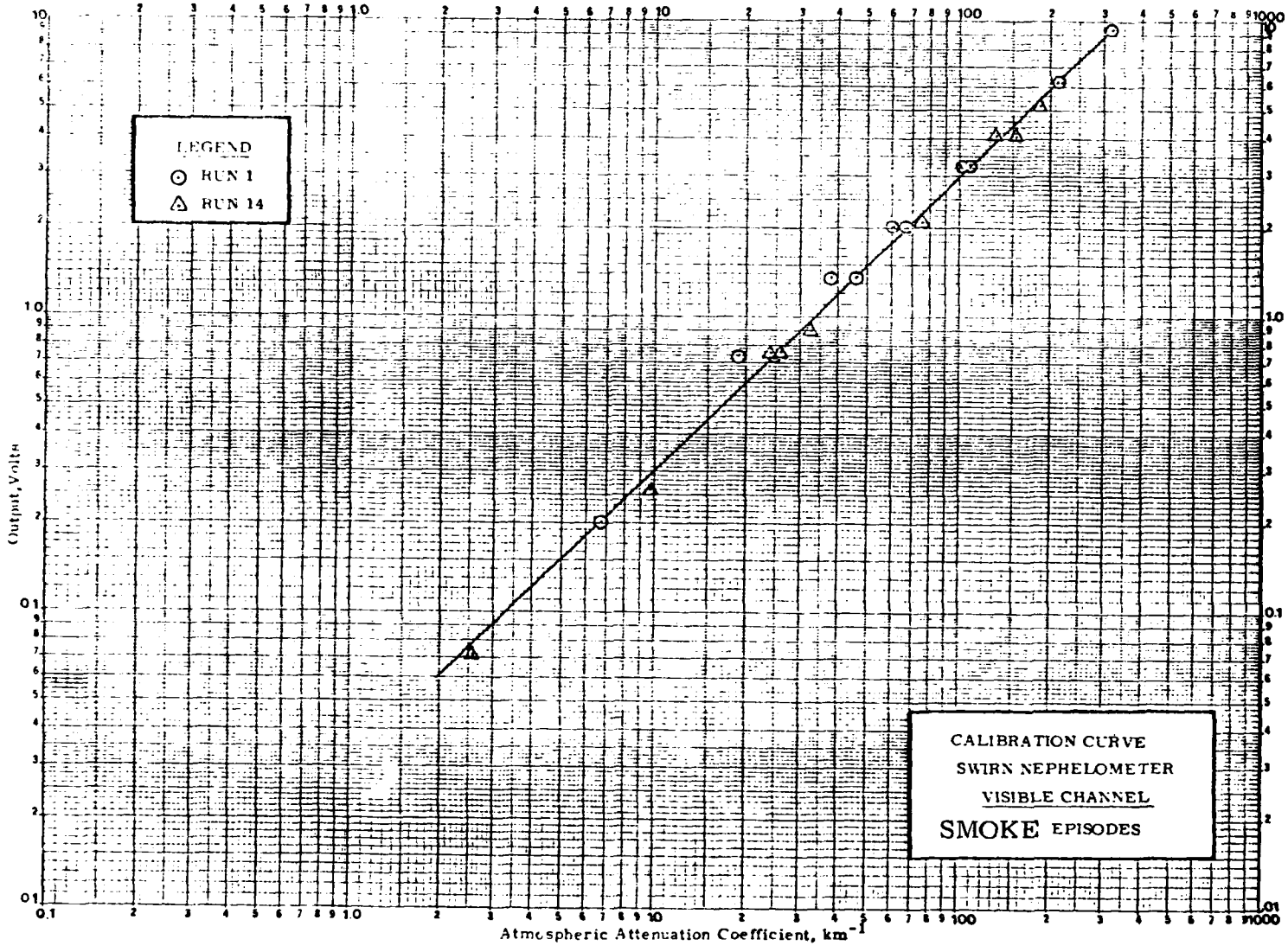

Figure 6.2. Visible channel calibration curve; Smoke Episodes 1 and 14.

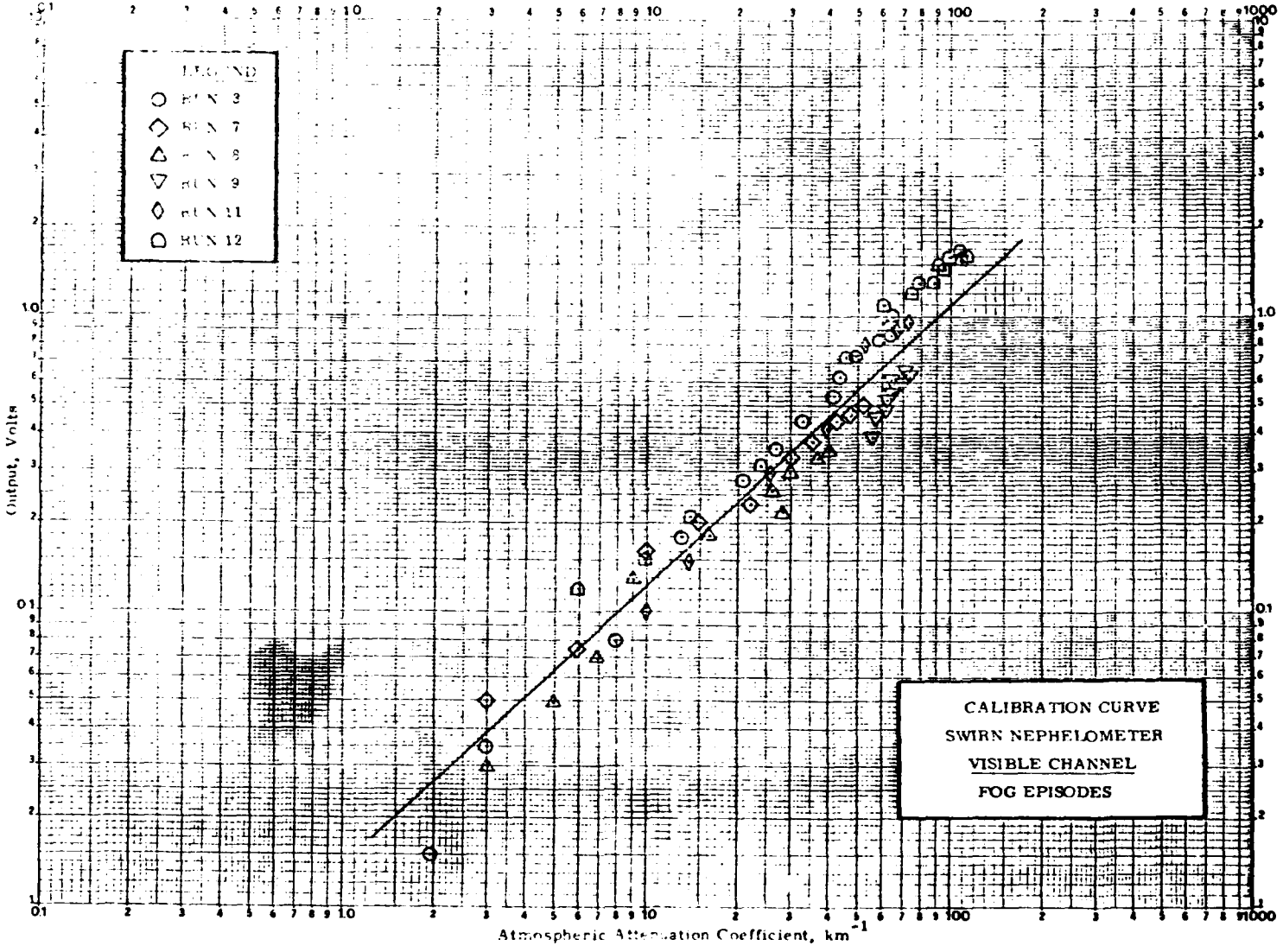

Figure 6.3. Visible channel calibration curve; Fog episodes 3, 7, 8, 9, 11 and 12.

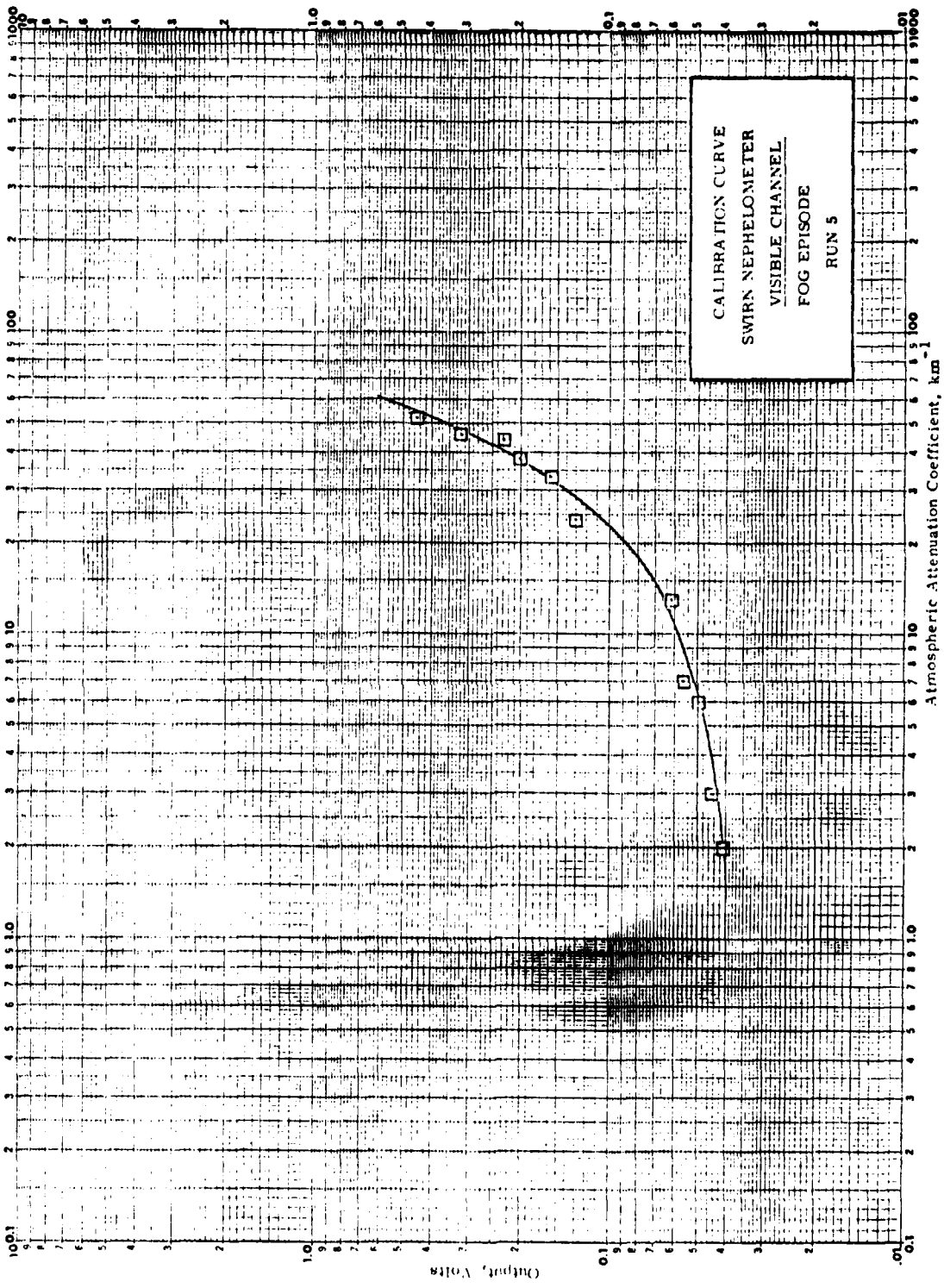

Figure 6.4. Visible channel calibration curve; Fog Episode 5.

nuclei. Little or no aerosol growth could occur due to the low humidity whereas in the high humidity episodes of Figure 6.1 aerosol growth could occur.

Fog Episodes: The basic visible channel calibration curve for fog is shown in Figure 6.3. There is relatively little difference between this calibration curve and that for haze episodes shown in Figure 6.1 in the regions where they overlap. If the two data sets were plotted as a composite data set one calibration curve for the visible channel would result. That one calibration curve would suffice for all natural fog and haze environments.

A mavrick fog calibration curve is shown in Figure 6.4. This curve is a result of drift in the collimated light beam of the CALSPAN transmissometer. On occasion the collimated beam would wander because of motion of the chamber wall during depressurization. Such data sets must be excluded from the calibrations because of the obvious instrumental error they introduce.

6.5.3 Infrared Channel

Calibration curves for the infrared channel are shown in Figure 6.5 and 6.6. Again the calibration data for the haze and fog episodes are treated separately.

Haze Episodes: The calibration curves obtained from three haze episodes are presented in Figure 6.5. There is an obvious disparity in the curves which we attribute to the type and size of the aerosol particles.

Two of the test runs (Episodes 10 and 13) simulated high humidity environments yet the particle sizes (see Table B2) were mostly submicron in size. The disparity between the data points on these two runs is however not significant and could be explained by a slight drift of the CALSPAN IR Transmissometer during one of the runs.

Data from Episode 14, which was a low humidity haze show a large disagreement with the data from the other two runs. This disparity

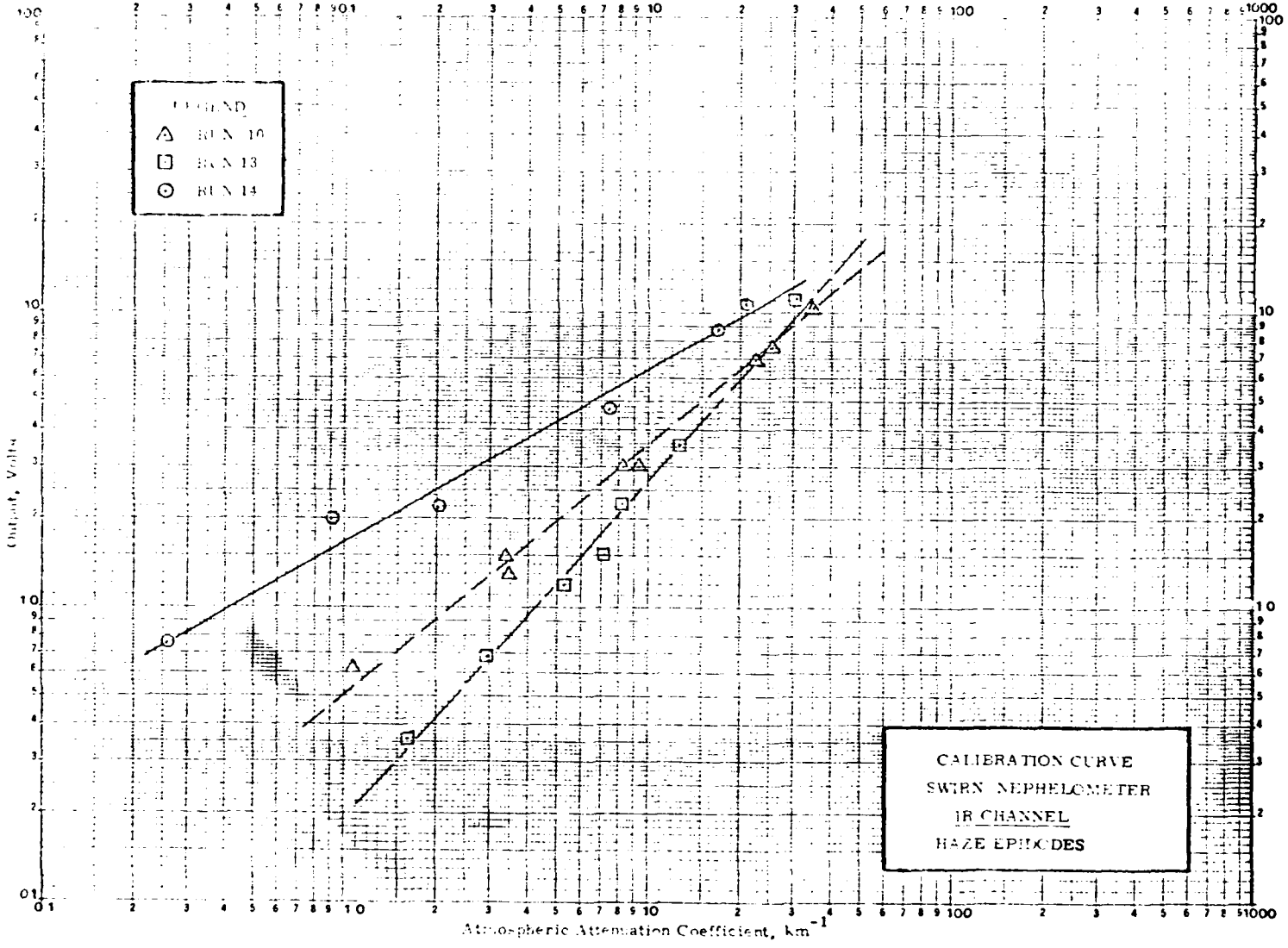

Figure 6.5. Infrared channel calibration curve; Haze Episodes.

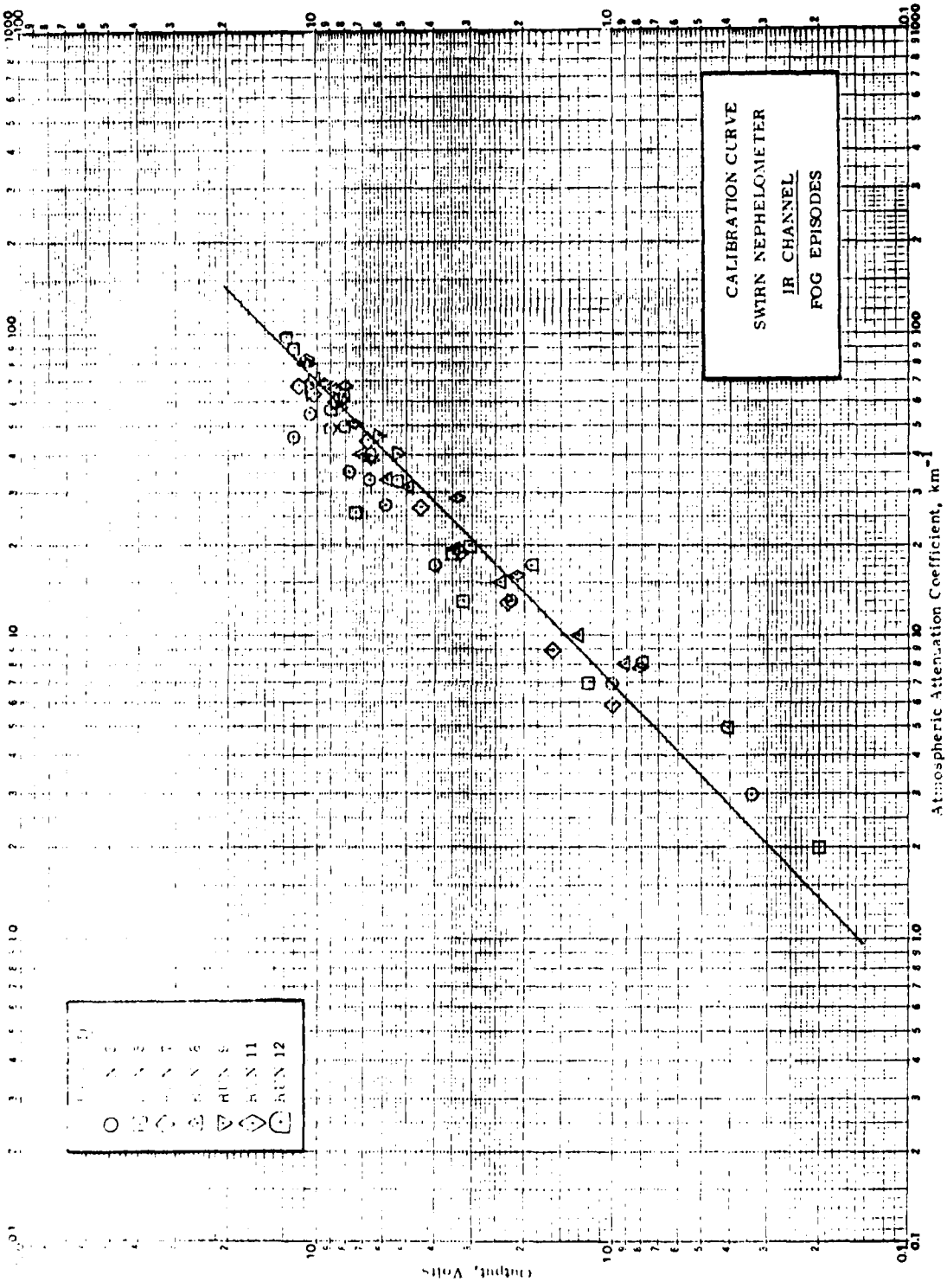

Figure 6.6. Infrared channel calibration curve; Fog Episodes.

is probably real and accounted for by the type of smoke particles (Phosphorous) which are not representative of the natural environment, although they may be representative of camouflage smoke particles. IR data for the other low humidity haze episode (Episode 1) was not obtained from the IR transmissometer (see Appendix B) thus the data from Episode 14 are unconfirmed.

A severe limitation of the haze calibration for the infrared channel is the lack of attenuation coefficients for high visibility situations. The short baseline IR transmissometer cannot provide useful data in such situations.

Fog Episodes: The data obtained from seven fog episodes are plotted in Figure 6.6. The combined data provide a single calibration curve which appears to be reasonable.

In the case of the visible channel the composite fog data and composite haze data (excluding Episodes 1 and 14) can be combined into a single calibration curve. This is not the case in the IR channel. This behavior could be real or it could result from the non-natural sizes of the haze particles. The question can probably only be resolved by operating the SWIRN against long path IR transmissometers in a real environment.

6.5.4 Calibration Equations

The general expression for the calibration equation of a forward scatter nephelometer is

$$\beta = K \left(\frac{V - b}{g} \right)^n \qquad (6.1)$$

where: β = atmospheric scattering coefficient, km^{-1}

v = output voltage, volts

b = zero offset voltage, volts

g = external amplifier gain

n = power-law exponent

For the CALSPAN tests a signal conditioner was employed to increase the output time constant of the instrument from 0.5 seconds to 15 seconds. This was done to insure that representative aerosol distribu-

tions would be sampled in a static operating situation. The signal conditioner provided X1 and X10 output signals for each of the two wavelength channels. In deriving the calibration curves all data points were plotted as if they were obtained from the X1 output of the signal conditioner.

Visible Channel: The calibration equation for the visible channel, based on a composite of the fog and haze calibrations is:

$$\beta = 106.4\ V \quad \text{(fogs and haze)} \tag{6.2}$$

Infrared Channel: The calibration curves for fog and haze differed significantly in the infrared channel. Until measurements are made against a long-path IR transmissometer in a real haze environment we shall treat the calibrations for fog and haze environments as being different for the infrared channel.

$$\beta = 7.00\ V \quad \text{(fog)} \tag{6.3}$$

$$\beta = 3.30\ V \quad \text{(haze)} \tag{6.4}$$

7. SPECIFICATIONS AND PERFORMANCE CHARACTERISTICS

7.1 Introduction

The specifications detailed herein pertain to the prototype SWIR Nephelometer. The performance characteristics are those which were measured during the tests and calibration at the CALSPAN Environmental Test Chamber, and are again those of the prototype instrument.

Some deficiencies in the prototype type instrument design were uncovered during fabrication and testing of the instrument. If and when a second instrument is built the corrections could lead to improved performance and to improved physical features. Whenever applicable, footnotes are used to indicate the improvements which could be affected in a later version of the instrument.

The performance characteristics as presented are influenced by the somewhat arbitrary settings of amplifier gains employed during the CALSPAN tests and by the time constant (15 seconds) used in the signal conditioner.

Characteristics which influence the range of atmospheric scattering coefficients that can be measured by a nephelometer are: (1) maximum linear output voltage, (2) amplifier gain settings, (3) detector/amplifier noise and (4) stability of the zero setting. Subsequent to the CALSPAN tests substantial effort was expended to improve the zero-set stability of the output amplifier of the Airborne Visibility Meter (AVM) -- an instrument with an identical amplifier design. Incorporation of these circuit modifications in SWIRN would improve the zero stability values shown in the specifications.

Finally, the full capability of the SWIRN can only be appreciated if its capabilities for a variety of gain settings and time constants are compared. An attempt to show some of the alternatives are made in the performance documentation and in the footnotes.

7.2 General Specifications

Wavelength Channels

Channel 1 ---------- Visible (Green)

Channel 2 ---------- NIR

Scattering Angle Coverage

Central Angle ---------- 55 deg.

Range of Angles ---------- $\pm$ 5 deg.

Sample Volume ---------- 2 cm^3

Source Characteristics

Type ---------- Tungsten Lamp

Model ---------- GE 1974D

Lifetime ---------- 10,000 hrs.

Power Req't (at 6 volts) ---------- 20 W

Temperature (color) ---------- 2550° K

Chopping Frequency ---------- 533 sec^{-1}

Physical Characteristics

Weight (Note 1) ---------- 9.5 lbs

Size ---------- 17.5"L x 4"W x 5.5"H

Optical Characteristics - Channel 1

Central Wavelength ---------- 0.55 μm

Optical Bandwidth ---------- 0.08 μm

Detector: Type ---------- Silicon P.V.

Model ---------- EG&G HUV 1000B

Receiver Lens: Type ---------- 2-Element Condensor

Material ---------- Pyrex

Wavelength Isolation Filter

Type ---------- 4 Cavity Inter.

Model ---------- Customized

Optical Characteristics - Channel 2

Central Wavelength ---------- 2.50 μm

Optical Bandwidth ---------- 1.0 μm

Detector: Type ---------- PbS

Model ---------- OTC-11S-82TC

Sensor Temperature ---------- (-)45° C

Detector Cooler: Type ---------- Thermoelectric

Model ---------- 11454-TP

Receiver Lens: Type ---------- 2-Element

Material ---------- Germanium

Wavelength Isolation Filter

Type (Note 2) ---------- None

Window Characteristics

Transmitter Section

Material ---------- COIR Quartz

Heater Power Req'ts ---------- 3 W

Receiver Section

Material ---------- CO IR Quartz

Heater Power Req'ts ---------- 4.5 W

Output Characteristics (Channels 1 and 2)

Output Voltage	Analog
Voltage Range	0 to 10 v
Time Constant (Note 3)	0.5 sec
Linearity	0.1%

Power Requirements (Note 4)

28 VDC power	14 W
6 VDC power	25 W
±15 VDC power	12 W

Environmental Capability (Note 5)

Temperature	-50°C to + 50°C
Altitude	0 to 10,000 ft
Weather	All Weather

7.3 Performance Characteristics

Channel 1 Performance Characteristics

Noise Voltage: (Note 6)

Nighttime (RMS Noise)	0.28 mv
Daytime (RMS Noise)	0.84 mv

Stability of Zero Setting: (Note 7)

Ambient Temp. Effects	2 mv
Long Term Drift	4 mv

Measurement Capability --- CALSPAN Results

Conditions	(Note 8)
Scattering Coefficient Range	1000 km^{-1} to 0.1 km^{-1}
Visual Range	3 m to 30 km

Measurement Accuracy (Note 9)

Rel.Error: At 30 km	100 %
At 10 km	29 %
At 7 km	20 %
3 m to 5 km	≤15 %

Measurement Capability --- Projected

Conditions	(Note 10)
Scattering Coefficient Range	100 km^{-1} to 0.3 km^{-1}
Visual Range Coverage	30 m to 10 km

Measurement Accuracy:

Rel. Error: At 10 km	100 %
At 2 km	20 %
30 m to 1.5 km	≤ 15 %

Channel 2 Performance Characteristics

Noise Voltage: (Note 6)

Nighttime (RMS Noise) ---------- 0.6 mv

Daytime (RMS Noise) ---------- 1.8 mv

Stability of Zero Settings (Note 7)

Ambient Temp. Effects ---------- 2 mv

Long Term Drift ---------- 4 mv

Measurement Capability --- CALSPAN Results

Conditions ---------- (Note 8)

Scattering Coefficient Range:

Fog ---------- 70 km^{-1} to 1.5 km^{-1}

Haze ---------- 1.5 km^{-1} to 0.006 km^{-1}

Seability: Fog ---------- 40 m to 2 km

Haze (Note 11) ---------- 2 km to 500 km

Measurement Accuracy (Note 9)

Rel. Error: At 200 km ---------- 100 %

At 50 km ---------- 20 %

90 m to 35 km ---------- ≤15 %

Measurement Capability --- Projected

Conditions ---------- (Note 10)

Scattering Coefficient Range ---------- 100 km^{-1} to 0.016 km^{-1}

Seability Range ---------- 30 m to 180 km

Measurement Accuracy:

Rel. Error: At 180 km ---------- 100 %

At 28 km ---------- 20 %

30 m to 22 km ---------- 15 %

Note 1. Excluding External Power Supplies

Note 2. The short wavelength cutoff (2 μm) of the passband is determined by the germanium lenses; the long wavelength cutoff (3.0 μm) is determined by the spectral responsivity of the PbS detector.

Note 3. The output time constant used for the CALSPAN tests was 0.5 seconds. Recent reviews of the Air Force requirements indicate that a time constant as long as 2 seconds is acceptable for airborne (RPV) use.

Note 4. These are the external source power requirements for all functions of the prototype instrument including the window heaters. In a second instrument we recommend that the $\pm$ 15 v external power supply for the chopper motor driver be combined with the internal DC/DC Converter which supplies $\pm$ 15 volts DC from the 28 VDC external power.

Note 5. These environmental capabilities are design goals which have not been subjected to test therefore are unproven.

Note 6. The nighttime noise figure was determined from the CALSPAN test records. The daytime noise figure was determined by multiplying the nighttime figure by a factor of three, which factor has been empirically established in a crude fashion by monitoring the AVM records at Otis AFB.

Note 7. The values assigned to the stability of the zero setting were not measured. They are based on early experience with similar circuits in the AVM.

Note 8. The measurement capability is based on the CALSPAN tests and calibration of the SWIRN. The time constant during the CALSPAN tests was 15 seconds. The daytime noise figure was used in the determination and the maximum visual range is established by setting the signal equal to the daytime noise. It is important to note that the potential zero drifts have not been utilized in establishing the upper limit to visual range. This was done under the assumption that the zero drift values could be improved in a later version instrument. The electronics gain setting for the visible channel (Channel 1) during the CALSPAN tests was obviously too low and should be set to a higher value in any future use of the instrument.

Note 9. The effects of zero drift have not been included in these estimates of the measurement capability. The estimate includes all other sources of error including the calibration error.

Note 10. The projected measurement capability of Channels 1 and 2 is based on a time constant of 2 seconds, an increase in the Channel 1 amplifier gain by a factor of ten, and a slight decrease in the Channel 2 amplifier gain. The effects of zero drift have not been included in the determination for reasons given in Note 8. Other criteria used in establishing the performance values are as set forth in Notes 8 and 9.

Note 11. The calibration runs at CALSPAN gave different calibration curves for fog and haze environments. We believe this may be due to the haze particle size distribution which was unlike normal atmospheric hazes in that the particle sizes were small and did not include the "tail" of large particles normally present in real haze environments.

8. EVALUATION OF THE SWIRN CONCEPT

8.1 Introduction

The basic premise underlying the development of the SWIR Nephelometer is that measurement of the atmospheric scattering coefficient at two widely separated short wavelengths, one in the visible the other in the near infrared, can be used to accurately predict the aerosol attenuation coefficient in the longwave 8 - 12 μm spectral region. The need for aerosol attenuation measurements at 8 - 12 μm is fundamental to the ability to provide pre-strike forecasts of the target lock-on range (LOR) for FLIR systems employed on strike aircraft carrying precision guided munitions.

One task under the present contract is to investigate, on a limited scale, empirical techniques for extrapolating the SWIRN measurements of atmospheric attenuation coefficient to the 8 to 12 μm spectral region to determine the aerosol scattering coefficient in that atmospheric window. The effort devoted to that task is described in this section of the report.

The approach taken consisted of three steps: (1) the search for possible empirical correlations between the aerosol scattering coefficients at the two wavelengths 0.55 μm and 2.5 μm and the aerosol scattering coefficient at 10 μm using the aerosol models of Shettle and Fenn (Reference 4); (2) testing of empirical relationships on the actual atmospheric transmission data reported by Clay and Lenham(Reference 10) and modifying the relations as necessary to improve their accuracy, and (3) testing the improved relations on the CALSPAN test data.

The development of empirical relationships of the type desired for the SWIR Nephelometer requires a data bank of simultaneous measurements of the atmospheric extinction coefficient of at least three wavelengths (.55 μm, 2.5 μm and 10 μm) for many types of atmospheric environments.

Any relationships which are derived from such a process must then be tested by operating the SWIR Nephelometer in many low-visibility natural environments alongside one or more long-path IR transmissometers.

There does not appear to be any such data bank,at least we were unable to locate one. Nor was the SWIRN operated in natural environments alongside long-path IR transmissometers.

The aerosol models of Shettle and Fenn were substituted for the primary data bank. Shettle and Fenn treat four classes of haze (rural, urban, maritime, and tropospheric) in eight conditions of relative humidity (0, 50, 70, 80, 90, 95, 98, and 99 %) making up 32 models. In addition, four fog models were treated, making a total of 36 models. Shettle and Fenn calculate extinction coefficients at a number of wavelengths including 0.55 μm, 2.2 μm, and 10 μm. Each of these calculations was made for a specific number density of the aerosol particles under consideration. If this number density is changed, the associated values of extinction coefficients change proportionally.

Using the Shettle-Fenn models an empirical relationship was developed which calculates the extinction coefficient at 10 μm when the extinction coefficients at 0.55 μm and 2.2 μm are given. The relationship, which involves 14 coefficients, holds for any number density of any of the 36 models. In general, the accuracies achieved involve errors of less than 10 % of the values given by Shettle and Fenn.

The empirical relationship derived from the Shettle-Fenn models was first tested using the atmospheric transmission data reported by M.R. Clay and A.P. Lenham. The test shows that the empirical relationship is deficient when transmission values from real fogs are treated. For this reason, the empirical relationship was upgraded using the Clay and Lenham data as guide.

The upgraded empirical relationship was finally tested using extinction coefficients obtained from the CALSPAN tests. These coefficients were derived from measurements made on fogs and hazes generated in the chamber to calibrate the SWIRN. These last tests of the empirical relationship are encouraging. They indicate that the fogs generated in the chamber have spectral extinction coefficients which confirm the relationships developed from the Clay-Lenham data. Each of the hazes generated in the chamber behaves in an orderly way as far as interrelationships of the extinction coefficients are concerned; however, such interrelationships are not those predicted from the Shettle-Fenn models of hazes.

In the final section of this chapter, we present some rather general comments on the relationship between measurements made with fixed angle nephelometers and the extinction coefficients of the aerosols involved. The magnitude of such measurements depends not only on the extinction coefficients of the aerosols but also on their albedos and phase functions. Since the albedos and phase functions change from one type of aerosol to another, the effects of these changes must be considered when nephelometer measurements are used to predict extinction coefficients at 10 μm.

It is shown that adequate corrections for these changes can be made if the ratios of the nephelometer measurements at 2.2 μm to those at 0.5 μm are known.

It is concluded that the studies presented in this section indicate reasonable possibility that extinction coefficients at 10 μm can be deduced from fixed angle nephelometer measurements made at 0.5 μm and at 2.2 μm. It is, therefore, recommended (1) that an effort be made to locate other extinction coefficients which can be used to check and to improve the relationships developed here and (2) that an experimental program be undertaken in natural environments to establish the relationship between nephelometer measurements as made by SWIRN and the extinction coefficients at 10 μm.

8.2 Correlation Equations from AFGL Aerosol Models

The SWIRN nephelometer makes measurements in narrow wavelengths bands centered on $\lambda = 0.5\ \mu m$ and $\lambda = 2.5\ \mu m$. For this stage of the discussion it is assumed the nephelometer can be calibrated so that the output readings are related in a known way to the aerosol extinction coefficients at these wavelengths. This being the case, extinction coefficients obtained from model calculations from experiments can be used to investigate correlations which may be achieved, down the line, using the SWIRN instrument.

The first correlation attempts were made using the calculations reported by Shettle and Fenn of AFGL (Ref. 4). Table 8.1 presents in columns 2, 3 and 4 the AFGL extinction coefficients $\gamma\ (.55)$, $\gamma(2.2)$ and $\gamma\ (10)$ at $\lambda = .55\ \mu m$, $\lambda = 2.2\ \mu m$ and $\lambda = 10\ \mu m$ respectively. Column 1 gives the relative humidity for each set of values used in the calculations. The values of extinction coefficient were calculated for each model using some specific aerosol number density. In an effort to be independent of number density in the correlation work, the ratio of the extinction coefficient at 2.2 μm to that at 0.5 μm was taken as the given value with the ratio of the coefficient at 10 μm to that at 0.5 μm as the value to be obtained by the correlation equations. With this in mind the ratio $R_2 = \gamma\ (2.2)/\gamma\ (.55)$ is given in column 5 and the ratio $R_{10} = \gamma\ (10)/\gamma(.55)$ is given in column 6.

In Figure 8.1 all values of R_{10} are plotted against the corresponding values of R_2. The plotted values fall into five distinct groups which can be isolated by limiting values of R_2 alone. Thus, values of R_2 of 0.11, 0.16, 0.3 and 1 may be used to separate the five groups.

A simple empirical equation was found for each group to relate the values of R_{10} to R_2. These relationships are given in Table 8.2 and their values plotted as the solid lines in Figure 8.1. The agreement shown here

Table 8.1. Extinction Coefficients at Three Wavelengths and their Ratios for AFGL Aerosol Models. (Units of the Extinction Coefficient are km^{-1}.)

%R.H.	γ (.55)	γ (2.2)	γ (10)	$\frac{\gamma (2.2)}{\gamma (.55)}$	$\frac{\gamma (10)}{\gamma (.55)}$
			RURAL MODEL		
0	0.1461	0.01944	0.01337	0.1331	0.09151
50	0.1514	0.02024	0.01377	0.1337	0.09095
70	0.1632	0.02221	0.01474	0.1361	0.09032
80	0.2245	0.03295	0.01962	0.1468	0.08739
90	0.3409	0.05046	0.02661	0.1480	0.07806
95	0.4271	0.06409	0.03183	0.1501	0.07503
98	0.5990	0.1127	0.05774	0.1881	0.09639
99	0.7828	0.1626	0.08665	0.2078	0.1107
			URBAN MODEL		
0	0.1767	0.03429	0.01732	0.1941	0.09802
50	0.1848	0.03570	0.01812	0.1932	0.09805
70	0.2377	0.04502	0.02285	0.1894	0.09613
80	0.3602	0.06477	0.03134	0.1798	0.08701
90	0.5563	0.09744	0.04434	0.1752	0.07971
95	0.8457	0.	0.06563	0.1780	0.07760
98	1.465	0.2849	0.1245	0.1945	0.08498
99	2.115	0.4562	0.2097	0.2157	0.09915
			MARITIME MODEL		
0	0.07976	0.03354	0.008156	0.4205	0.1023
50	0.08685	0.03821	0.009109	0.4400	0.1049
70	0.1099	0.05523	0.01282	0.5025	0.1167
80	0.2195	0.1505	0.03907	0.6856	0.1780
90	0.3146	0.2272	0.06498	0.7222	0.2065
95	0.4373	0.3471	0.1126	0.7937	0.2575
98	0.6998	0.6137	0.2428	0.8770	0.3470
99	1.035	0.9611	0.4497	0.9286	0.4345
			TROPOSPHERIC MODEL		
0	0.04419	0.001707	0.0007082	0.03863	0.01603
50	0.09580	0.001796	0.0007424	0.03921	0.01621
70	0.04932	0.001995	0.0008148	0.04045	0.01652
80	0.06764	0.003152	0.001165	0.04660	0.01722
90	0.1037	0.005861	0.001794	0.05652	0.01730
95	0.1306	0.008193	0.002251	0.06273	0.01724
98	0.1777	0.01282	0.003056	0.07214	0.01720
99	0.2293	0.01857	0.003955	0.08099	0.01775

Table 8.1. Extinction Coefficients at Three Wavelengths and their Ratios for AFGL Aerosol Models. (Units of the Extinction Coefficient are km^{-1}).

Fog Model	β (.55)	β (2.25)	β (10)	$\frac{\beta (2.25)}{\beta (.55)}$	$\frac{\beta (10)}{\beta (.55)}$
Advec. 1	28.74	30.08	35.25	1.047	1.226
Advec. 2	18.49	19.49	22.84	1.054	1.235
Rad. 1	16.61	18.39	11.31	1.107	0.6809
Rad. 2	8.672	12.07	2.093	1.392	0.2412

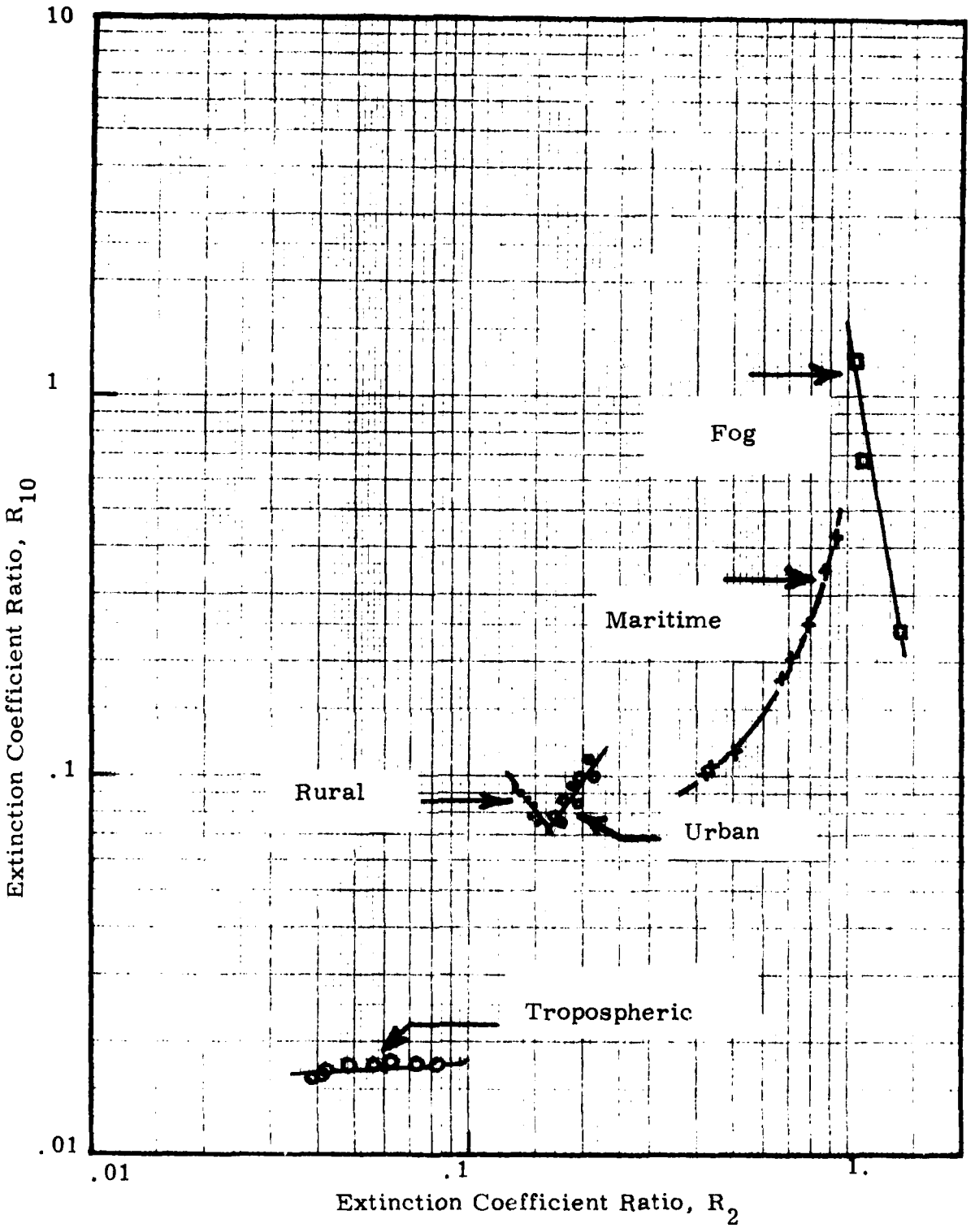

Figure 8.1. Relationships between R_{10} and R_2 for the AFGL Aerosol Models.

Table 8.2. Empirical Relationships Derived from the Shettle-Fenn Atmospheric Aerosol Models. (Note 1)

R_2 Categories	Derived Relation
For: $0 < R_2 < 0.11$	$R_{10} = 0.0217\ R_2^{.0867}$
For: $0.11 < R_2 < 0.16$	$R_{10} = .006\ R_2^{-1.36}$
For: $0.16 < R_2 < 0.3$	$R_{10} = .826\ R_2^{1.325}$
For: $0.3 < R_2 < 1$	$R_{10} = .030\ \exp^{(2.77\ R_2)}$
For: $1 < R_2$	$R_{10} = 1.49\ R_2^{-5.62}$
Also: $\gamma(10) = R_{10}\ \gamma(.55)$	

Note 1: The derivation of five empirical relations for different ranges of R_2 probably assumes a closer relation between the real world and the details of the Shettle-Fenn models than is reasonable. Also, some non-physical discontinuities appear because of the use of five relationships. Perhaps all that is justified is a single smooth curve through all the Shettle-Fenn models for the whole range of R_2. Obviously, much more work is required before issues such as this are settled.

also holds for calculations of γ (10), given γ (.55) and γ (2.2), since γ (10) = (.55) R_{10}.

Inspection of Figure 8.1 shows that the empirical relationship represented in Table 8.2 leads to an adequate correlation for the AFGL model. The good agreement in the figure is only a measure of the ability of the empirical relationship to represent the calculated points.

Deirmendjian (Ref. 11) developed several aerosol models within the range of hazes and fogs covered by Shettle and Fenn. His calculated extinction coefficients γ_D (.55), γ_D (2.2) and γ_D (10) for four of his models are given in Columns 2, 3 and 4 of Table 8.3. Column 5 of the table gives our derived value of γ_{SF} (10), i.e. the extinction coefficient at 10 μm, calculated using Diermendjian's values of γ (.55) and γ (2.2) and the empirical relationships of Table 8.2. Agreement between values in column 4 and 5 is excellent for Model C1; i.e. Deirmendjian's model for a cumulus cloud. This should be expected because Deirmendjian's model C_1 is identical to Shettle and Fenn's radiation fog Model No. 1. The agreement for the three hazes is poor. Deirmendjian's extinction coefficients at 10 μm are one-half to one-fifth those predicted from the HSS empirical relations.

Derimendjian assigned aerosol size distributions to his models which were different from those assigned to the corresponding models of Shettle and Fenn. A comparison of the size distributions is made in Figures 8.2, 8.3, and 8.4. In all cases the size distributions have been scaled so as to produce a value of γ(.55) equal to 0.17 km^{-1}. The Shettle-Fenn models are for 70% relative humidity. (Deirmendjian does not include relative humidity as a variable). The models which are compared follow:

	Model Type	
Figure Number	Deirmendjian	Shettle-Fenn
8.2	Land	Rural RH = 70%
8.3	Maritime	Maritime RH = 70%
8.4	High	Tropospheric RH = 70%

Table 8.3. Test of the Derived Empirical Relations Using Deirmendjian's Calculated Values of Extinction Coefficient. Units of the Extinction Coefficient are km^{-1}.

Atmospheric Model	$\gamma_D(.55)$	$\gamma_D(2.2)$	$\frac{\gamma_D(2.2)}{\gamma_D(.55)}$	$\gamma_D(10)$	$\gamma_{SF}(10)$
Haze M	1.06×10^{-1}	4.21×10^{-2}	3.98×10^{-1}	4.2×10^{-3}	9.5×10^{-3}
Haze L	4.22×10^{-2}	6.4×10^{-3}	1.52×10^{-1}	6×10^{-4}	3.3×10^{-3}
Haze H	1.43×10^{-2}	4.22×10^{-4}	2.95×10^{-2}	10^{-4}	2.28×10^{-4}
Cloud C1	1.52×10^{1}	1.75×10^{1}	1.13	1.12×10^{1}	1.15×10^{1}

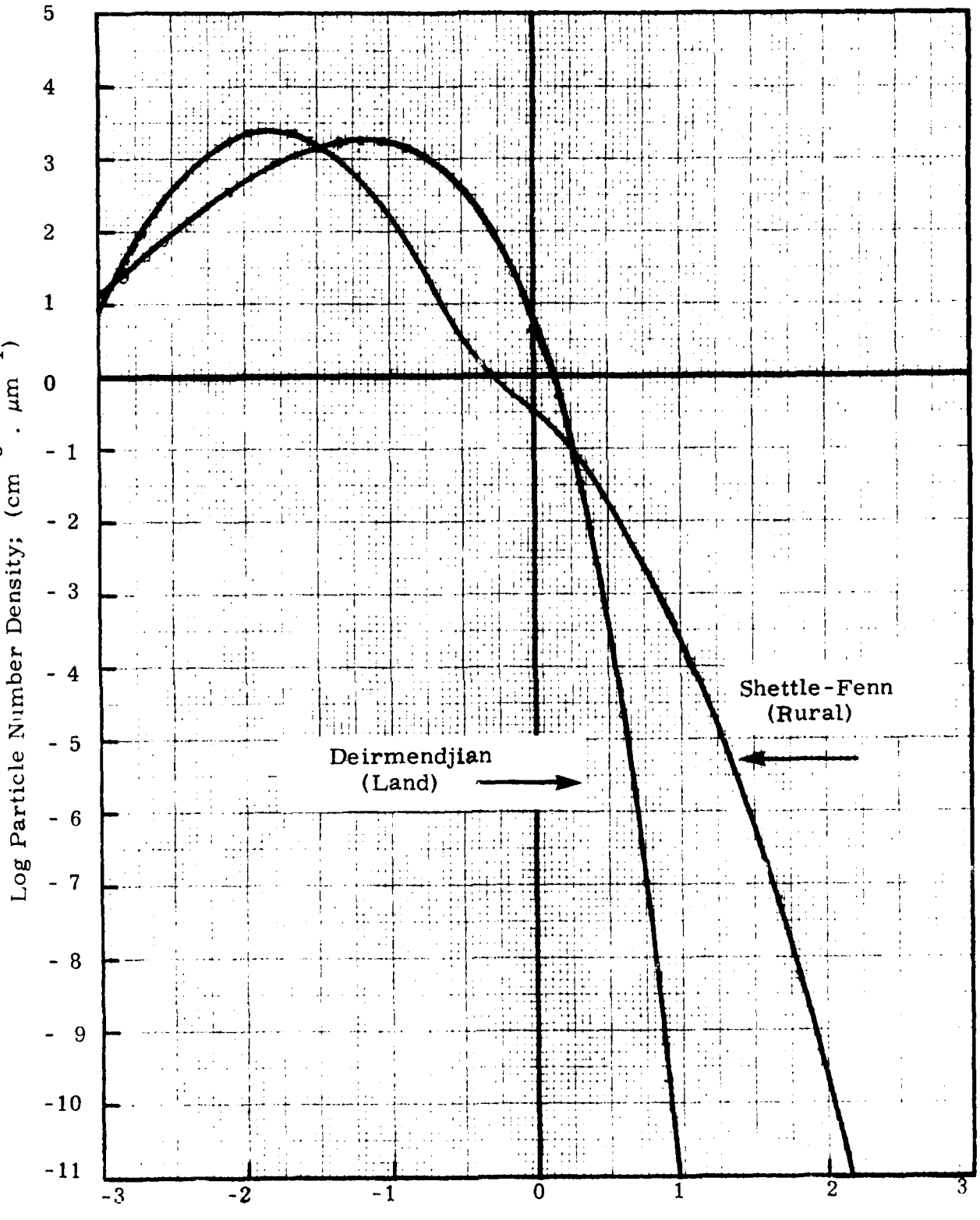

Figure 8.2. Comparison of Aerosol Number Distributions: Deirmendjian Land Model and Shettle-Fenn Rural Model.

AD-A126 676 THE DEVELOPMENT OF A TACTICAL DUAL-WAVELENGTH NEPHELOMETER(U) H S S INC BEDFORD MA D F HANSEN ET AL. 24 NOV 82 HSS-B-093 AFGL-TR-82-0374 F19628-81-C-0008 2/2

UNCLASSIFIED F/G 14/2 NL

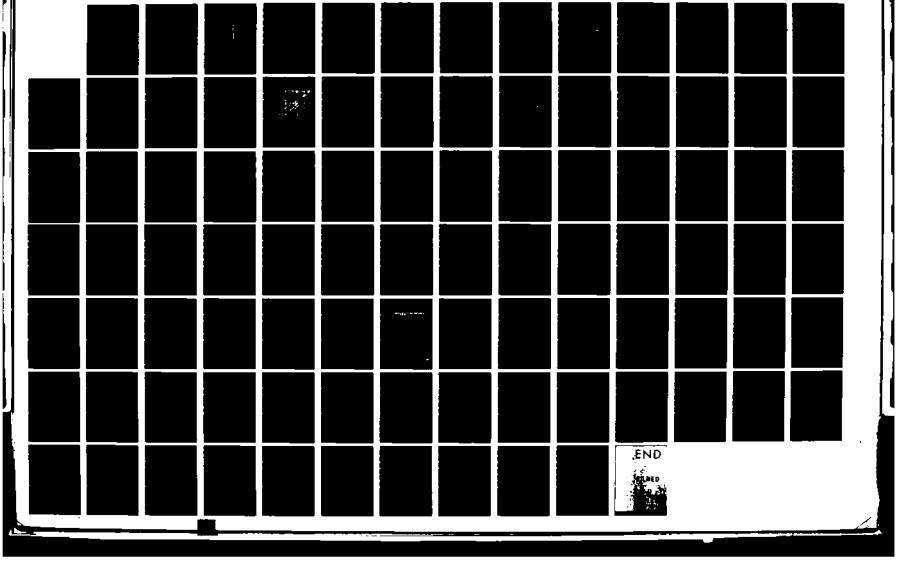

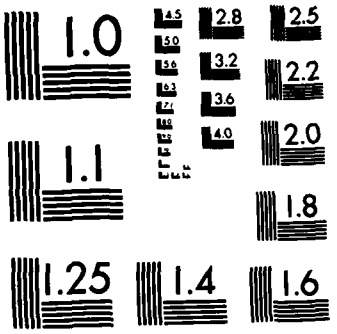

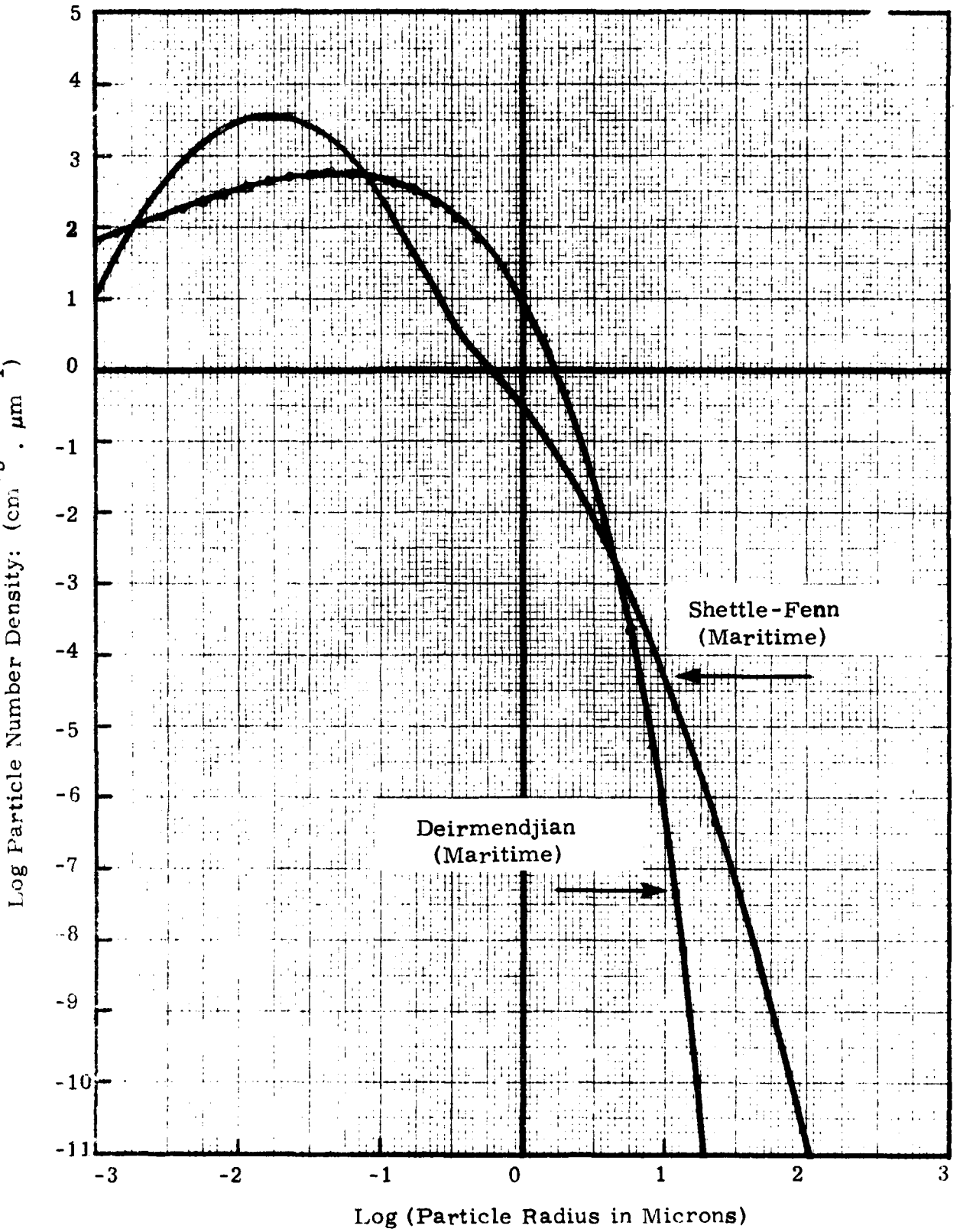

Figure 8.3. Comparison of Aerosol Number Distributions: Deirmendjian Maritime Model and Shettle-Fenn Maritime Model.

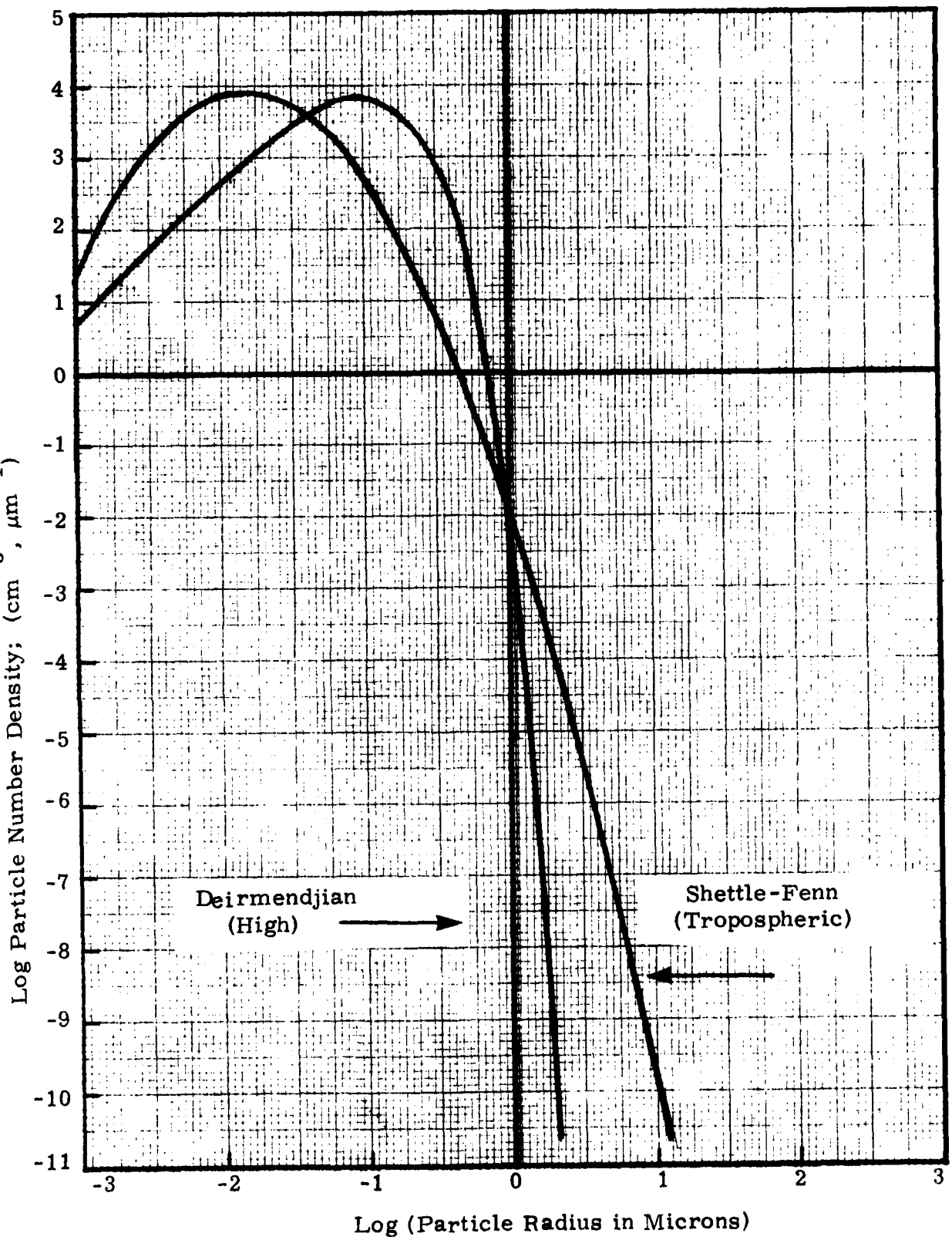

Figure 8.4. Comparison of Aerosol Number Distributions; Deirmendjian High Model and Shettle-Fenn Tropospheric Model.

Inspection of the figures shows that the aerosol size distributions used by Deirmendjian to describe haze models have fewer large particles than the corresponding distributions used by Shettle and Fenn. These account for a large fraction of the differences in extinction coefficients at 10 μm. (Differences in values of refractive index also contribute.)

8.3. Modification of Correlation Relations Using Clay-Lenham Data

Clay and Lenham (Reference 10) measured the atmospheric transmission in several wavelength bands during fogs. Measurements were made at the Field Station of the Royal Military College of Science, Shrivenham, Swidon, Wiltshire, U.K. The transmission path was 17 meters long. The half peak band widths, $\Delta\lambda$, at the wavelengths of interest here were:

λ	$\Delta\lambda$
0.53 μm	0.08 μm
2.2 μm	0.1 μm
10.1 μm	1.9 μm

Measurements were made during 20 fogs occurring in October, November, and December of 1980 and January 1981. Extinction coefficients for selected times during six of these fogs are published in the reference. All of the values published for λ = 0.53, 2.2 and 10.1μ are repeated in Table 8.4. Column 4 presents values of γ (10) labeled $\gamma_{SF}(10)$ calculated using the method described in the previous section and stated in Table 8.2. A comparison of column 3 and column 4 shows reasonable correlation considering the simplicity of the correlation equations. The equations are such that fog is treated as concentrated maritime haze for all conditions involving β (2.2) < β (.5).

Table 8.4. Test of the Correlation Relations Using the Data of Clay and Lenham; All Extinction Coefficients are in km^{-1}.

	γ (.53)	γ (2.2)	γ (10)	$\gamma_{SF}(10)$	$\gamma_{HSS}(10)$
31 October	10.2	4	2.8	0.9	2.18
	10.5	9.7	5.5	4.1	4.48
	21.2	14.2	11.3	4.06	11.2
	30.4	25.2	23.0	9.06	23.0
	27.8	22.7	22.2	8.01	20.5
	25.9	21.9	22.2	8.10	20.3
	21.6	19.5	19.2	7.9	18.9
	16.9	15.4	12.3	6.3	6.9
	10.5	7.4	7.9	2.2	6.04
	5.9	3.4	2.9	.87	2.4
	3.8	2.0	1.3	.49	1.3
10 November	5.5	1.7	.5	.64	.78
	5.1	1.9	0	.43	1.0
	13.8	10.3	1.6	3.3	8.7
	9.7	6.8	0.8	2.1	5.5
	6.5	3.7	0	.9	2.5
	2.8	1.1	.5	.25	.6
11 December	7.2	6.4	2.6	2.5	2.7
	16.7	17.1	6.7	21.7	9.9
	28.4	29.4	17.6	34.8	17.5
	6.9	6.4	2.0	2.7	3.0
	11.2	12.0	6.7	11.3	7.7
	9.2	8.5	2.3	3.5	3.9
	5.0	4.1	1.4	1.4	1.5
	3.2	1.6	1.4	.38	1.0
	3.2	2.4	1.7	.76	.7
	3.5	3.0	2.9	1.12	1.17
	4.4	4.1	3.8	1.7	1.9
	5.3	5.8	5.4	4.8	3.9
	3.8	3.0	1.7	1.01	1.0
24 January	11.5	11.8	3.0	14.8	6.8
	20.5	19.7	5.5	8.8	9.9
	35.4	35.7	21.9	50.3	2.0
	28.5	28.9	25.4	39.3	16.4
	7.2	6.0	3.0	2.1	2.2
	7.2	5.2	2.4	2.0	4.3
	11.5	10.9	7.8	4.8	5.3

Table 8.4 (Continued) Test of the Correlation Relations Using the Data of Clay and Lenham; All Extinction Coefficients are in km^{-1}.

	γ (.53)	γ (2.2)	γ (10)	$\gamma_{SF}(10)$	$\gamma_{HSS}(10)$
24 January	15.8	15.8	10.6	23.5	8.7
	13.1	13.5	10.3	16.4	7.9
	13.1	13.8	10.6	14.5	8.5
	13.5	13.8	9.6	17.8	8.0
	3.8	3.2	1.8	1.17	1.2
	14.2	16.5	12.8	4.2	12.6
	12.7	14.5	12.4	8.98	10.7
	18.3	20.5	8.5	14.4	14.5
	18.8	19.7	13.5	21.5	12.0
	13.1	14.8	9.2	9.8	10.6
	5.5	5.4	2.7	2.5	2.8
27/28 January	3.4	2.4	1.2	.72	.61
	5.1	5.5	2.7	5.0	3.6
	7.8	8.8	4.6	5.9	6.3
	11.0	12.5	9.6	8.0	9.1
	12.9	14.5	10.7	10.0	10.3
	11.8	13 2	12.1	9.36	9.3
	16.1	17.7	14.7	14.1	12
	14.1	16.3	13.2	9.3	12.3
	13.7	16.3	13.6	7.7	13.6
	11.0	12.2	11.0	9.2	8.4
	7.8	8.1	5.6	9.4	4.8
	4.4	4.3	1.8	2.0	2.2
29/30 January	17.3	13.8	4.2	4.7	12.3
	16.5	14.8	7.8	5.9	6.4
	25.2	24.7	20.6	11.4	13.0
	38.9	38.1	33.2	17.6	39
	64.5	65.1	64.0	91.2	68.1
	50.0	51.0	57.3	66.7	54
	29.6	31.9	36.4	29	20.7
	17.3	19.0	21.0	15.2	12.8

The Clay-Lenham measurements were used to improve the correlation relations for fog environments. The correlation relations for other environments as shown in Table 8.2 were not modified. The approach taken to modify the relationship for fog is outlined here.

The improved fog correlation relation is based on two assumptions: (1) haze exists when $\beta(.5) < 2\ km^{-1}$ and fog exists when $\beta(.5) > 2\ km^{-1}$, and (2) the extinction coefficients published by Clay and Lenham can be used to develop the correlation equations appropriate to fog. Some of the correlation equations which were studied included an accommodation for the modeled transmission values for fog published by Shettle and Fenn. The latter effort is not discussed.

A linear plot was made of the values of R_{10} taken from Table 8.4 against the corresponding values of R_2. These values are shown in Figure 8.5. The line A-A divides what appears to be one group of points from the other. The intent is to establish two equations for R_{10} given R_2, under the assumption that nature divides fog into two classes, therefore, two correlation relations are required to treat the two classes of fogs.

In an effort to find a way to separate those points on one side of the line A-A in Figure 8.5 from those on the other, the values R_2 involved were plotted against the corresponding values of $\gamma(.53)$ on a log-log plot. This is shown in Figure 8.6. The line D-D was drawn to separate points corresponding to those to the left of A-A in Figure 8.5 from those to the right of A-A. This approach was reasonably successful. Points below D-D in Figure 8.6 correspond to points to the left of A-A in Figure 8.5. Thus, values of $\gamma(.53)$ and $R_2 = \gamma(2.2)/\gamma(.53)$ can be used to select the best function for relating R_{10} to R_2. In Figure 8.6 the line D-D is given by

$$\log R_2 = -0.24 + 1.5 \log \gamma(.53) \qquad (8.1)$$

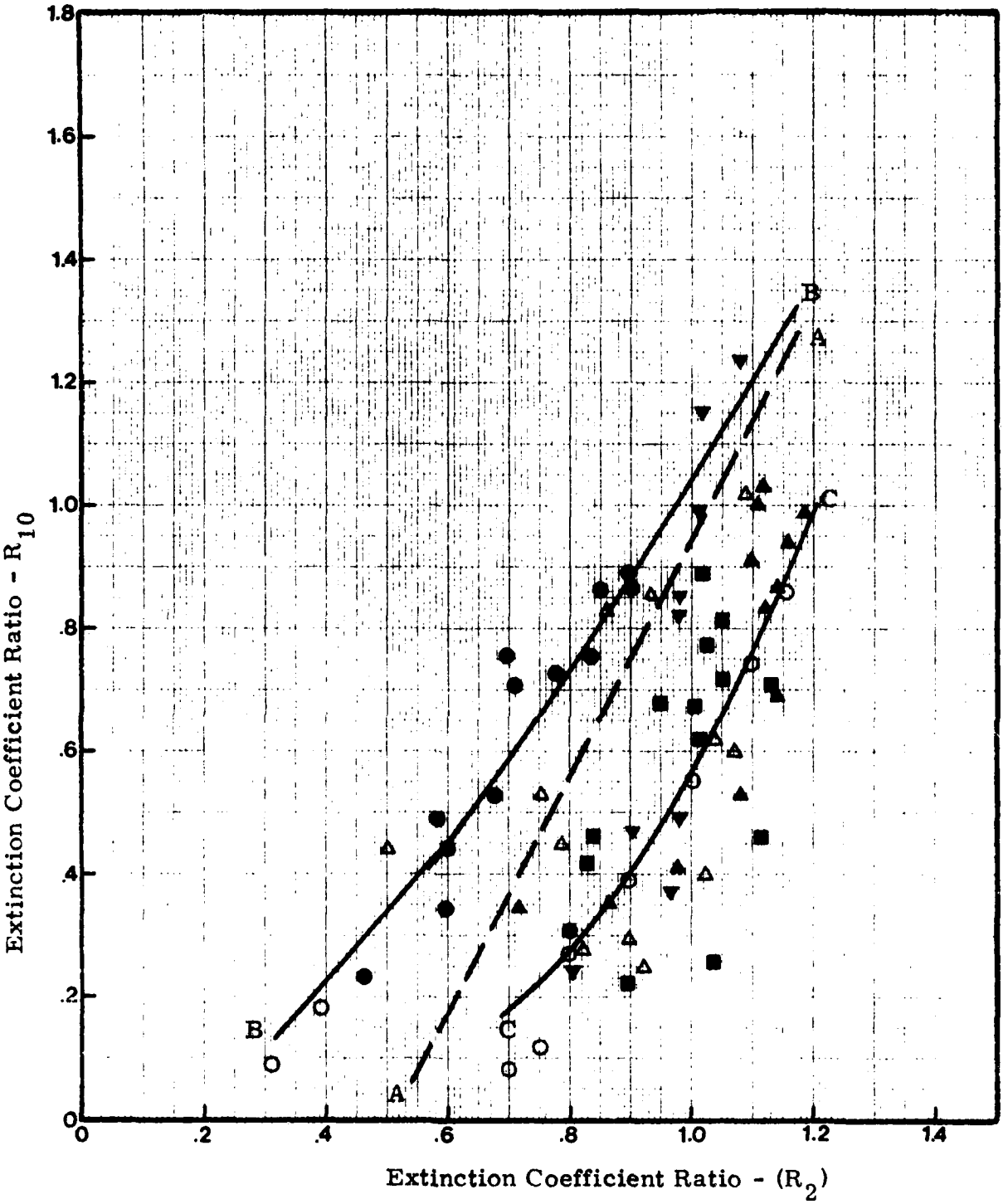

Figure 8.5. Relationships between R_{10} and R_2 for the Clay-Lenham measurements of fog extinction coefficients. (The different symbols represent separate environmental episodes).

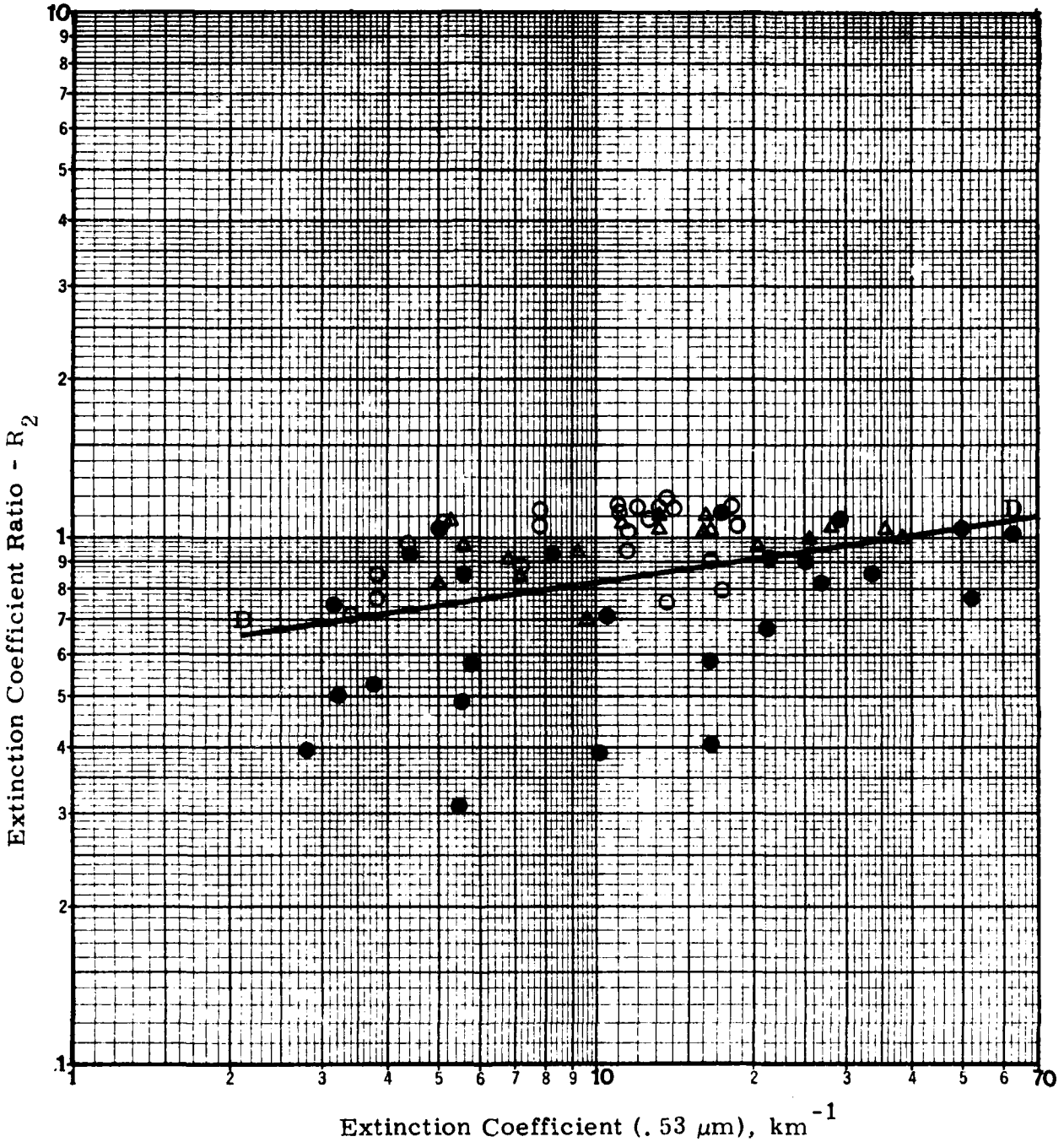

Figure 8. 6. Relationship between R_2 and γ (. 53 μm) for Clay and Lenham fog data. (Each type of symbol represents a separate fog episode).

The two groups of points determine two "best fit" curves. These were determined to be:

when: $\log R_2 > -0.24 + 1.5 \log \gamma(.53)$

then; $R_{10} = 0.55\, R_2^{3.21}$ (8.2)

and when; $\log R_2 < -0.24 + 1.5 \log \gamma(.53)$

then; $R_{10} = 1.04\, R_2^{1.69}$ (8.3)

Table 8.5 provides the complete set of correlation relations to be used to obtain $\gamma(10)$ including the Equations 8.2 and 8.3 to be used for fogs. New values of the 10 μm extinction coefficient were calculated using Equations 8.2 and 8.3. These values are shown in column 5 of Table 8.4. In general, the correlation seems better than that determined using our fit to the Shettle-Fenn Fog Model.

The improvement which results from the use of the modified correlation relation is illustrated in Figures 8.7 and 8.8. In Figure 8.7 the unmodified predicted values of $\gamma_{SF}(10)$ are plotted against the Clay-Lenham measured values. In Figure 8.8 the modified predicted values of $\gamma_{HSS}(10)$ are plotted against the Clay-Lenham data.

8.4 Tests of Empirical Correlation Equations Using CALSPAN Data

Haze and fog extinction coefficient measurements were made during the time period 3 May 1982 to 7 May 1982 in the CALSPAN environmental test chamber. Many concentrations of haze and fog were generated in the chamber. Extinction coefficient and other measurements made by CALSPAN include: (1) optical transmission through the test chamber for the visible spectral region and at narrow wavelength intervals centering on 2.2 μm and 10μm, (2) the scattering coefficient in the visible region measured by an integrating nephelometer, (3) the aerosol size distirubtion and (4) the relative humidity. Simultaneously HSS Inc recorded the voltage outputs

Table 8.5. Complete Set of Empirical Correlations Derived from the Shettle-Fenn Aerosol Models Including Improved Relations Based on the Clay-Lenham Measurements.

R_2 Categories	Relation
For $0 < R_2 < 0.11$	$R_{10} = 0.0217\ R_2^{0.0867}$
For $0.11 < R_2 < 0.16$	$R_{10} = 0.006\ R_2^{-1.36}$
For $0.16 < R_2 < 0.3$	$R_{10} = 0.826\ R_2^{1.325}$
For $0.3 < R_2$ and $\gamma(.5) < 2$	$R_{10} = 0.030 \exp^{2.77 R_2}$
For $0.3 < R_2$ and $\gamma(.5) > 2$	
Case a: $\log R_2 > -0.24 + 1.5 \log \gamma(.5)$	$R_{10} = 0.55\ R_2^{3.21}$
Case b: $\log R_2 < -0.24 + 1.5 \log \gamma(.5)$	$R_{10} = 1.04\ R_2^{1.69}$
Also: $\gamma(10) = \gamma(.5)\ R_{10}$	

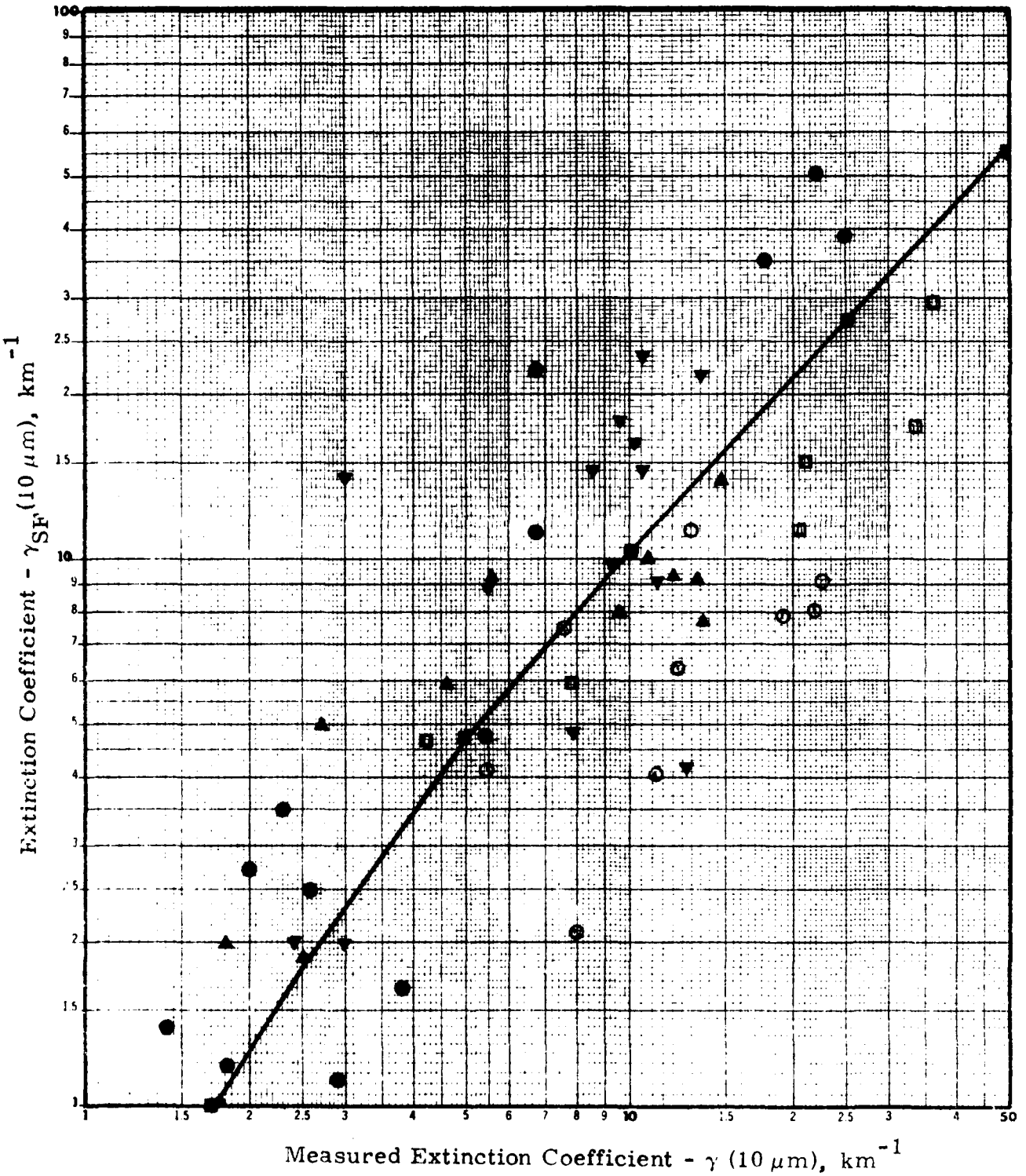

Figure 8.7. Comparison of calculated extinction coefficients vs measured (Clay-Lenham) 10 μm extinction coefficients.

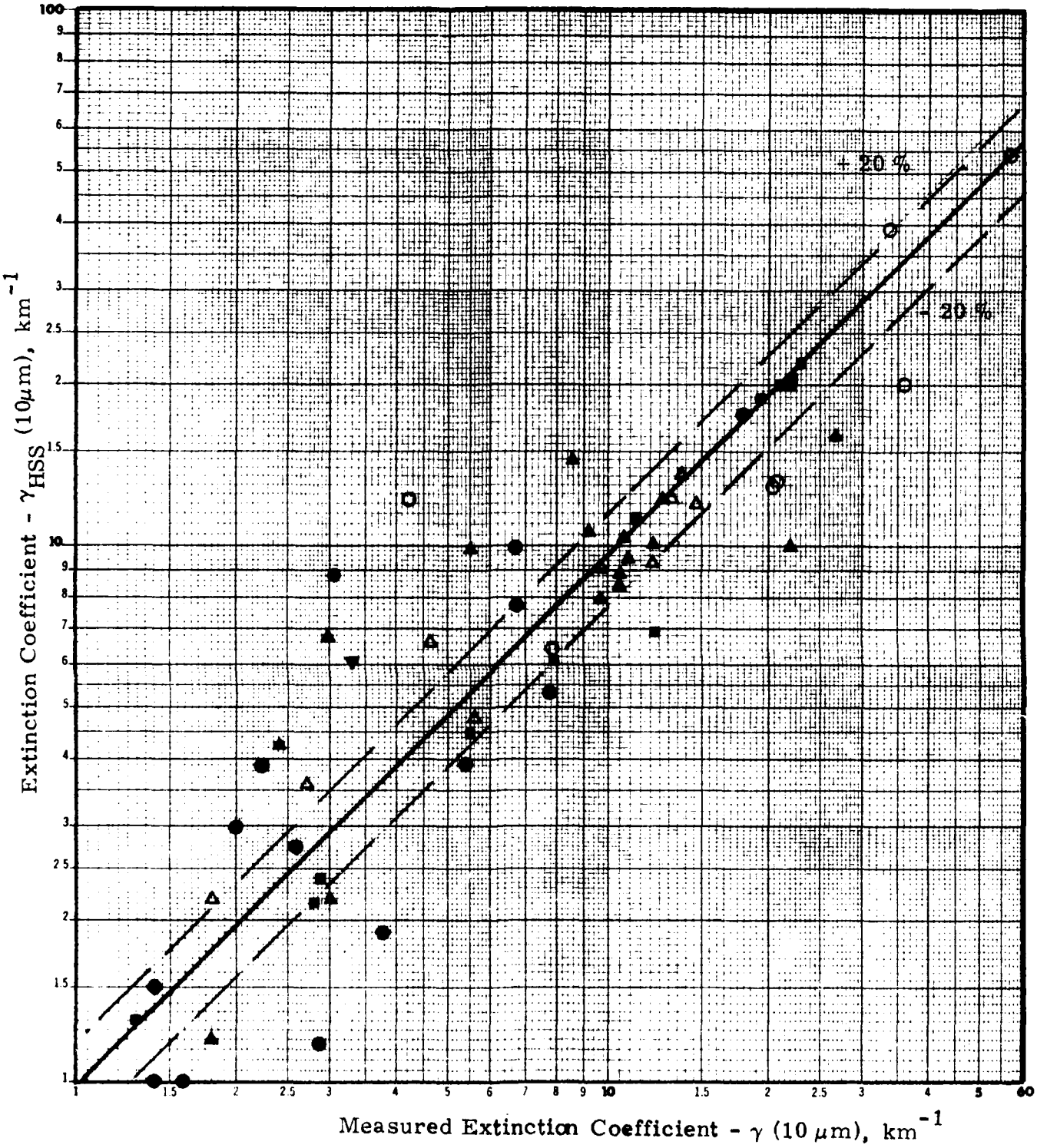

Figure 8.8. Comparison of predicted 10 μm extinction coefficients (from improved relations) vs measured (Clay-Lenham) 10 μm extinction coefficients.

of the SWIR Nephelometer, which measured the scattering coefficient in narrow wavelength intervals centering on 0.5 μm and 2.5 μm.

The tests at CALSPAN were numbered Episodes 1 through 14. The CALSPAN IR transmissometer was restricted to making measurements at two wavelengths using narrow band interference filters for wavelength isolation. Measurements were made alternately at each wavelength by manually moving the filter wheel. Many times during the tests no transmission results at $\lambda = 10\ \mu$m were recorded because of the short baseline of the IR transmissometer. Table 8.6 presents all of the transmission data available at times when results were obtained at $\lambda = 10\ \mu$m. CALSPAN did the primary data reduction and provided the resulting values in a report to HSS Inc. The data used here were extracted from the CALSPAN Final Report (Appendix B). Note that the reduced data are given as extinction coefficients in the units km^{-1}.

Table 8.6 gives the number and type of episode in column 1. Values of γ (.5), γ (2.2) and γ (10) as reported by CALSPAN are given in columns 2, 3 and 4. In column 5 values of $\gamma_{HSS}(10)$ calculated using the correlation equations of Table 8.5 are given. The predicted values of extinction coefficient $\gamma_{HSS}(10)$ have a fair correlation with the measured values γ (10).

The fog and haze episodes generated by CALSPAN have very high extinction coefficients. In fact, the only infrared measurements for haze episodes were obtained when the extinction coefficients were extremely abnormal and unlike those of any natural environment.

At this point in the analysis the assumption was made that if the concentration of particles producing the CALSPAN fogs and hazes were reduced then the ratio R_2 would remain unchanged. Given that assumption the values of γ (0.5) and (2.2) were reduced by a factor of ten.

Table 8.6 CALSPAN Data Used to Test Empirical Correlation Relations in Table 8.5; All values of Extinction Coefficient are in Units of km^{-1}.

Episode	γ (.5)	γ (2.2)	γ (10)	$\gamma_{HSS}(10)$	$\gamma_{HSS}(10)$ (1/10 Dilution) X10	$\gamma_{HSS}(10)$ (1/100 Dilu) X100
3 Fog	64	50.5	23	44.6	16.5	17
	27	22	(7)	20	7.7	7.7
4 Fog	40	33	(11)	30	11.9	11.7
	18	10	(5)	7	2.5	2.5
5 Fog	52	23	(6)	13.6	13.6	5.3
	24	4	(2)	1.85	1.85	1.85
6 Salt	80	5.03	(.33)	1.37	1.37	1.37
Haze	153	9.01	(.73)	2.6	2.6	2.6
	267	15.1	(1.26)	4.5	4.5	4.5
7 Fog	53	62	42	48	48	40.5
	15	23	16	--	31.4	31.4
8 Fog	44	40	23	39	17.8	16.3
	28	25	15	24	10.7	9.9
	5	(8)	(6)	--	12.6	12.6
9 Fog	73	66	26	64	29	26.7
	57	53.5	23	53	25.6	23
10 Haze	126	3.37	(.9)	2	2	2
(Salt)	246	8.42	(2.15)	4	4	4
	469	25.3	(4.22)	7.9	7.9	7.9
	569	34.4	5.42	9.68	9.68	9.68
	366	22.5	(1.71)	6.23	6.23	6.23
11 Fog	92	82	29	79	35	32.5
	83	75	28	73	33	30.3
12 Fog	107	96	28	93	41.5	38

Table 8.6 (Continued) CALSPAN Data Used to Test Empirical Correlation Relations of Table 8.5; All values of Extinction Coefficients are in Units of km^{-1}.

Episode	γ (.5)	γ (2.2)	γ (10)	$\gamma_{HSS}(10)$	$\gamma_{HSS}(10)$ X10	$\gamma_{HSS}(10)$ X100
13 Haze (Salt)	30	(1.65)	(.12)	.51	.51	.51
	61	(2.96)	(.23)	1.0	1.0	1.0
	108	5.4	(.23)	1.8	1.8	1.8
	193	8.5	(.29)	3.1	3.1	3.1
	367	23	(.47)	6.25	6.25	6.25
	448	31.5	(.82)	7.7	7.7	7.7
	172	(13.3)	(.53)	3	3	3
	(70)	(7.4)	.41	1.25	1.25	1.25
14 Haze White Phos.	62	(.46)	(.44)	.88	.88	.88
	156	(2.05)	(1.38)	2.32	2.32	2.34
	265	7.12	8.6	4.2	4.2	4.2
	525	17.5	30.8	8.5	8.5	8.5
	774	30.8	60.0	12.7	12.7	12.7
	487	20.7	31.1	8.0	8.0	8.0
	189	(7.5)	(3.5)	3.1	3.1	3.1
	76	(0.92)	0.8)	1.1	1.1	1.1

(1) Values given in parenthesis have probable errors equal to or greater than $\pm$ 20 percent.

The predicted values of $\gamma_{HSS}(10)$ were then recalculated for the diluted extinction coefficients and for comparison purposes the resultant value of $\gamma_{HSS}(10)$ was multiplied by 10. The results are given in column 6 of Table 8.6. The process was repeated again using a dilution factor of 100. Those results are given in column 7 of the same table.

A comparison of values given in columns 4 with those in columns 6 and 7 shows a better agreement for the fog episodes than do the values of column 5. In the case of hazes the $\gamma_{HSS}(10)$ extinction coefficients for hazes are essentially unchanged by the dilution and normalization process with only fair to poor correlation. On the basis of the results shown in Table 8.6 it appears that application of the correlation equations to the CALSPAN measurements gives encouraging results for light fogs but not for hazes of the types generated by CALSPAN.

In Figure 8.9 the predicted values of extinction coefficient at 10 μm, $\gamma_{HSS}(10)$, for (1/100 concentration of aerosols) x 100 are plotted against measured values. The predicted fog values agree quite well with the measured values, and are well-behaved in that they fall along a straight line with shape 0.5 on a log-log plot.

The high humidity hazes of episodes 6, 10 and 13 were generated by burning Salty Dog pyrotechnic material. These points are distributed about a line with shape 0.66 on the log-log plot. The haze of Episode 14 was generated by burning white phosphorous in a low humidity environment which provided little or no aerosol growth. Of all the haze episodes Episode 14 is most unlike any natural environment.

Relative size distributions of the aerosols were measured routinely by CALSPAN during the haze runs employing a TSI Model 3030 Electrostatic Aerosol Analyzer (0.01 to 1.0 μm diameter) and a Royco Model 225 Aerosol Particle Counter (0.56 to 10 μm diameter). These data are presented in Table 2 of Appendix B. The total aerosol

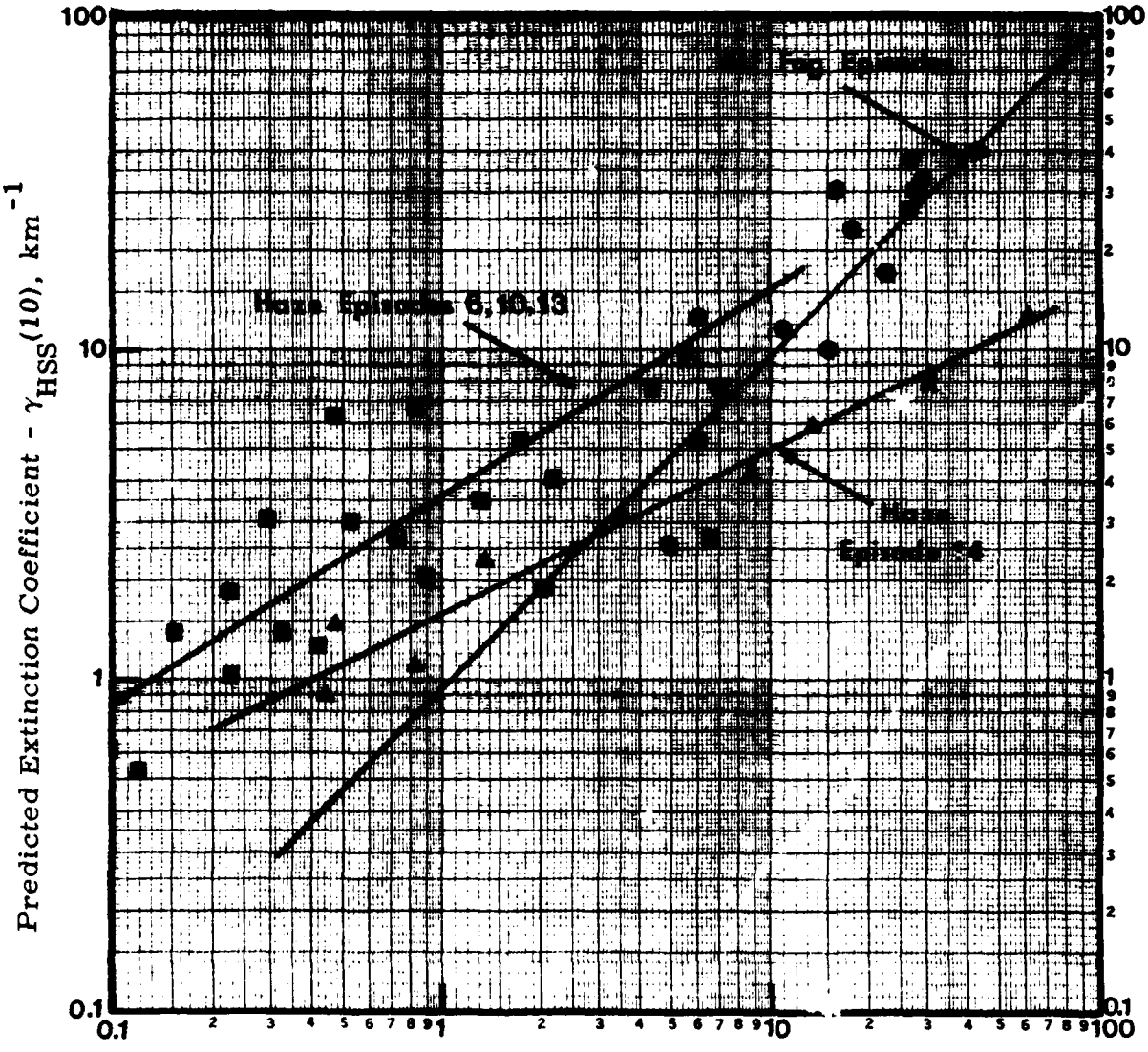

Figure 8.9. Comparison of predicted and measured extinction coefficients at 10 μm for the CALSPAN test data.

concentration, measured by a Gardner Small Particle Detector, was used to determine the absolute size distribution in hazes.

A CALSPAN Droplet Sampler was used to obtain measurements of fog droplet size spectra. Reduction of data taken by this instrument is labor-intensive and therefore expensive. HSS Inc and AFGL contracted with CALSPAN for the reduction of 12 fog droplet size spectra spread over seven fog episodes. These size distributions are given in Table 3 of Appendix B and Figure 1 of Appendix B.

The fog droplet size distributions were used by M. Shuler to calculate the fog extinction coefficient using Eric Shettle's AFGL program "MIE 3, Mie Scattering Analysis". This program calculates the extinction coefficients at any designated wavelength given the aerosol size distribution and the refractive index of the aerosol particles. For the calculations discussed here the refractive index was taken to be that of water.

Extinction coefficients were calculated for wavelengths of 0.55 μm, 2.2 μm and 10 μm. The results are given in Table 8.7. The times shown in column 3 are specific to the times at which the particle size distribution measurements were made by CALSPAN. (In some cases it was necessary to extrapolate the values of extinction coefficients which were measured at slightly different times to the times shown.)

The agreement between the computed and the measured values of extinction coefficient at 0.55 μm is impressive. This is illustrated in Figure 8.10(a) where the computed values are plotted against the measured values. Note that the "best fit" straight line does not pass through the origin. Figure 8.10 (b) presents the same type of plot for the values at 2.2 μm.

Figure 8.11 (a) presents a similar comparison for the 10 μm wavelength. The agreement between computed and measured values is fair at wavelength 2.2 μm, but at 10 μm the agreement is poor.

Table 8.7. Comparison of Computed Extinction Coefficients to the Measured Extinction Coefficients.

Date	Episode	Time	Extinction Coefficient, km^{-1}					
			Computed			Measured		
			λ 0.55	2.2	10 μ	λ 0.55	2.2	10
May 4	4	1457	43.9	54.5	14.6	33	25	8
May 4	5	1559	52.2	59.0	30.7	52	22.5	(6)
May 5	7	1007	48.4	51.7	25.6	53	62	42
5	7	1013	23.7	25.2	10.4	15	23	16
May 5	8	1111	48.6	63.9	11.2	44	39	23
	8	1116	31.1	34.1	10.3	28	25	(15)
May 5	9	1242	78.5	98.0	23.6	73	66	26
	9	1247	79.1	91.0	34.4	57	53	23
May 6	11	1048	97.5	108.6	49.8	92	82	29
	11	1053	82.8	94.8	41.9	83	75	28

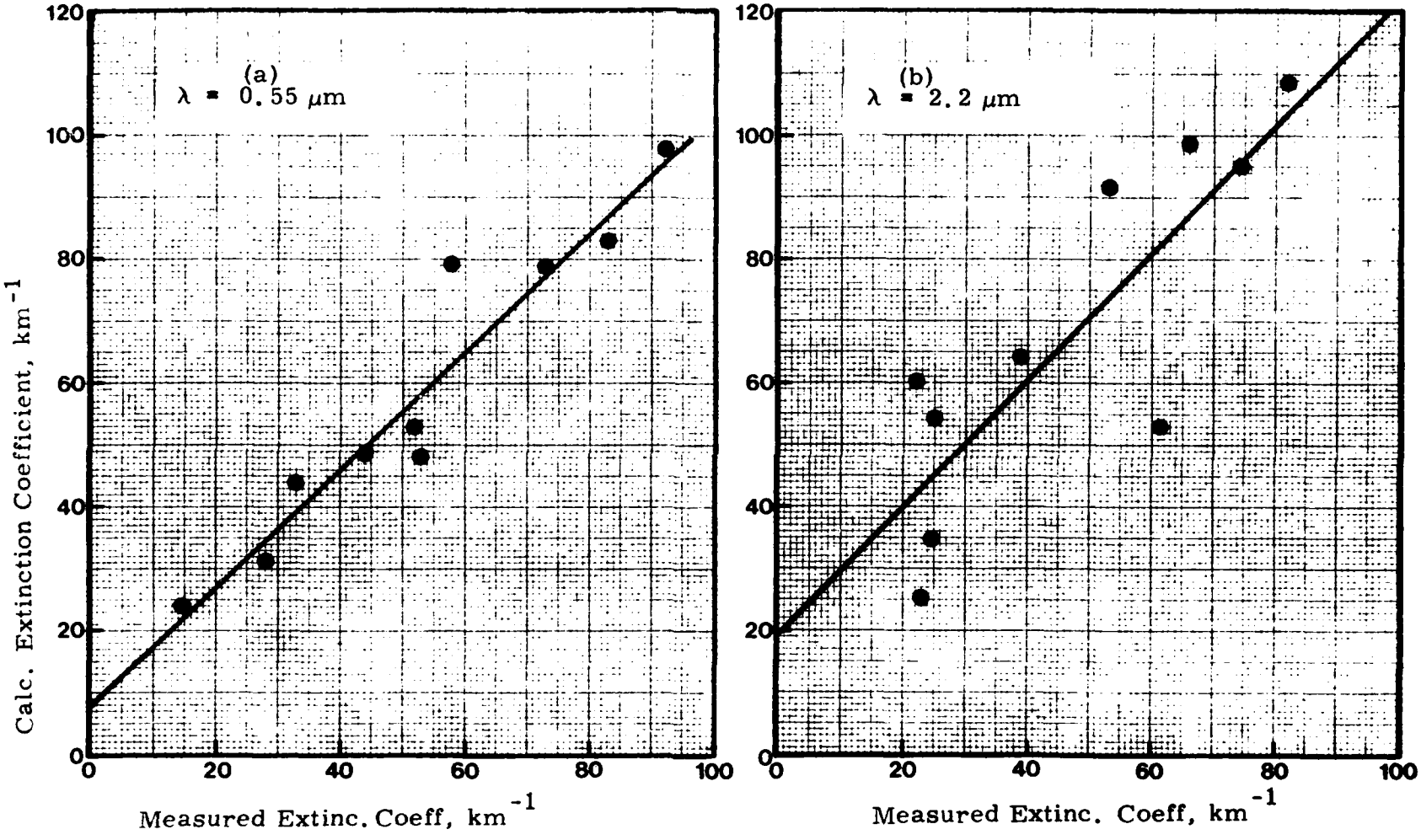

Figure 8.10. Comparison of calculated and measured values of extinction coefficients: (a) for λ = 0.55 μm, (b) for λ = 2.2 μm.

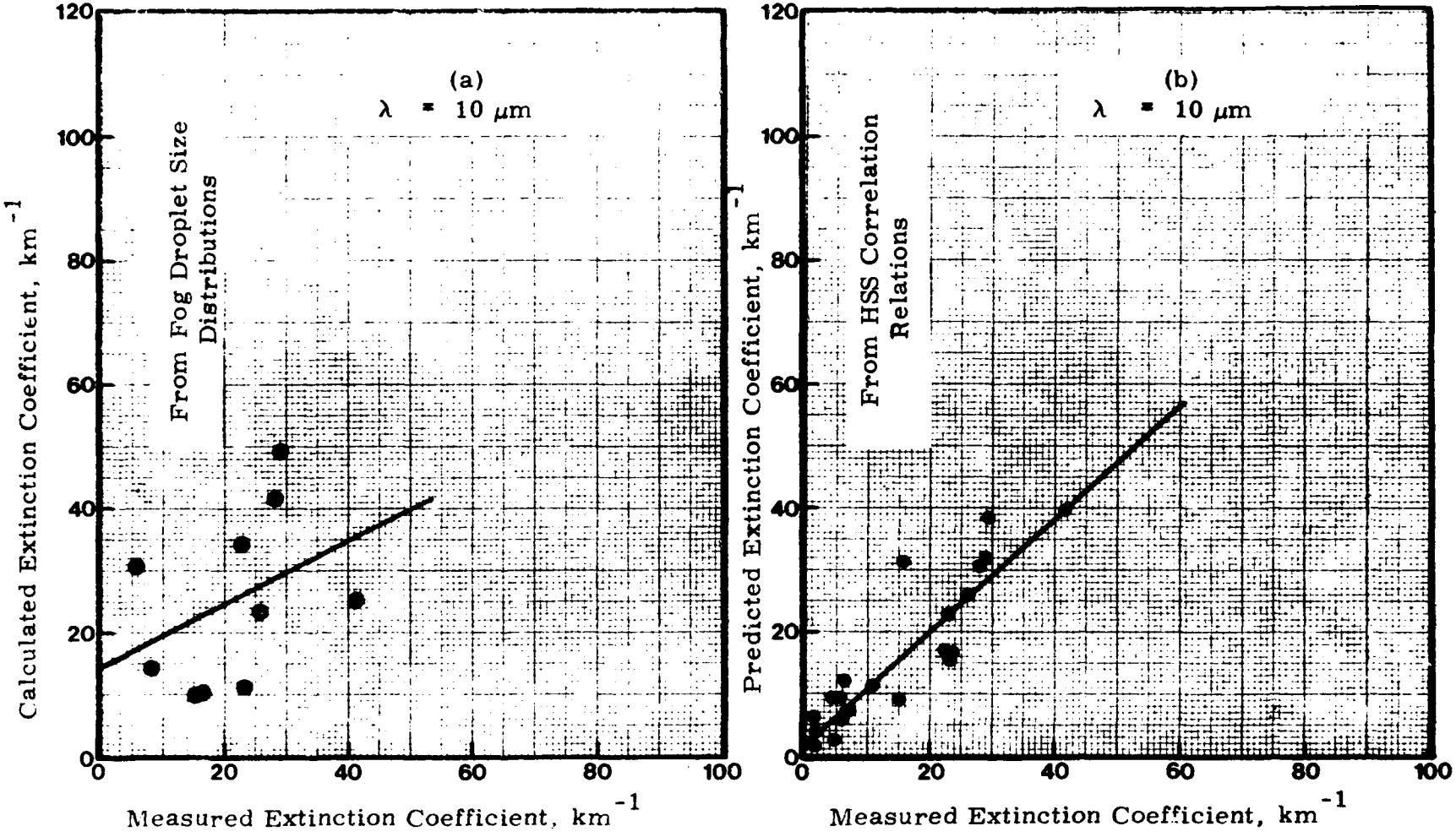

Figure 8.11. (a) Comparison of calculated and measured values of extinction coefficient at 10 μm; (b) Comparison of predicted and measured values of extinction coefficient at 10 μm.

Figure 8.11 (b) presents a plot of the extinction coefficients predicted by the HSS correlation relations given in Table 8.5. For the very limited number of test cases represented by the CALSPAN data better values of extinction coefficient at 10 μm are obtained from predictions using the correlation relations than from calculations using the actual aerosol size distributions.

8.5 Relationship Between Nephelometer Measurements and Aerosol Extinction Coefficients

Two properties of aerosols, the albedo and the phase function, along with the total scattering coefficient influence the measurement characteristics of a forward scatter nephelometer such as the SWIRN. In the following sections we examine the wavelength dependence of these properties. The wavelength dependence of the albedo and scattering phase function of aerosol particles has a bearing on the ability to predict the aerosol scattering coefficient at 10 μm from the SWIRN measurements at 0.55 μm and 2.5 μm. The purpose in discussing these properties is to understand how they might influence the derivation of more accurate correlation relations--not to attempt any further improvement in the empirical correlation relations given in Table 8.5 until such time as a data base of measurements in real atmospheric environments is available.

8.5.1 Aerosol Albedo

The preceding attempts to derive empirical correlation relations capable of predicting the 10 μm atmospheric aerosol extinction from measurements at 0.55 μm and 2.2 μm are based on measurements of the aerosol extinction coefficient at those two wavelengths and not on the aerosol scattering coefficient. The SWIR Nephelometer, however, measures the atmospheric scattering coefficient. It responds to light scattered from the sample volume in a narrow range of angles centered on 55°. The response of the SWIRN is thus proportional to the total

scattering coefficient and the albedo and phase function of the scattering aerosols.

At a particular wavelength, λ, the extinction coefficient of an air sample, (γ), is considered to be made up of the sum of the molecular absorption coefficient, $k_m(\lambda)$, the molecular scattering coefficient, $\sigma_m(\lambda)$, the aerosol absorption coefficient, $k_a(\lambda)$ and the aerosol scattering coefficient $\sigma_a(\lambda)$. That is:

$$\gamma(\lambda) = k_m(\lambda) + \sigma_m(\lambda) + k_a(\lambda) + \sigma_a(\lambda) \qquad (8.4)$$

The visible channel of SWIRN is outside of any molecular atmospheric absorption bands. The IR channel is on the edge of an H_2C absorption band; but because the pathlength of the IR radiation in air is so short, the molecular absorption can be neglected. The sensitivity of the SWIRN is such that $k_m(\lambda)$, the molecular absorption coefficient, can be treated as equal to zero in the two wavelength bands of interest. This is also true of molecular scattering. That is: $\sigma_m(\lambda)$ may also be treated as equal to zero in the two bands of interest. Thus, for the SWIRN, the following approximation is acceptable

$$\gamma(\lambda) = k_a(\lambda) + \sigma_a(\lambda) \qquad (8.5)$$

The albedo for single scattering, A, is defined as

$$A(\lambda) = \frac{\sigma(\lambda)}{\gamma(\lambda)}$$

$$\text{or } \sigma_a(\gamma) = A(\lambda)\,\gamma(\lambda) \qquad (8.6)$$

When scattering coefficients are measured, as with the SWIRN, extinction coefficients can be calculated if the albedo for single scattering is known. Values of the albedo at 0.55 μm and 2.2 μm have been published

by Shettle and Fenn (Reference 4) for their rural, urban, maritime and tropospheric haze aerosol models at eight values of relative humidity and also for their four fog models. The albedo values for the hazes are plotted as a function of relative humidity in Figure 8.12. The albedo values for fog are given in Table 8.8. If the relative humidity and the haze or fog type are known albedo values can be determined. There is almost a one-to-one relationship between $R_2 = \gamma(2.2)/\gamma(.53)$ and the appropriate albedo values. This is shown in Figure 8.13. Here the ratio of the albedo at 2.25 μm to that value at 0.55 μm is plotted against the ratio R_2, i.e. the extinction coefficient at 2.2 μm to that at 0.55 μm. These points make up the upper set of curves. The lower set are the ratios of albedos at 10 μm to those at 0.55 μm and also plotted against the ratio R_2. The lower set of curves is presented to indicate some of the problems which might arise in 10 μm nephelometry. The upper set of curves relates to the use of the SWIRN. There can be ambiguity in the value of A(2.2)/A(.55) for values of R_2 between $R_2 = 0.17$ and $R_2 = 0.21$ because both the rural and the urban models can have values of R_2 in this range.

8.5.2 Aerosol Scattering Phase Function

The probability that radiation of wavelength λ which is scattered by an aerosol will be deviated through an angle θ is symbolized by $\Phi(\theta, \lambda)$ which is called the phase function. It is normalized so that

$$2\pi \int_0^{\pi} \Phi(\theta, \lambda) \sin\theta \, d\theta = 1. \qquad (8.7)$$

The units of $\Phi(\theta, \lambda)$ are sr^{-1}.

A fixed angle nephelometer measures a fraction of the amount of light scattered through some range of angles θ_1, to θ_2. The efficiency of measurement, $E(\theta)$ depends on the design of the fixed angle nephelometer. The scattered light measured by the nephelometer, Z, is proportional to

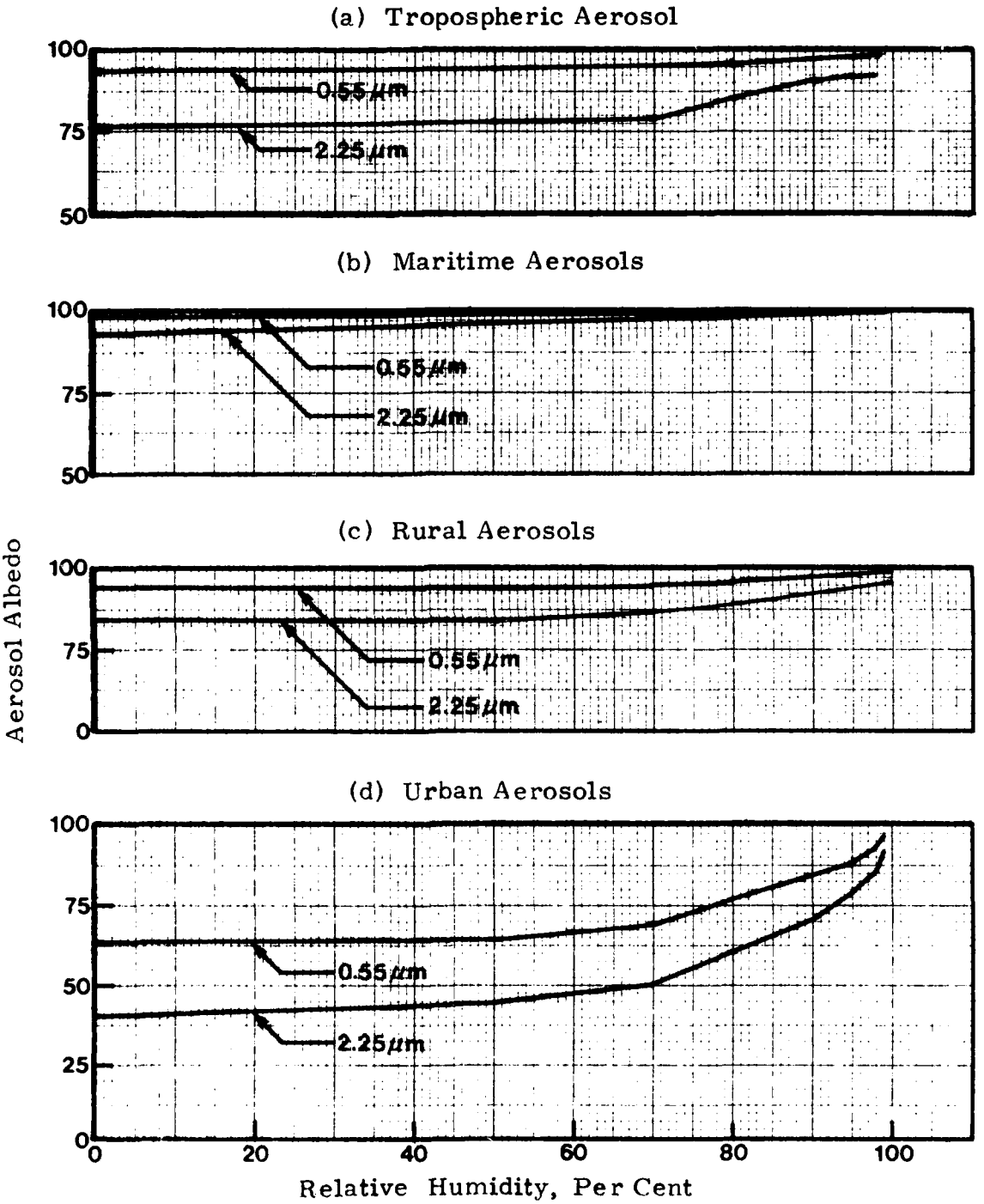

Figure 8.12. Aerosol Albedo for single particle scattering used in Shettle-Fenn Aerosol Models.

Table 8.8. Albedo Values for Fog Droplets Used in the Shettle-Fenn Aerosol Models.

Shettle-Fenn Fog Model	Aerosol Albedo Value For Wavelength		
	0.55 μm	2.25 μm	10 μm
Advective No. 1	1	0.9628	0.6153
Advective No. 2	1	0.9695	0.6482
Radiation No. 1	1	0.9881	0.6477
Radiation No. 2	1	0.9956	0.4893

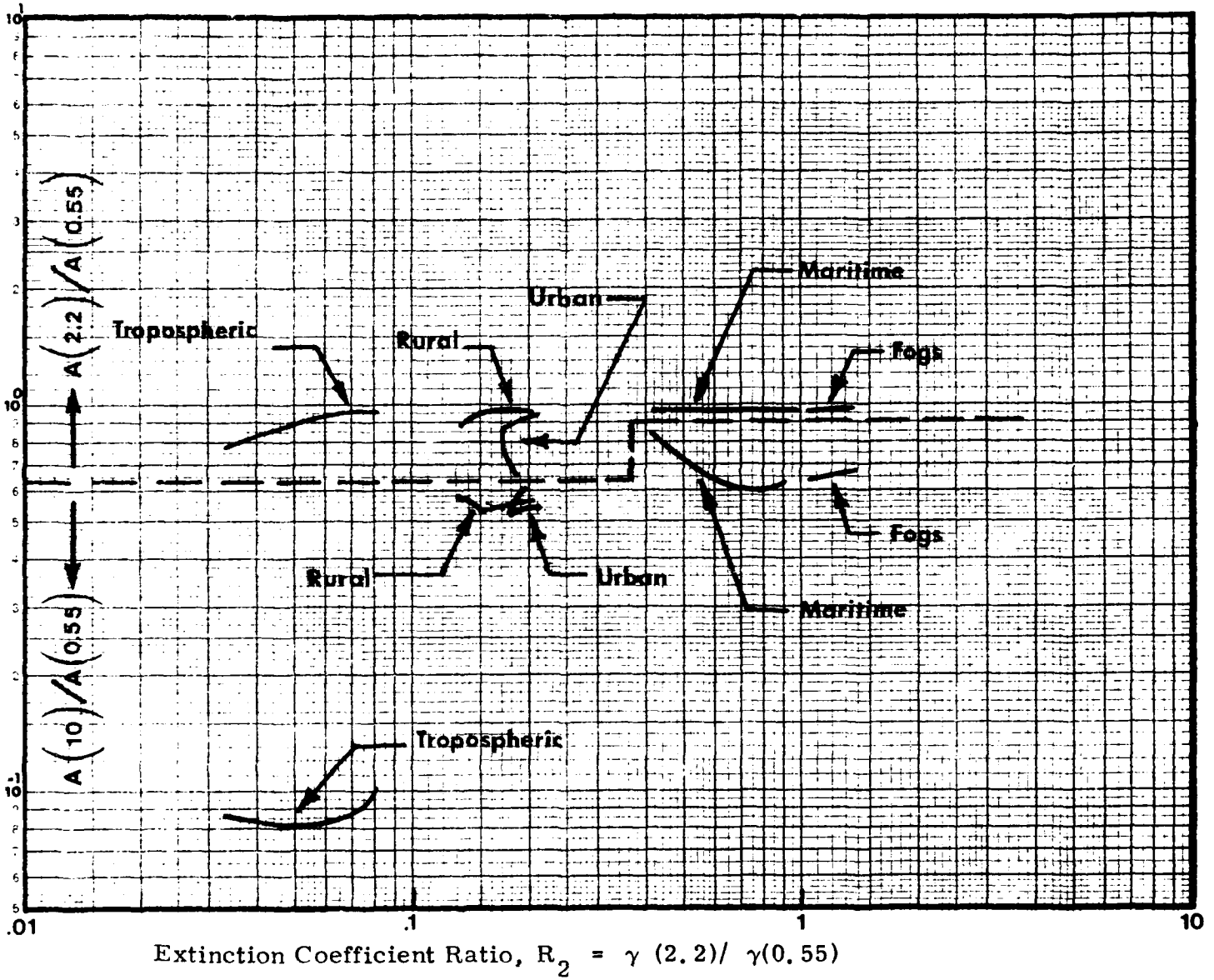

Figure 8.13. Relationships between R_2 and ratios of albedo at two sets of wavelengths.

$$b\,Z = A(\lambda)\,\gamma(\lambda)\int_{\theta_1}^{\theta_2} \Phi\,(\theta, \lambda)\,E(\theta)\,\sin\theta\,d\theta \qquad (8.8)$$

where b is some constant.

At any wavelength the phase function $\Phi(\theta, \lambda)$ depends upon the size distribution and the composition of the aerosols involved. Deirmendjian (Reference 11) has described three haze models in some detail. They are: Haze M, representing maritime or coastal types of distributions; Haze L, representing the continental-type aerosol; and Haze H, representing high-level or stratospheric aerosol or dust layers. These models are forerunners to Shettle and Fenn's models for maritime, rural, and trospheric aerosols, respectively. Deirmendjian calculated the phase functions for his models at a number of wavelengths. Figures 8.14 through 8.17 use some of Deirmendjian's phase functions, but present them in a way pertinent to this discussion of fixed angle nephelometers.

In Figures 8.14 through 8.17, the abscissa values are ratios of the extinction coefficients at 1.94 μm to those at 0.45 μm. These are the wavelengths closest to 2.2 μm and 0.5 μm available from the Deirmendjian models. Ordinate values are the phase functions at 20°, 40°, 50°, 60° and 70°. Figure 8.14 shows the phase function for a wavelength of λ = 0.45 μm, Figure 8.15 for λ = 0.7 μm, Figure 8.16 for λ = 1.94 μm, and Figure 8.17 for λ = 10.0 μm. Figure 8.14 is for λ = 0.7 μm, 8 for λ = 1.94 and Figure 8.17 is for λ = 10 μm. Phase function values for Deirmendjian's cloud model C1 are also given. Deirmendjian describes C1 as representative of cumulus clouds.

Deirmendjian used a function he called a modified gamma distribution to describe the size distribution of aerosols in his various haze and cloud models. Shettle and Fenn have used the same form of function to describe size distributions in fogs. The function has the form

$$n(r) = a\,r^{\alpha}\exp(-br^{\gamma}) \qquad (8.9)$$

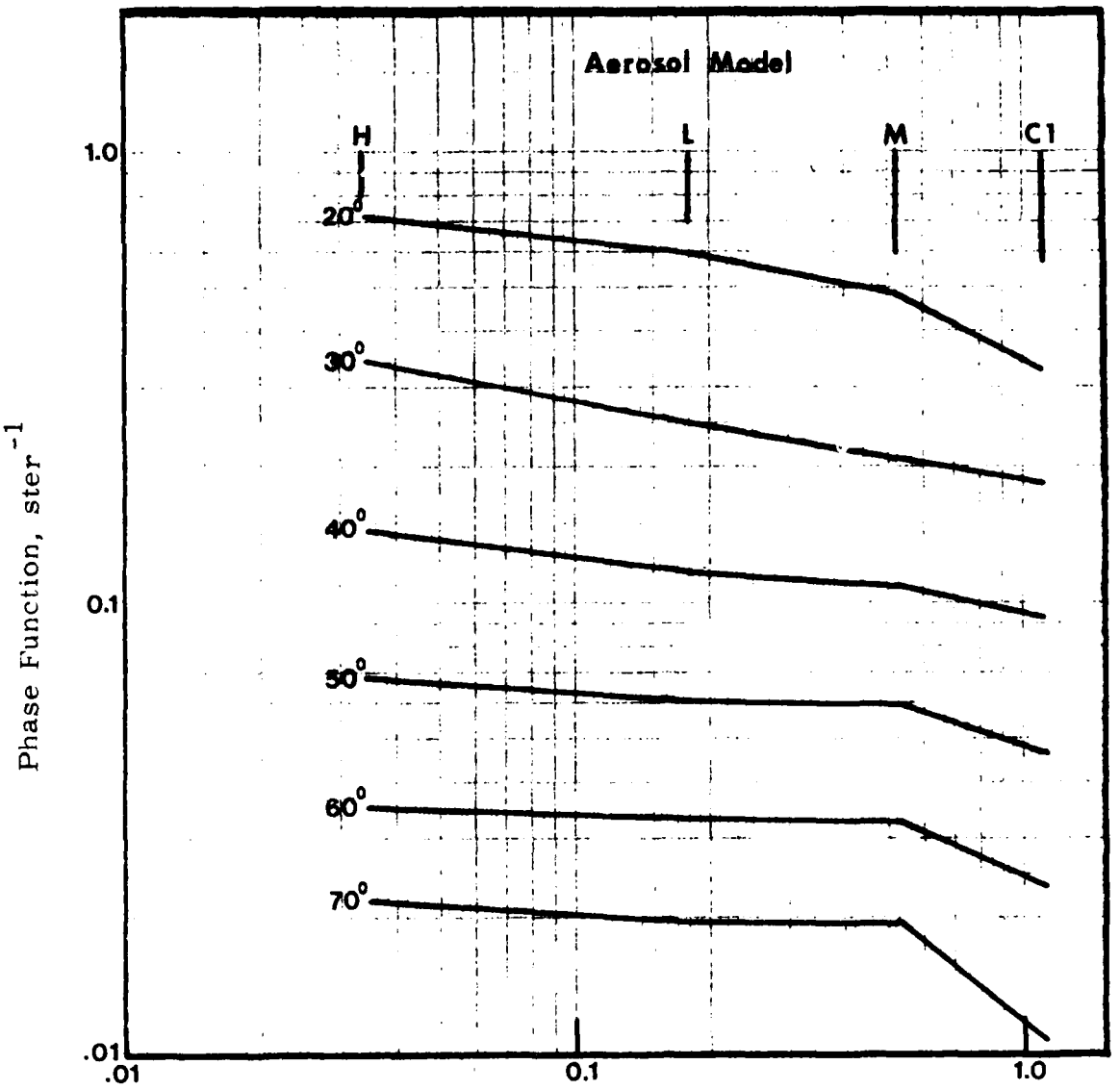

Figure 8.14. Aerosol scattering phase function at $\lambda = 0.45\ \mu m$ vs extinction coefficient ratio R_2 at six forward scattering angles for four Deirmendjian aerosol models.

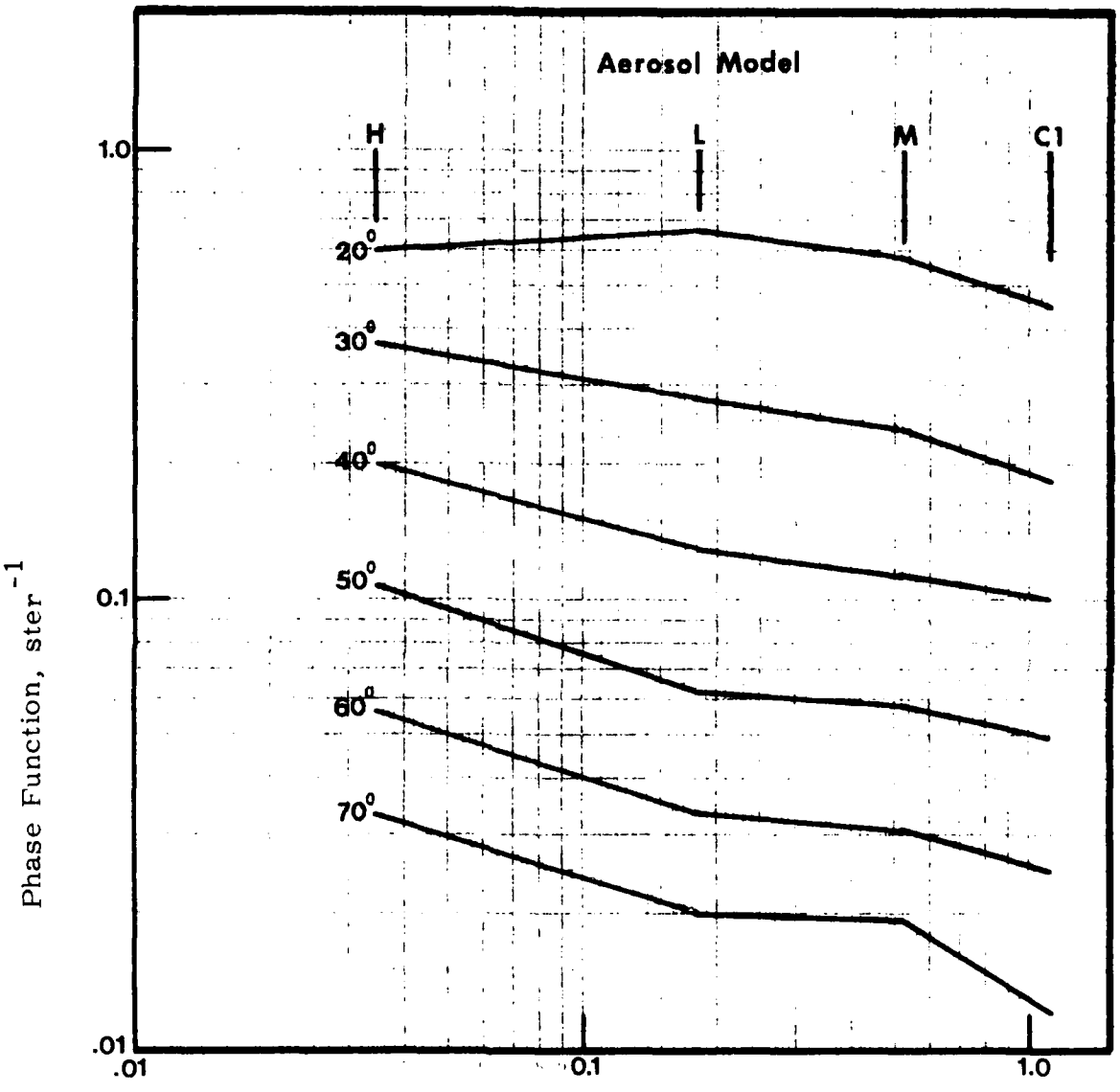

Figure 8.15. Aerosol scattering phase function at $\lambda = 0.7\ \mu m$ vs extinction coefficient ratio R_2 at six forward scattering angles for four Deirmendjian aerosol models.

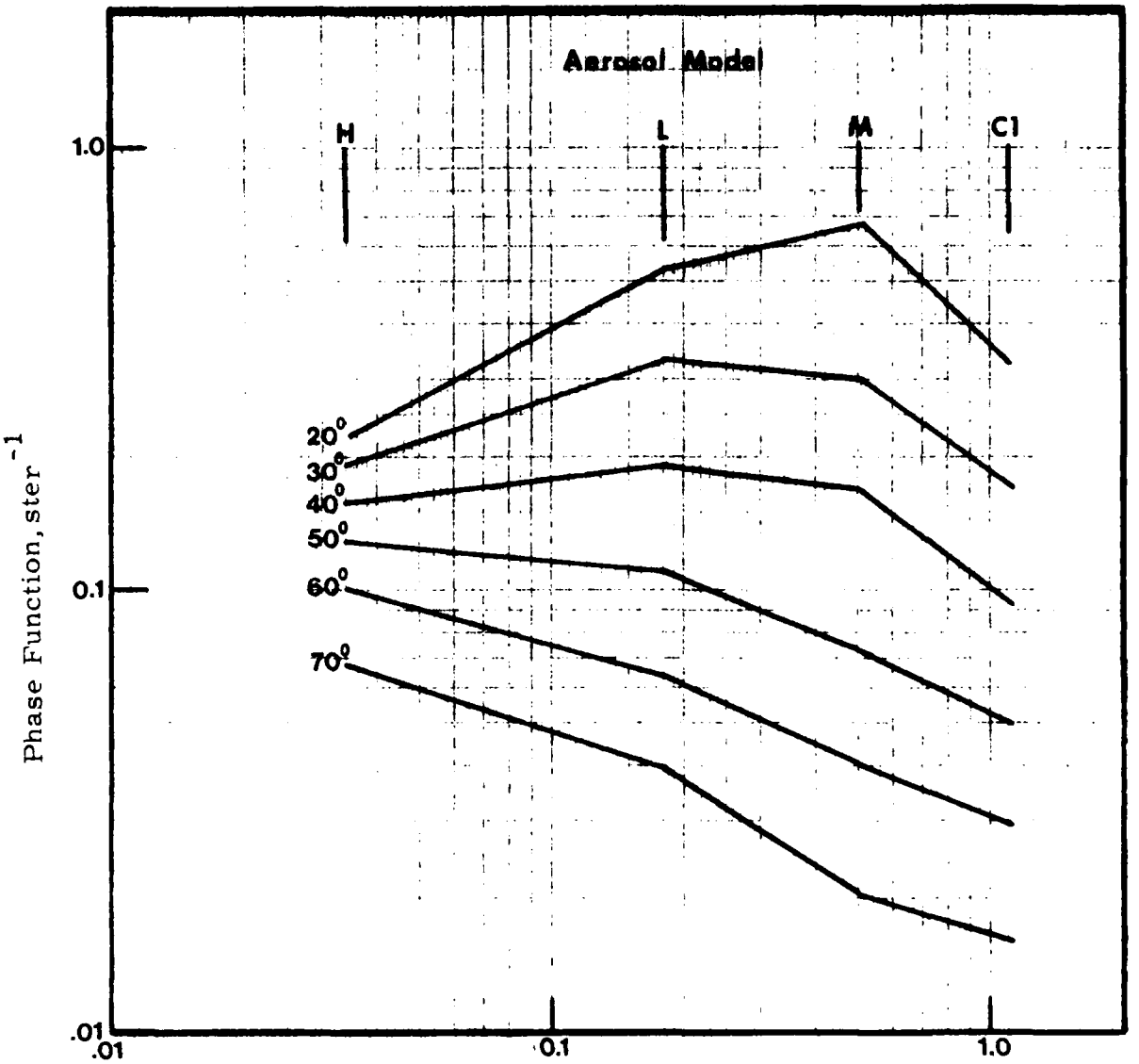

Figure 8.16. Aerosol scattering phase function at $\lambda = 1.94\ \mu m$ vs extinction coefficient ratio R_2 at six forward scattering angles for four Deirmendjian aerosol models.

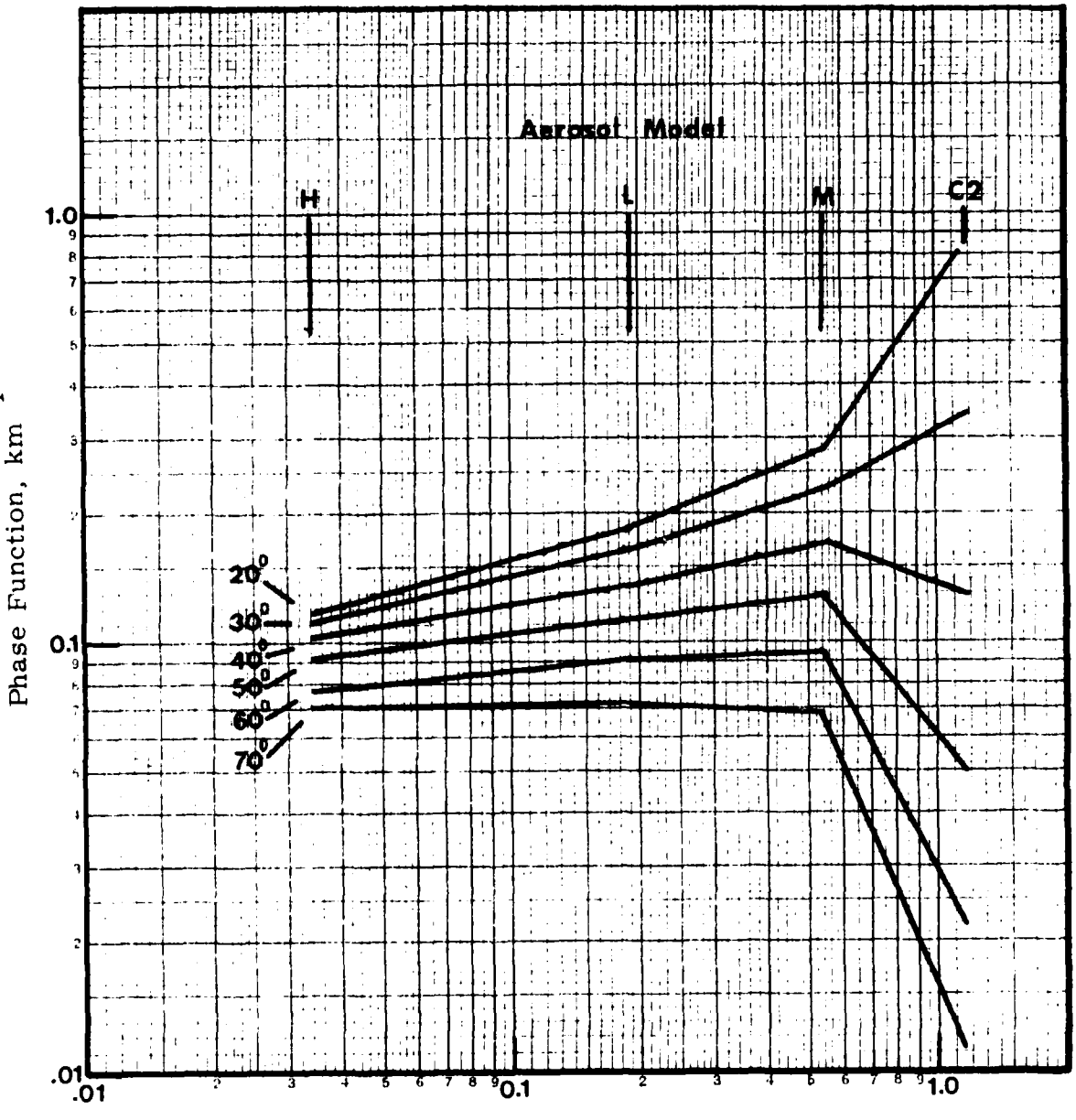

Figure 8.17. Aerosol scattering phase function at $\lambda = 10\ \mu m$ vs extinction coefficient ratio R_2 at six forward scattering angles for four Deirmendjian aerosol models.

Deirmendjian described cloud type C1 using the coefficients

$$a = 2.373$$

$$\alpha = 6$$

$$\gamma = 1$$

$$b = 1.5$$

Shettle and Fenn used the same coefficients to describe their radiation fog model 1 (also called fog model 3). Deirmendjian's calculated values of phase function for cloud model C1 can also be used in this discussion to describe the phase function of Shettle and Fenn's radiation fog model 1. In Figures 8.14 through 8.17 solid lines connect the phase function values for high, continental and maritime hazes and cloud type C1. Table 8.9 presents Deirmendjian's values of γ (0.45), γ (1.94) and their ratio for his models H, L, M and C1.

Equation 8.8 describes the dependence of the signal Z, measured by a fixed angle nephelometer, on angle θ and phase constant b includes the source intensity, optical filter characteristics and other optical and geometric parameters. The topic of interest here is the relationship of extinction coefficient to the amount of scattered light as the scattering model changes. For a fixed angle nephelometer sensitive over a very limited angular range the following approximation is valid

$$\gamma(\lambda) = \frac{b\,Z}{A(\lambda)\Phi(\theta,\lambda)\,E(\theta)\sin\theta\;\Delta\theta} \qquad (8.10)$$

and since $E(\theta)$ = constant, $\sin\theta$ = constant and $\Delta\theta$ = constant then

$$\gamma(\lambda) = \frac{k\,Z}{A(\lambda)\Phi(\theta,\lambda)} \qquad (8.11)$$

where k is a collection of constants.

Table 8.9. Aerosol Extinction Coefficients at Two Wavelengths and their Ratio for Four Deirmendjian Aerosol Models.

Model	$\gamma(0.45)$ (km^{-1})	$\gamma(1.94$ (km^{-1})	$\frac{\gamma(1.94)}{\gamma(0.45)}$
H	0.0201	0.000696	0.0346
L	0.048	0.0089	0.185
M	0.1056	0.0555	0.5256
C1	16.33	18.05	1.105

The potential for phase function and albedo effects to influence empirical correlation relations intended to predict aerosol scattering behavior at 10 μm from measurements at 0.55 μm and 2.5 μm is demonstrable on the basis of the foregoing discussions. In any future program intended to pursue the SWIRN concept the magnitude of these effects should,therefore,be evaluated and, if necessary, included in the empirical correlation relations.

9. CONCLUSIONS AND RECOMMENDATIONS

9.1 Measurement Performance

The measurement performance requirements of the SWIRN are determined by its primary operational function, which is to perform atmospheric aerosol scattering measurements at two short wavelengths such that in turn those measurements can be used to predict the atmospheric aerosol extinction coefficient in the 8 to 12 μm atmospheric window. The two wavelengths chosen for the SWIRN measurements were 0.55 μm and 2.5 μm.

By making realistic assumptions about target characteristics, atmospheric conditions and FLIR system capabilities (Table 3.1) we arrived at the requirement for a SWIRN capability of predicting atmospheric aerosol attenuation coefficients of $\beta = 0.1\ km^{-1}$ in the 8 to 12 μm spectral region.

Also underlying the requirement to predict aerosol extinction coefficients as low as $0.1\ km^{-1}$ is the PRESSURS Program Requirement (Reference 12) for predicting Lock-On ranges as great at 10 km with an accuracy of $\pm$ 20 per cent. Throughout most of the report we stated that the accuracy with which the value of $\beta = 0.1\ km^{-1}$ (in the 8 - 12 μm region) should be predicted was $\pm$ 20 per cent. This is undoubtedly too stringent a measurement requirement as we will show.

From Figure 3.1 (and the conditions of Table 3.1)., we had concluded that the minimum total atmospheric extinction coefficient of concern was $\beta = 0.47\ km^{-1}$. We had also found that water vapor absorption (continuum and molecular) accounted for an appreciable amount, $\beta = 0.37\ km^{-1}$, of the total extinction coefficient and aerosol attenuation accounted for the remainder (i.e. $\beta = 0.1\ km^{-1}$).

A 100 percent error in the aerosol component ($\beta = 0.1\ km^{-1}$) of the total extinction coefficient ($\beta = 0.47\ km^{-1}$) would introduce less than 20 per cent error in the value of the total extinction coefficient, assuming that errors in the measurements propagate as independent errors. Consequently, we believe that the performance requirement for predicting the aerosol extinction coefficient at 8 to 12 μm should be relaxed to an error of $\pm$ 20 per cent when $\beta = 0.3\ km^{-1}$ for the aerosol component of the total extinction coefficient.

Based on the earlier requirement to determine the 8 to 12 μm aerosol extinction coefficient to an accuracy of $\pm$ 20 percent when $\beta = 0.1\ km^{-1}$ we had concluded, as a worst case situation, that the SWIRN must be capable of measuring the aerosol scattering coefficients at 0.55 μm and 2.5 μm to an accuracy of $\pm$ 20 per cent when the scattering coefficients were $\beta = 0.1\ km^{-1}$ at each wavelength. We believe this requirement can be relaxed by the amount permitted by the 8-12 μm requirement. That is, the SWIRN need only measure aerosol scattering coefficients of $\beta = 0.3\ km^{-1}$ to an accuracy of $\pm$ 20 per cent at each of two wavelengths. Further work is needed to confirm this.

The measurement accuracy imposed on the SWIRN in the above arguments also has imposed on it one further constraint--the time constant of the measurement. We had concluded, based on the analysis in Reference 1) that the maximum time constant for the SWIRN measurements should be $\tau = 2$ seconds. We believe that requirement still holds.

Table 7.3 gives the actual measurement performance of the SWIRN with the 15 second time constant used at CALSPAN. The projected measurement performance for a 2 second time constant is also given. The 2.5 μm channel of the prototype SWIRN is more than capable of meeting the measurement requirement; the 0.55 μm channel is not.

The measurement performance requirement of the 0.55 μm channel can probably not be improved with the present SWIRN transmitter components or the present 55 degree scattering angle. An increase of a factor of five in signal strength is required. A factor of two may be achieved by reducing the scattering angle to say 40 degrees. It is not feasible to increase the size of the light source which already requires 20 Watts of power.

A more attractive alternative would be to have two light sources in the transmitter section of the SWIRN. The second source could be similar to the IRED used in the AVM (Reference 1). More powerful IRED sources have been developed since the fabrication of the prototype AVM. One of these sources, combined with a smaller scattering angle would permit the 0.55 μm channel to meet its performance requirement.

9.2 Physical Features

The primary and overriding objective in the development of the prototype SWIRN was to achieve an instrument whose measurements could be used to predict the aerosol extinction coefficient in the 8 to 12 μm atmospheric window. Whenever size, weight or power considerations come into conflict with the primary objective they were sacrificed in favor of trying to meet the primary objective.

As an instrument concept the SWIRN will first and foremost succeed on the basis of the ability to predict the 8 to 12 μm aerosol extinction coefficient using two short wavelengths. If that goal can be achieved,then the problems of minimizing the size, weight, and power demands of the instrument can be addressed. We are confident that these physical features can be made compatible with the capabilities of an RPV.

9.3 Correlation Relations

Using the aerosol models of Shettle and Fenn, preliminary correlation relations were developed for using the SWIRN measurements to predict aerosol extinction coefficients in the 8 to 12 μm atmospheric window. These relations were then tested against the fog transmission measurements of Clay and Lenham. Improvements to the relations were made based on the Clay-Lenham data.

A set of five empirical correlation relations was arrived at by the above process. These relations were then tested using IR transmission measurements in the simulated haze and fog environments generated by CALSPAN in their environmental test chamber. The ability to predict the 10 μm extinction coefficient for fog environments (especially "diluted" fogs--where the density of particles was numerically scaled down) was shown to be good. The ability to predict the 10 μm extinction coefficient for the extremely unreal hazes generated by CALSPAN was only fair to poor.

We believe that thus far the SWIRN concept has not undergone sufficient testing to be able to formulate any judgment as to its success or failure. The empirical correlation equations are based on aerosol models and a small amount of fog data. The tests of these relations were performed on simulated fog and haze environments. Haze environments were generated which were extremely unreal because of the necessity of obtaining any kind of readings with a very short path 18.3 meter IR transmissometer.

The results obtained thus far in predicting the 10 μm extinction coefficient for fog offers enough encouragement, we believe, to warrant further investigation and testing of the SWIRN objectives. In any future program of that nature, the SWIRN should be operated against one or more long path IR transmissometers. All low visibility environmental episodes should be well characterized by standard meteorological measurements and by particle sizing instruments.

REFERENCES

1. D. F. Hansen, "Development of an "Airborne Visibility Meter", HSS-B-092, Final Report on Contract F19628-81-C-0005, 15 November 1982 (to be published).

2. Lucien M. Biberman, "Uncertainties in Comparison of FLIR Performance in the 3-5 and 8-12 μm Bands", IDA Paper P-1128, Sept. 1979.

3. Kit G. Cottrell et al, "Electro-Optical Handbook, Volume I, Weather Support for Precision Guided Munitions", Air Weather Services (MAC) AWS/TR-79,002, May 1979.

4. Eric P. Shettle and Robert W. Fenn, "Models for the Aerosol of the Lower Atmosphere and the Effects of Humidity Variations on Their Optical Properties", AFGL-TR-0214, 20 September 1979.

5. SWIRN Design Review Meeting at AFGL on 4 June 1981. Staff Members of HSS Inc and AFGL were in attendance.

6. Dr. J. A. Mauro, Ed and Contributing Author, "Optical Engineering Handbook", General Electric, Electronics Lab of the Defense Electronics Division, Syracuse, N.Y.

7. D. F. Hansen et al, "Design of a Prototype Multi-Wavelength Abridged Polar Nephelometer", AFGL-TR-82-0154, Final Report on Contract F19628-81-C-0008, 10 May 1982.

8. William L. Wolfe, "The Infrared Handbook", The Infrared Information and Analysis Center, Environmental Research Institute of Michigan, 1978.

9. D. F. Hansen, "Design, Develop, Fabricate and Test and Expendable Air Deployable Infrared Nephelometer (SWIRN), HSS Inc Report, HSS-B-086, 10 Dec 1981.

10. M. R. Clay and A. P. Lenham "Transmission of Electromagnetic Radiation in Fogs in the 0.53 - 10 μm Wavelength Range", App. Opt. 21, p. 3831 - 3832, 1981.

11. D. Deirmendjian, "Electromagnetic Scattering on Spherical Polydispersions", American Elsevier, New York, 1969.

12. F. Brousaides, "Meteorological Sensors for the PRESSURS Program and an Assessment of the AN/GMQ-13 Cloud Height Set", AFGL Rpt, Sep 1981.

APPENDIX A

R & D TEST AND ACCEPTANCE PLAN

HSS-B-086

10 Dec 1981

Contract: F19628-81-C-0008

HSS-B-086

DESIGN, DEVELOP, FABRICATE, AND TEST AN EXPENDABLE AIR DEPLOYABLE INFRARED NEPHELOMETER (SWIRN)

Rand D TEST AND ACCEPTANCE PLAN

D. F. Hansen

10 December 1981

Contract: F19628-81-C-0008

Line Item: 0002 Seq. No. 103

This Report is Intended Only for the Internal Management Use of the Contractor and the U. S. Air Force.

Prepared For:

AIR FORCE GEOPHYSICS LABORATORY (LYP)

AIR FORCE SYSTEMS COMMAND

HANSCOM AFB, MASS 01731

1. BACKGROUND

The present contract for the development of the SWIR Nephelometer requires that after fabrication and in-house testing is complete that HSS Inc install that instrument at the AFGL Weather Test Facility (WTF) at Otis AFB for a calibration, test and evaluation period of approximately six months duration. At WTF the output signals of the instrument are to be recorded by AFGL and routinely furnished to HSS Inc for data processing and evaluation. AFGL is to conduct infrared transmission measurements at selected wavelengths over long horizontal paths in the vicinity of the SWIRN to provide a data base for comparison with and evaluation of the SWIRN measurements.

The present document; i.e. the R&D Test and Acceptance Plan for the SWIR Nephelometer, was to be based upon implementing the above program at Otis AFB. However, a problem has developed which in effect precludes the implementation of the planned effort at Otis AFB. The problem has surfaced because the Atmospheric Optics Branch (OPA) at AFGL no longer intends to send their optical-measurements-trailer to Otis AFB. Without the OPA trailer at Otis AFB, there will be no capability for performing measurements of the instrared transmission over long horizontal paths for purposes of calibration of the SWIRN and comparison with and evaluation of the SWIRN data. The transmissometer measurements are essential to the calibration and evaluation of both the instrument and program objectives.

In light of the above development, a meeting was held at AFGL on 4 December 1981 to consider alternative test sites for the SWIR Nephelometer. Participants at the meeting were the contract technical monitor, Fred Brousaides, Eric Shettle from the Atmospheric Optics Branch of AFGL, and Donald Hansen of HSS Inc. Those present at the meeting concluded that a substitute program could be formulated to take the place of the planned program at Otis AFB. The substitute program would, however, require that measurements be conducted at other locations and under circumstances different from those originally planned. What was once a single test program may become a group of test programs.

2.0 TEST OBJECTIVES

2.1 Program Test Objectives

A primary objective of the Air Force PRESSURS program is the ability to forecast the Target-Acquisition-Range (TAR) and the system Lock-On-Range (LOR) for infrared imaging systems operating in the atmospheric window between 8 μm to 12 μm. Three physical mechanisms contribute to the attenuation of optical radiations in this wavelength interval; they are: water vapor absorption, water vapor continuum absorption and aerosol extinction.

For most environmental situations the two effects of water vapor on atmospheric transmission are well predicted by computer codes employing inputs from basic meteorological measurements. This is not true for aerosol extinction processes as has been recognized by all investigators who have attempted to model a correlation between aerosol extinction and the basic meteorological parameters (Reference 1).

Aerosol extinction is composed of two components, scattering and absorption. For most environments aerosol scattering dominates the aerosol absorption in the atmospheric windows of military interest. Thus, it is usually only necessary to measure the attenuation due to scattering to arrive at the aerosol extinction coefficient. Instruments which measure aerosol scattering, such as the SWIRN, are called nephelometers.

Physical constraints have been imposed on the SWIRN because the contemplated method for deployment is by Remote Piloted Vehicle (RPV). To be deployed on an RPV the instrument must be small in size, light in weight and have low power consumption. To perform the required aerosol scattering coefficient measurements in the 8 μm to 12 μm spectral region, given these constraints, is considered to be beyond the state-of-the-art in aerosol nephelometry.

An alternative approach has been taken by AFGL to the direct measurement of aerosol scattering in the 8 to 12 μm region. That approach has

led to the development of the SWIR Nephelometer. In this approach two widely separated short-wavelength measurements are to be used as inputs to a Predictive Model to obtain the atmospheric extinction coefficient in the long-wavelength (8 μm to 12 μm) spectral region. The two central wavelengths adopted in the prototype SWIRN are one in the visible spectral region (at 0.55 μm) and one in the near infrared (at 2.5 μm).

The indirect approach outlined above is based on the premise that a predictive model can, using the SWIRN measurements and basic meteorological measurements, determine atmospheric aerosol extinction properties at long wavelengths. This hypothesis has yet to be tested, and is contemplated to be one part of the overall SWIRN test program. Logically, however, it must be isolated as an entirely separate objective from the test and evaluation of the instrument itself.

2.2 SWIRN Test Objectives

Primary test objectives of the prototype SWIR Nephelometer relate specifically to an evaluation of its measurement performance as a nephelometer. Secondary objectives of the SWIR tests relate to: (1) the long term stability of the instrument calibration (once established), (2) environmental and temperature effects on the instrument calibration and, (3) the degree and type of maintenance required to maintain peak performance.

The measurement objectives of the SWIR Nephelometer must be stated in terms of the range of aerosol scattering coefficients to be measured by each of the two instrument channels. Before these ranges can be established it is necessary to quantify the operational objectives of the PRESSURS program in terms of the performance of FLIR systems operating in the 8 to 12 μm spectral region. Once those objectives are quantitatively specified the AFGL Atmospheric Aerosol Models (Reference 2) can be used to find the approximate range of scattering coefficients at 0.55 μm and 2.5 μm which correspond to the 8 to 12 μm operational conditions.

The operational objectives of the PRESSURS program insofar as they pertain to the SWIR Nephelometer were defined quantitatively by AFGL and HSS Inc personnel as inputs to the Design Evaluation of the SWIRN (Reference 3). Briefly stated these objectives are as follows:

The design goal of the SWIRN is to provide a capability to the Air Force for forecasting whether the Lock-On-Range of an 8 to 12 μm FLIR system is greater or less than 10 kilometers. If the Lock-On-Range is less than 10 kilometers then the range is to be determined to an accuracy of $\pm$ 20 percent. The operational situation for FLIR systems was further defined in terms of an worst-case dew point temperature of 20° C. It is also required that the threshold temperature transmittance of the atmosphere be no greater than 0.01 in order to achieve lock-on. (Threshold temperature transmittance is defined as the ratio of the system minimum-detectable-radiative-temperature-contrast to the inherent-radiative-temperature-contrast between the target and its background).

The Electro-Optical Handbook of the Air Weather Service (Reference 4) was used to determine the values of water vapor absorption coefficient and aerosol extinction coefficient in the 8 to 12 μm region which correspond to a FLIR Lock-On-Range of 10 kilometers under the foregoing specified conditions. The total extinction coefficient corresponding to this operational situation is 0.5 km^{-1}, of which 0.4 km^{-1} is due to water vapor absorption and 0.1 km^{-1} to aerosol extinction.

The analysis outlined above defined the minimum value of aerosol extinction coefficient, for the 8 to 12 μm region, which is of concern in an operational situation. The AFGL Atmospheric Aerosol Models were then employed to find the approximate minimum values of aerosol scattering coefficients at 0.55 μm and 2.5 μm which must be measured by SWIRN to an accuracy of $\pm$ 20 percent. These values are given in Table 1.

The atmospheric aerosol models used in the preparation of Table 1 were selected from the AFGL models given in Reference 2. In the case of the

Table 1. Atmospheric Extinction and Scattering Coefficients Pertinent to the Design Goals of the SWIRN Nephelometer

AFGL Model	λ = 10 μm		Scattering Coeff. (km^{-1})	
	Extinction Coeff. (km^{-1})	Scattering Coeff. (km^{-1})	2.5 μm	.55 μm
Rural (99% RH)	.09	.05	.13	.77
Urban (98% RH)	.12	.063	.20	1.35
Maritime (95% RH)	.11	.067	.31	.44
Light Radiation Fog	2	1.0	12	8.7
Heavy Advection Fog	35	22	26	29

Rural, Urban and Maritime aerosol models a value of relative humidity was chosen from amongst those available which gave a total aerosol extinction coefficient at 10 μm which was closest to the limiting value of 0.1 km^{-1}. The scattering coefficients at 10 μm, 2.5 μm, and 0.55 μm were then read directly from the tables in that document.

Approximate minimum values of the scattering coefficients to be measured by the SWIRN may be obtained using Table 1 as a guideline. The minimum aerosol scattering coefficient required to be measured by the 2.5 μm channel is taken to be 0.1 km^{-1}; for the 0.55 μm channel the minimum value required to be measured is taken to be 0.3 km^{-1}.

AFGL fog models were used to define typical limits to the measurement range of the SWIRN. Table 1 indicates that scattering coefficients as great as 30 km^{-1} can be expected. To prevent saturation of the instrument electronics a maximum value of 60 km^{-1} was taken as a design parameter for the instrument.

3.0 TEST PLAN

3.1 Potential Test Locations

Three possible locations for testing of the SWIRN have been suggested as alternatives to the Otis AFB site. These three locations are: (1) the SNOW 1A Exercise in Burlington, Vermont during the month of January, (2) the CALSPAN Environmental Test Chamber in Ashford, New York, and (3) ad hoc tests at Hanscom AFB during environmental episodes of importance to the evaluation of the SWIRN and to the testing of a predictive model.

3.2 Testing of a Predictive Model

When the SWIRN development program was initiated it was contemplated that by the time the testing of the instrument began there would be a predictive atmospheric aerosol model available which could be adopted for use in the SWIRN test program. If was further assumed that several parameters of the model would be available for adjustment in order to optimize the predictive behavior of the model.

To our knowledge, no predictive model is yet available from any source. In the absence of predictive model an attempt will be made to find an empirical correlation of the aerosol scattering coefficients measured by SWIRN with the 8 to 12 μm aerosol extinction coefficients measured using a long path transmissometer.

There is a low probability that an empirical correlation of the type just described will meet with success. Investigators who have searched for such correlations indicate in the literature that aerosol particle size distribution and aerosol number density are key parameters in being able to predict the long wavelength attenuation properties of the atmosphere. A predictive model having the most likelihood of success would thus have the aerosol size distribution and number density as internal parameters which are automatically adjusted to fit the SWIRN data. Basic meteorological

data (temperature and relative humidity) will quite likely be required as inputs to the model also, since these parameters, especially relative humidity, have an influence on the size of the atmospheric aerosols.

3.3 Calibration of SWIRN

The SWIRN is a state-of-the-art fixed-angle nephelometer. Tests with another state-of-the-art nephelometer, the Airborne Visibility Meter (AVM), indicate that the response (i.e. the output signal) of such instruments is not quite linearly related to the aerosol scattering coefficient, but instead obeys a mild power law (Reference 5). The deviation from a linear response is probably not apparent in calibration curves of conventional fixed-angle nephelometers or forward-scattering visibility meters. In the case of SWIRN and AVM, with their extreme dynamic range capability, the non-linearity is not only apparent but must be dealt with by a calibration of the instrument over the full range of response. Thus, before the SWIRN can be of any use for testing predictive models or for deducing empirical scaling laws, it must be calibrated.

Calibration of the first SWIRN will require that the instrument be operated in a variety of natural or simulated environmental situations ranging in character from heavy fogs to very light hazes. We believe that the most expedient method for calibrating the SWIRN is by a combination of two complimentary programs: (1) the simulation of a wide variety of environments in a short period of time at the CALSPAN Environmental Test Chamber, and (2) measurements of opportunity during a variety of naturally occurring environmental episodes (hereinafter referred to as the Ad Hoc Program).

3.4 Calspan Test Program

3.4.1 General Considerations

Past experience in conducting a similar test program at the CALSPAN Environmental Test Chamber has shown that the contemplated program should be somewhat flexible to accommodate unexpected events or unpredicted results. The program outlined here should, therefore, only be taken as a guideline for a series of tests at CALSPAN.

A four-day test program should be sufficient to cover all the environments necessary to calibrate the SWIR Nephelometer. It should include large and small droplet fogs and a variety of high humidity and low humidity hazes. Haze and fog particle densities should be varied over the maximum ranges permitted by the exercise of controls over the chamber environmental conditions. Seed nuclei with varying degrees of hydroscopicity should be used in the generation of the hazes in order to vary the aerosol particle sizes. Based on conversations with CALSPAN personnel, a tentative test program has been drawn up. That program is given in Table 2.

Several hours must be alloted at the beginning and the end of the four day test program for set-up and roll-up of equipment. Actual time available for testing in a four day period is such that CALSPAN will only guarantee that ten tests will be conducted. The probability that more than ten tests can be conducted is high. Fourteen tests were conducted for AFGL/HSS Inc during the calibration of the AVM.

A test program at CALSPAN would not be conducted in the sequence indicated in Table 2. The preferred daily sequence to get maximum use of the chamber is to start out with a large droplet fog test followed by a small droplet fog test, then to begin a series of haze tests starting with high humidity hazes. A description of how the simulated fogs and hazes are produced may be found in References 6 and 7.

Table 2. Preliminary Environmental Test Program for the SWIR Nephelometer at the CALSPAN Test Facility

TEST RUN	OBJECTIVE	AEROSOL NUCLEI
1	Large Droplet Fog	Ambient
2	Large Droplet Fog	Seed at 6 Min
3	Small Droplet Fog	1 gm Salty Dog
4	Small Droplet Fog	Cigar Smoke
5	High Humidity Haze	0.1 gm Salty Dog
6	High Humidity Haze	0.1 gm Phosphorous
7	High Humidity Haze	Cigar Smoke
8	Low Humidity Haze	1 gm Salty Dog
9	Low Humidity Haze	Cigar Smoke
10	Low Humidity Haze	Diesel Fuel
11	Small Droplet Fog	.2 gm Phosphorous
12	High Humidity Haze	1 gm Salty Dog
13	Low Humidity Haze	6 gm Salty Dog
14	Low Humidity Haze	1 gm Phosphorous

3.4.2 CALSPAN Instrumentation

A list of the instrumentation available at the CALSPAN test facility which are pertinent to the calibration and testing of the SWIR Nephelometer is given in Table 3. Temperature and relative humidity are monitored almost continuously during the course of each test run. Particle sizing instruments appropriate to the particular fog or haze test will be employed. The visible light transmissometer will be used during all fog simulations to measure the visible light extinction coefficient. The MRI integrating nephelometer will be used to measure the visible light scattering coefficient in all haze environments.

The infrared measuring capability at the CALSPAN facility will be a limitation to the calibration and testing of the SWIR Nephelometer. In the past year CALSPAN switched over from an IR filter-transmissometer to a Circular-Variable-Filter transmissometer. The new IR transmissometer was bolted to the chamber wall, as opposed to the old method of mounting which employed pillars external to the chamber. The bending and vibration of the chamber wall which takes place during pressurization and expansion of the chamber on fog tests degrades the instrument performance to the point where it cannot be used for measurement of IR transmission in fogs. It can be utilized in hazes, however, with no degradation of performance. CALSPAN plans to remount the IR transmissometer to eliminate the above problem, but this change will not be made until mid to late summer of 1982.

Gene Mack of CALSPAN indicates that he may be able to give us one to two minutes of IR measurements once during each fog run. This would occur at the time the chamber pressure is passing from its overpressure state through ambient pressure, and at the time when they would normally turn on pumps to continue expansion of the chamber and thus maintain the fog environment. By halting the expansion process when ambient pressure is reached, the chamber wall is returned to its normal

Table 3. Measurement Instrumentation Available at CALSPAN Pertinent to the Calibration and Test of the SWIR Nephelometer.

INSTRUMENT	PARAMETER
1. Thermo-Systems Electric Aerosol Analyzer Model 3030.	Aerosol Size Distribution (.004 to 0.75 μm)
2. Royco Model 225 Particle Counter	Aerosol Size Distribution (.3 to 10 μm)
3. CALSPAN Fog Droplet Sampler	Drop Size Distribution (3 to 100 μm)
4. MRI Integrating Nephelometer Model 2050	Visible Light Scattering Coefficient (.08 to 8 km^{-1})
5. Temperature and Relative Humidity	Unspecified Systems
6. CALSPAN Visible Light Trans.	Visible Light Extinction Coefficient (1 to 200 km^{-1})
7. CALSPAN IR Transmissometer (Circular-Variable-Filter Type)	IR Extinction Coefficient: Wavelength Range = 2 to 14 μm Wavelength Resolution = 2 % Extinction Coefficient Range = (Unspecified) Cycle Time = 4 minutes

position and IR measurements can be made. The fog will hold for one to two minutes, Gene estimates, and then rapidly evaporate.

One to two minutes is not adequate time to allow the CVF IR transmissometer to complete its cycle from 2 to 14 microns. As it now stands that cycle time is 4 minutes. CALSPAN intends to halve the cycle time to 2 minutes in the near future. Even so, we can probably expect changing fog conditions during a two minute period such that the transmission at 2 $m\mu$ and the transmission at 10 $m\mu$ will refer to quite different fog conditions.

CALSPAN has indicated the possibility of manually moving the filter wheel to different wavelength positions thus providing a better time-correlation between measurements at different wavelengths. This potential should be explored further. Also the possibility of enlarging the spectral band width of the instrument must be explored. Used as a fixed-filter, the 2 per cent band width is probably too narrow to provide a proper calibration of the near-IR channel or to attempt serious correlation with the 8 to 12 μm spectrum interval.

A further limitation of the CALSPAN transmissometer is its short baseline (18.3 meters). This path length represents two traversals of the chamber; obviously, however, it is not adequate to deal with other than fog and heavy haze situations. We estimate that the CALSPAN IR transmissometer has a useful extinction coefficient measurement range of 1 km^{-1} to 200 km^{-1}.

The above synopsis of the CALSPAN instrumentation and its capabilities indicates that to complete the calibration and testing of the SWIRN will require that tests be conducted at another location, one where a long-baseline IR transmissometer is available.

At CALSPAN the SWIRN can be calibrated and tested over a range of 0.1 km^{-1} to 100 km^{-1} in the visible channel and probably from 1 km^{-1} to 60 km^{-1} in the near-IR channel. Calibration of the near-IR channel in the range from 0.1 km^{-1} to 1.0 km^{-1} must be left to comparisons with long-path transmissometers.

At the AFGL meeting on 4 December, Eric Shettle indicated that in the absence of IR transmission measurements during CALSPAN simulated fogs, it may be possible to calculate the atmospheric extinction coefficient at 2 μm and at 10 μm using the measured particle size distribution and his Mie-Code. This suggestion was advanced to Gene Mack as a possibility; he countered with the idea of making the fog transmission measurement at ambient pressure, a procedure which was described above. Gene suggested the exercise of caution in the calculational approach. They have attempted it with a somewhat limited Mie-Code without great success. He admits, however, that a full Mie-Code might be more successful.

One problem would be how to tell whether the calculational approach was successful or not. That question could only be answered if measurements and calculations were compared on a specific experiment. Such an experiment is possible using measurements of fog transmission and particle distribution at ambient pressure.

3.5 Ad-Hoc Test Program

The objectives of the Ad-Hoc Test Program will be: (1) to calibrate the SWIRN in those environments which were not covered by the CALSPAN instrumentation capabilities (2) to gather data for formulating empirical LWIR aerosol attenuation scaling laws and/or for eventual use in evaluating a Predictive LWIR Atmospheric Aerosol Attenuation Model if one becomes available, and (3) to subject the instrument to prolonged use and exposure to the outdoor elements in order to evaluate the instrument stability.

The capability for conducting a limited Ad-Hoc test program will be available during the SNOW 1A exercise in Burlington, Vermont during mid-to-late January 1982. A number of long-path IR transmissometers will be operating at the SNOW 1A site including two such instruments which will be operated by the OP Laboratory of AFGL.

A more comprehensive program for completing the calibration and testing of SWIRN will be possible at AFGL after the SNOW 1A Exercise. The OPA group have indicated the likelihood of conducting occasional measurements with their instrumented trailer for the SWIRN program over a several month period. Specific instruments that would be used by OPA and their instrument capabilities are not in the possession of HSS Inc at this time. Program details and the instrumentation will be a subject of discussion at a later date when it is convenient for the OPA group who are now heavily engaged in the SNOW 1A Exercise.

4. TEST SCHEDULE

The Ad-Hoc program is constrained to the time periods when the OPA instrumented trailer is available as outlined in the preceeding discussion. The CALSPAN test program is constrained by the availability of the test chamber. Conversations with Gene Mack at CALSPAN indicate that the following time periods are the earliest times available: the last two weeks in February, the last week in April and the first week in May.

REFERENCES

1. Lucien M. Biberman, "Uncertainties in Comparison in FLIR Performance in the 3-5 and 8-12 μm Bands", IDA Paper P-1128, Sept. 1979.

2. Eric P. Shettle and Robert W. Fenn, "Models for the Aerosols of the Lower Atmosphere and the Effects of Humidity Variations on Their Optical Properties", AFGL-TR-79-0214, 20 September 1979.

3. D. F. Hansen and A. H. Pierson, "Design Evaluation of a SWIRN Nephelometer"; To Be Published. HSS-B-085.

4. Kit G. Cottrell et al, "Electro-Optical Handbook, Volume I, Weather Support for Precision Guided Munitions", Air Weather Services (MAC) AWS/TR-79/002, May 1979.

5. D. F. Hansen; "Development of An Airborne/Expendable Visibility Meter"; Monthly Status Report to AFGL; Oct.-Nov. 1981.

6. HSS Inc; "Development of an Airborne/Expendable Visibility Meter; R&D Test and Acceptance Plan No. 1"; 1 September 1981.

7. E. J. Mark; "Collection and Reduction of Drop Size Data in Simulated and Natural Fogs"; Interim Technical Report; May 1980 - AFGL Contract No. F19628-80-C-0041.

APPENDIX B

ARVIN CALSPAN
DOCUMENTATION OF EXTINCTION AND PARTICLE SIZE MEASUREMENTS FOR CHAMBER TESTS OF MAY 1982

for

HSS Inc

ARVIN/CALSPAN

DOCUMENTATION OF EXTINCTION AND PARTICLE SIZE MEASUREMENTS FOR CHAMBER TESTS OF MAY 1982

By

J. T. Hanley

FINAL REPORT

July 1982

Prepared for:

HSS Incorporated
2 Alfred Circle
Bedford, MA 01730

ADVANCED TECHNOLOGY CENTER

P.O. BOX 400 BUFFALO, NEW YORK 14225 TEL (716) 632-7500

APPLIED TECHNOLOGY GROUP
ARVIN

INTRODUCTION

Under contract (P.O. No. 2232) with HSS Inc., Calspan Corporation performed a series of chamber tests to aid in the evaluation of several visibility meters under development by HSS. The tests involved the measurement of extinction, at visible and IR wavelengths, simultaneously with Calspan instrumentation and the HSS devices in fogs and hazes generated in Calspan's 600 m^3 Environmental Test Chamber. A total of fourteen tests, consisting of nine fogs and five hazes as summarized in Table 1, was performed.

The fogs were formed by the expansion of near saturated (i.e., RH $\geq$ 97%) air and, through control of the pre-expansion aerosol concentration, the resultant fog droplet size range and concentration was varied. Hygroscopic hazes were generated by burning either white phosphorus or a pyrotechnic containing KCl and NaCl.

Test logs providing extinction coefficient, total particle concentration and relative humidity data as functions of time for each of the tests are found in Appendix A. Table 2 presents the aerosol size distributions for the haze tests. Fog droplet size distributions are presented graphically in Figure 1 and tabulated in Table 3. The following section discusses instrumentation and procedures used to obtain these data.

INSTRUMENTATION AND PROCEDURES

Extinction Coefficient (β)

Visible wavelength extinction was measured with three instruments; an MRI Integrating Nephelometer model 1550B ($0.01\ Km^{-1} < \beta < 10\ Km^{-1}$) and two Calspan-assembled transmissometers operating over pathlengths of 18.3 m ($3\ Km^{-1} < \beta < Km^{-1}$) and 2.7 m ($19\ Km^{-1} < \beta < 1110\ Km^{-1}$). The nephelometer provided a direct read-out of the scattering coefficient with a stated accuracy of $\pm$ 0.1 Km from 0-1 Km^{-1} and $\pm$ 1.0 from 1-10 Km^{-1}. For the transmissometers, the extinction coefficient was computed from Bouguer's Law, $I = I_o\ e^{-\beta x}$ where I_o and I are the incident and received intensities

Table 1

TEST LOG

TEST NO	DATE	TYPE OF OBSCURANT	MAXIMUM MEASURED EXTINCTION AT		
			Visible λ	2.2 λ	10 λ
1	3 May 82	Haze; mixed salt aerosol @ low RH	449	-	-
2	4 May 82	Fog; ambient nuclei	FOG DID NOT DEVELOP		
3	4 May 82	Fog; ambient nuclei	64	63	23
4	4 May 82	Fog; ambient nuclei	40	37	11
5	4 May 82	Fog; cigar smoke nuclei	52	26	6
6	4 May 82	Haze; mixed salt aerosol @ high RH	267	15	1
7	5 May 82	Fog; ambient nuclei	60	69	42
8	5 May 82	Fog; ambient nuclei	44	40	23
9	5 May 82	Fog; cigar smoke nuclei	74	67	26
10	5 May 82	Haze; mixed salt aerosol @ high RH	569	34	5
11	6 May 82	Fog; ambient nuclei	92	84	29
12	6 May 82	Fog; cigar smoke nuclei	107	96	28
13	6 May 82	Haze; mixed salt aerosol @ high RH	448	31	0.8
14	7 May 82	Haze; white phosphorus @ low RH	487	31	60

respectively, and X is the pathlength. The extinction coefficient measurement accuracy obtained with the 18.3 m pathlength transmissometer is estimated to be ±10% or ±0.5 km^{-1} whichever is greater and for the 2.7 m pathlength transmissometer ±10% or ±4 km^{-1} whichever is greater*

Extinction at IR wavelengths was measured with an IR transmissometer utilizing an 18.3 m pathlength, a 900°C black body source, and an HgCdTe detector operated at liquid nitrogen temperature. The source beam, chopped and collimated, was directed through the chamber (at a height of ∿1.5 m) and folded back to the detector by spherical front-silvered mirrors. Two band pass filters were alternately placed in front of the detector to provide measurement of extinction in the discrete wavelength bands of 2.117-2.325 μm and 9.13-10.33 μm. Prior to periods of filtration, pressurization, or expansion, the accuracy of the IR system is estimated to be ±10% or ±1 km^{-1} whichever is greater. During or after these operations, the accuracy is estimated to be ±10% or ±3 km^{-1} whichever is greater**.

Based on the above estimates of accuracy, values of the extinction coefficient reported in Appendix A are placed in parentheses if their measurement accuracy is not within ±20%.

Aerosol Concentration and Size Distribution

A Gardner Small Particle Detector (Type CN) provided measurement of the total particle concentration (#/cc) during the haze tests and during the pre-expansion period of the fog tests.

Aerosol size distributions were obtained during the haze tests with a TSI Model 3030 Electrostatic Aerosol Analyzer (0.01 to 1.0 μm diameter) and a Royco Model 225 Aerosol Particle Counter (0.56 to 10 μm diameter). These data are presented in Table 2. Tests 6, 10 and 13 were all high-humidity,

*Accuracy estimates based on transmissometer pathlength and measurement agreement of the two transmissometers.

**Accuracy estimate based on transmissometer pathlength, repeatibility of band pass filter placement and alignment shifts due to wall vibrations.

TABLE 2

HAZE TEST PARTICLE SIZE DISTRIBUTIONS

	% OF PARTICLE POPULATION IN INDICATED DIAMETER (μm) SIZE RANGE											
	EAA								ROYCO			
	0.01-0.0178	0.0178-0.0316	0.0316-0.0562	0.0562-0.1	0.1-0.178	0.178-0.316	0.316-0.562	0.562-1.0	0.562-1.78	1.78-3.16	3.16-5.62	5.62-10
Test 1 @ 1712	19%	34%	12%	12%	14%	7.7%	1.6%	0.27%				
1720	9.1	26	9.2	15	23	14	3.1	0.51				
1730	13	10	6.9	14	30	21	4.6	0.83				
1740	11	7.5	5.5	12	31	26	6.0	1.1				
1750	12	4.2	5.5	10	33	28	6.5	1.1				
Test 6, 10 and 13	0	0	8.7	3.2	12	36	25	→	12%	2.8%	0.011%	0%
Test 14	0	0	0	0	21	37	25	→	16	1.2	0	0

mixed-salt haze tests and had similar size distributions. The data presented for these tests is taken from Test 10 which had the most size distribution data available for analyses. Data for tests 10 and 14 were obtained after all burns were completed and after sufficient filtration had taken place so that the aerosol equipment was not overloaded. For test 10 this was at 1720 and for test 14 at 1200. As filtration removes particles evenly from all the size categories, the reported size distributions are believed to be representative of the distributions subsequent to the last burn of each test.

By using the total aerosol concentration values reported in the logs (see Appendix A), the absolute size distribution during the hazes is readily obtainable.

A Calspan Droplet Sampler was used to obtain measurement of fog droplet size spectra. In operation, foggy air is drawn through a sampling tube by a high capacity blower, and droplets are collected by impaction on gelatin-coated slides. The sampling airspeed is measured by a pitot tube and static source mounted in the unit, and a standard aircraft airspeed indicator is used to read the airspeed through the sampler. Airspeed is adjustable from 20 to 80 m sec^{-1}, but typically an impaction velocity of $\sim$40 m sec^{-1} was used.

Droplet samples are taken by injecting a narrow, gelatin-coated, glass slide into a high-speed flow through an opening in the sampling tube. Slide injection is accomplished through the use of a modified 35 mm photographic slide changer. When the coated slide is exposed to the air flow in the tube, droplets in the air volume swept out by the 4 mm wide glass slide impinge on the gelatin coating and form crater-like depressions. Development work on this technique (Jiusto, 1965 and Mack, 1966)* has shown that

*Jiusto, J.E., 1965: Cloud Particle Sampling, Pennsylvania State University, Department of Meteorology, Report No. 6, NSF G-24850.

Mack, E.J., 1966: "Techniques for Analysis of Cloud Particle Samples," Pennsylvania State University, Department of Meteorology, Report No. 14, NSF GP-4743.

there is approximately a 2:1 ratio between the crater diameter and the diameter of the impinging droplet. Exposure times are typically ∿0.2 sec, but can be extended to minutes as might be required for light hazes. Reduction of the droplet data is performed manually from photomicrographs (of the sample slides) obtained with a phase contrast microscope.

The raw distributions produced from measurements of the droplet replicas provide input to a computer program which first corrects for collection efficiency of the slide and then produces a normalized drop size distribution, $N(r_i)$, where $N(r_i)$ is the fraction of drops of radius r_i. Droplet concentration is then computed by using the measured extinction coefficient (β) and the expression

$$\beta = 2\pi n \sum N_i(r_i) r_i^2$$

where n = total number of drops per unit volume.

The computation of LWC, ω, is then straightforward, where

$$\omega = \frac{4\pi n}{3} \sum N_i(r_i) r_i^3.$$

As directed by HSS, selected impaction samples were analyzed. Results of these analyses are presented in Figure 1 and Table 3.

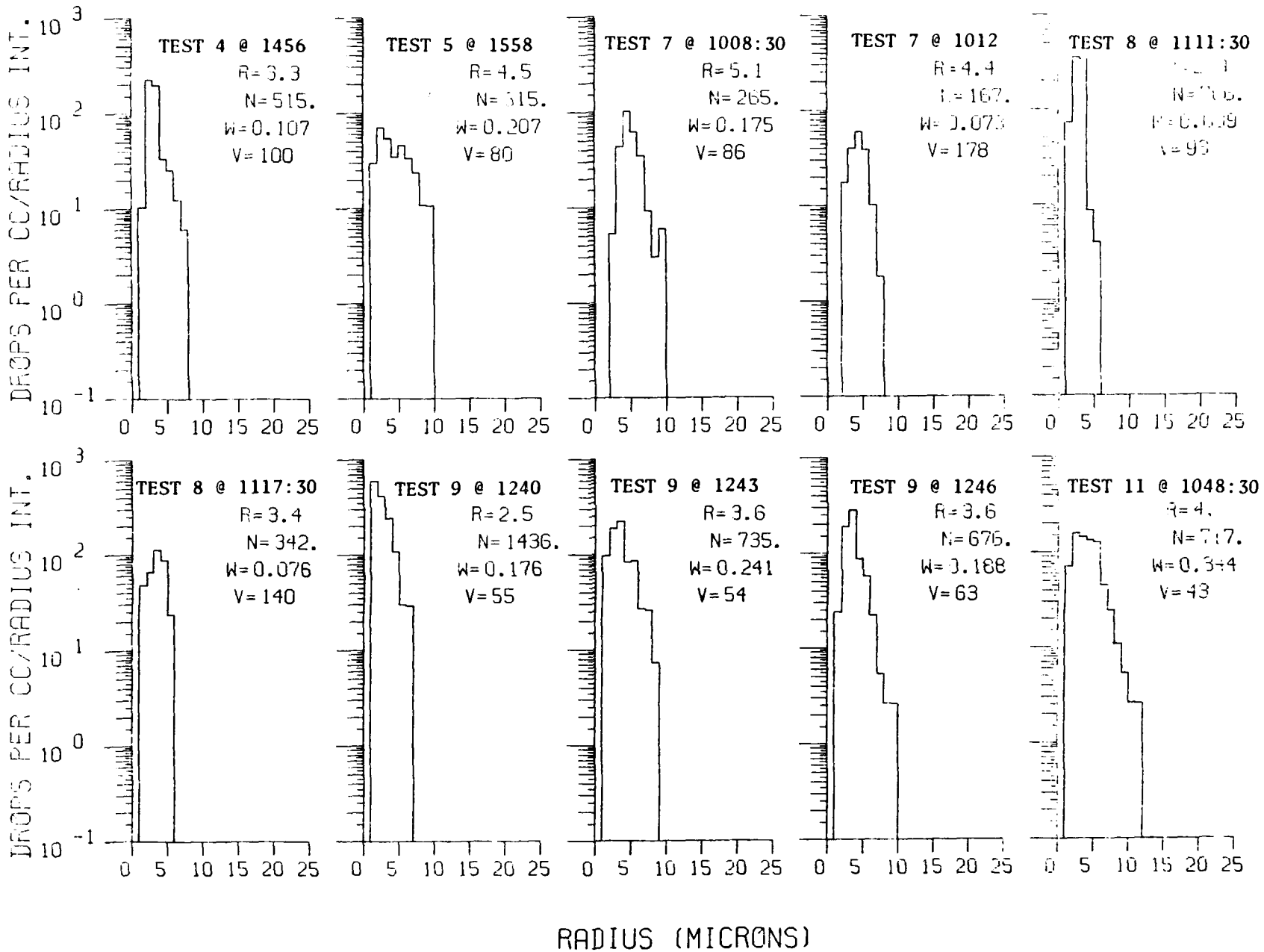

Figure 1. FOG DROPLET SIZE DISTRIBUTIONS

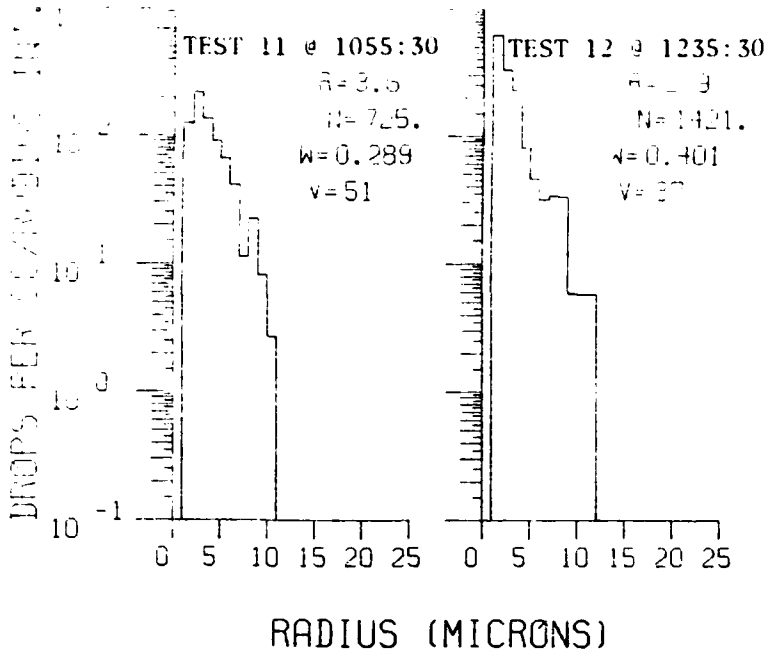

R = mean radius (μm)
N = drop number concentration (cm^{-3})
W = liquid water content (g/m^3)
V = measured visibility (m)

Figure 1. Continued

Table 3

TABULATION OF FOG DROPLET SIZE DISTRIBUTIONS

TEST NO	DATE	TIME	DROP CONCENTRATION (#/CC) PER INDICATED RADIUS INTERVAL (MICRONS)										
			1-2	2-3	3-4	4-5	5-6	6-7	7-8	8-9	9-10	10-11	11-12
4	4 May 82	1456	10.6	227.1	198.1	34.2	26.0	12.6	6.2	0	0	0	0
5	4 May 82	1558	29.9	71.2	54.0	34.8	46.5	33.7	23.8	10.8	10.7	0	0
7	5 May 82	1008:30	0	5.2	43.2	101.7	62.4	34.6	9.2	3.0	5.9	0	0
7	5 May 82	1012	0	17.4	39.8	59.4	38.6	10.2	1.8	0	0	0	0
8	5 May 82	1111:30	71.5	351.8	329.9	8.6	4.0	0	0	0	0	0	0
8	5 May 82	1117:30	48.3	66.6	114.7	88.8	23.7	0	0	0	0	0	0
9	5 May 82	1240	603.8	419.5	244.7	108.4	30.2	29.2	0	0	0	0	0
9	5 May 82	1243	96.3	187.2	221.0	83.5	86.8	26.7	26.0	7.3	0	0	0
9	5 May 82	1246	24.1	190.7	283.7	87.7	57.1	22.0	5.4	2.6	2.6	0	0
11	6 May 82	1048:30	71.0	155.7	142.5	131.5	126.7	44.3	24.3	10.6	5.2	2.6	2.6
11	6 May 82	1055:30	125.5	219.4	137.4	90.7	66.8	40.8	11.3	22.3	8.2	2.7	0
12	6 May 82	1235:30	619.3	333.1	226.1	81.1	46.1	31.5	33.7	33.0	5.9	5.8	5.8

APPENDIX A

Extinction Coefficient, Total Particle Concentration, and Relative Humidity as Functions of Time for the Performed Tests

TEST 1

HAZE; MIXED SALT AEROSOL @ LOW HUMIDITY

TIME	COMMENT	EXTINCTION COEFFICIENT (km^{-1}) @ λ =				
		VISIBLE WAVELENGTH			2.1-2.3 μm	9.1-10.3 μm
		MRI Nephelometer	18.3 m Trans.	2.7 m Trans.	18.3 m IR Trans.	18.3 m IR Trans.
3 May 82						
1705	Burn 0.3 g pyrotechnic					
1710	15,000/cc; 26% RH				NO USEFUL IR DATA	
1715	Burn 0.7 g pyrotechnic					
1720	22,000/cc		(0.8)	(2)		
1725	Burn 2 g pyrotechnic					
1730	26,000/cc		3.4	(7)		
1735	Burn 7 g pyrotechnic					
1740	54,000/cc		19	25		
1745	Burn 10 g pyrotechnic					
1750	88,000/cc		39	47		
1756	Burn 10 g pyrotechnic					
1801	97,000/cc		61	69		
1807	Burn 20 g pyrotechnic					
1815	108,000/cc		101	109		
1820	Burn 50 g pyrotechnic					
1825	160,000/cc		208	218		
1830	Burn 50 g pyrotechnic		Window Contaminated			
1835				320		
1840	Burn 50 g pyrotechnic					
1845				449		
1852	Start Filtration; End of Test					

TEST 2

FOG; AMBIENT NUCLEI

TIME	COMMENT	EXTINCTION COEFFICIENT (km^{-1}) @ λ =				
		VISIBLE WAVELENGTH			2.1-2.3 μm	9.1-10.3 μm
		MRI Nephelometer	18.3 m Trans.	2.7 m Trans.	18.3 m IR Trans.	18.3 m IR Trans.
4 May 82						
1120	Start Pressurization					
1128	Stop Pressurization					
1130	Begin Expansion		---FOG DID NOT DEVELOP---			
1148	End Expansion					

TEST 3

FOG; AMBIENT NUCLEI

TIME	COMMENT	EXTINCTION COEFFICIENT (km^{-1}) @ λ =				
		VISIBLE WAVELENGTH			2.1-2.3 μm	9.1-10.3 μm
		MRI Nephelometer	18.3 m Trans.	2.7 m Trans.	18.3 m IR Trans.	18.3 m IR Trans.
4 May 82						
1342	Start pressurization; 3,400/cc					
1350	End Pressurization					
1352	Begin Expansion					
1353						
1354						
1355			59		55	
1356			66		63	
1357			71		55	
1358			64			23
1359			59		46	
1400			49		45	
1401			44		35	
1402			42		33	
1403			33		27	
1404			27			(7)
1405			21		17	
1406			13		(13)	
1407			8		(7)	
1408			(3)		(3)	
1409			(2)			
1410						
1411						
1412						
1413	End Expansion					

TEST 4

FOG; AMBIENT NUCLEI

TIME	COMMENT	EXTINCTION COEFFICIENT (km^{-1}) @ λ =				
		VISIBLE WAVELENGTH			2.1-2.3 μm	9.1-10.3 μm
		MRI Nephelometer	18.3 m Trans.	2.7 m Trans.	18.3 m IR Trans.	18.3 m IR Trans.
4 May 82						
1440	Start Pressurization; 3,400/cc					
1448	End Pressurization					
1450	Begin Expansion					
1451						
1452						
1453						
1454			34		37	
1455			40			(11)
1456			39		29	
1457			33		25	
1458			28		21	
1459			22		(15)	
1500			18			(5)
1501			11		(4)	
1502			6		(4)	
1503			(3)		(2)	
1504			(1)			
1505	End Expansion					

TEST 5

FOG; CIGAR SMOKE NUCLEI

TIME	COMMENT	EXTINCTION COEFFICIENT (km^{-1}) @ λ =				
		VISIBLE WAVELENGTH			2.1-2.3 μm	9.1-10.3 μm
		MRI Nephelometer	18.3 m Trans.	2.7 m Trans.	18.3 m IR Trans.	18.3 m IR Trans.
4 May 82						
1543	Start Pressurization; 100,000/cc					
1551	End Pressurization					
1553	Begin Expansion					
1554						
1555						
1556						
1557			39		10	
1558			49		26	
1559			52			(6)
1600			46		19	
1601			44		20	
1602			38		(13)	
1603			34		(7)	
1604			24			(2)
1605			13		(2)	
1606			7			
1607			6			
1608			(3)			
1609			(2)			
1610	End Expansion					

TEST 6

HAZE; MIXED SALT AEROSOL @ HIGH HUMIDITY

TIME	COMMENT	EXTINCTION COEFFICIENT (km^{-1}) @ λ =				
		VISIBLE WAVELENGTH			2.1-2.3 μm	9.1-10.3 μm
		MRI Nephelometer	18.3 m Trans.	2.7 m Trans.	18.3 m IR Trans.	18.3 m IR Trans.
4 May 82						
1700	Burn 5 g pyrotechnic					
1703	75,000/cc; 88% RH		80	76	(5)	(0.3)
1705	Burn 5 g pyrotechnic					
1708	95,000/cc		153	136	9	(0.7)
1710	Burn 10 g pyrotechnic					
1715	110,000/cc; 87% RH		267	260	15	(1.3)
1718	Start Filtration					
1725			116			
1728	Stop Filtration					
1730	60,000/cc		96	85		
1735	Start Filtration					
1740			65			
1745	Stop Filtration					
1750			46	37		
1752	Start Filtration					
1755			36			
1800			23			
1805			16			
1810	4,800/cc		11			
1815		8.2	8			
1816	Stop Filtration	7.5				
1817		7.7	(7)	(4)		
1818		7.7				
1820	2,400/cc	6.5				

TEST 6 (Continued)

TIME	COMMENT	EXTINCTION COEFFICIENT (km^{-1}) @ λ =				
		VISIBLE WAVELENGTH			2.1-2.3 μm	9.1-10.3 μm
		MRI Nephelometer	18.3 m Trans.	2.7 m Trans.	18.3 m IR Trans.	18.3 m IR Trans.
1822		5.5				
1824		4.8				
1826		3.9				
1828		3.4				
1830	1,100/cc; 79% RH	2.9				
1832		2.3				
1834		2.0				
1836		1.7				
1838		1.4				
1840	600/cc	1.2				
1842	Change Scale on Nephelometer	-				
1844		0.85				
1845	End of Test	0.79				

TEST 7

FOG; AMBIENT NUCLEI

TIME	COMMENT	EXTINCTION COEFFICIENT (km^{-1}) @ λ =				
		VISIBLE WAVELENGTH			2.1-2.3 μm	9.1-10.3 μm
		MRI Nephelometer	18.3 m Trans.	2.7 m Trans.	18.3 m IR Trans.	18.3 m IR Trans.
5 May 82						
0948	Start Pressurization; 1,000/cc					
0956	End Pressurization					
1000	Begin Expansion					
1001						
1002						
1003			53		51	
1004			59		63	
1005			60		69	
1006			57		65	
1007			53			42
1008			48		59	
1009			43		50	
1010			36		45	
1011			30		40	
1012			22		27	
1013			15			16
1014			10		19	
1015			6		(13)	
1016			(3)		(9)	
1017			(2)		(6)	
1018					(4)	
1019	End Expansion					(1)

TEST 8

FOG; AMBIENT NUCLEI

TIME	COMMENT	EXTINCTION COEFFICIENT (km^{-1}) @ λ =				
		VISIBLE WAVELENGTH			2.1-2.3 μm	9.1-10.3 μm
		MRI Nephelometer	18.3 m Trans.	2.7 m Trans.	18.3 m IR Trans.	18.3 m IR Trans.
5 MAY 82						
1052	Start Pressurization; 1,500/cc					
1102	End Pressurization					
1106	Begin Expansion					
1107						
1108			17		24	
1109			30		35	
1110			40		39	
1111			44			23
1112			40		40	
1113			37		39	
1114			32		33	
1115			26		31	
1116			28			(15)
1117			16		19	
1118			9		(15)	
1119			8		(10)	
1120			5		(8)	(6)
1121			(2)		(5)	
1122			(1)		(4)	
1123	End Expansion				(3)	

TEST 9

FOG; CIGAR SMOKE NUCLEI

TIME	COMMENT	EXTINCTION COEFFICIENT (km^{-1}) @ λ =				
		VISIBLE WAVELENGTH			2.1-2.3 μm	9.1-10.3 μm
		MRI Nephelometer	18.3 m Trans.	2.7 m Trans.	18.3 m IR Trans.	18.3 m IR Trans.
5 MAY 82						
1220	Start Pressurization; 43,000/cc					
1228	Stop Pressurization					
1235	Begin Expansion					
1236						
1237						
1238			41		20	
1239			63		53	
1240			71		64	
1241			74		65	
1242			73			26
1243			73		67	
1244			65		61	
1245			65		60	
1246			62		60	
1247			57			23
1248			56		47	
1249	End Expansion		50		41	

TEST 10

HAZE; MIXED SALT AEROSOL @ HIGH HUMIDITY

TIME	COMMENT	EXTINCTION COEFFICIENT (km^{-1}) @ λ =				
		VISIBLE WAVELENGTH			2.1-2.3 μm	9.1-10.3 μm
		MRI Nephelometer	18.3 m Trans.	2.7 m Trans.	18.3 m IR Trans.	18.3 m IR Trans.
5 MAY 82						
1510	Burn 2 g pyrotechnic					
1515	25,000/cc; 83% RH		18	23		
1518	Burn 3 g pyrotechnic					
1522	66,000/cc		57	60	(1.1)	
1524	Burn 5 g pyrotechnic					
1530	110,000/cc; 83% RH		126	128	(3.4)	(0.9)
1532	Burn 10 g pyrotechnic					
1540			246	248	8.4	(2.1)
1543	Burn 20 g pyrotechnic					
1547				469	25	(4.2)
1550	Burn 10 g pyrotechnic					
1554				569	34	5.4
1556	Start Filtration					
1600	Stop Filtration					
1603				366	22	(1.7)
1605	Start Filtration					
1615	Stop Filtration					
1618	70,000/cc; 81% RH		164	158	(9.3)	
1620	Start Filtration					
1630	Stop Filtration					
1633	27,000/cc		69	66	(3.5)	
1635	Start Filtration					

TEST 10 (Continued)

TIME	COMMENT	EXTINCTION COEFFICIENT (km^{-1}) @ λ =				
		VISIBLE WAVELENGTH			2.1-2.3 μm	9.1-10.3 μm
		MRI Nephelometer	18.3 m Trans.	2.7 m Trans.	18.3 m IR Trans.	18.3 m IR Trans.
1645	Stop Filtration					
1648	12,000/cc; 81% RH		28	29		
1651	Start Filtration					
1700	Stop Filtration					
1703	4,500/cc		11	(15)		
1705	Start Filtration					
1715	Stop Filtration					
1720	2,000/cc; 80% RH	8.1	(3)	(7.4)		
1730	Start Filtration	8.1				
1732		6.8				
1734		5.5				
1736		4.7				
1738		4.0				
1740	Stop Filtration	3.4				
1742		3.4				
1744	1,000/cc; 79% RH	3.4				
1746		3.4				
1748		3.5				
1750	Start Filtration	3.5				
1752		3.0				
1754		2.4				
1756		2.0				
1758		1.7				

TEST 10 (Continued)

TIME	COMMENT	EXTINCTION COEFFICIENT (km^{-1}) @ λ =				
		VISIBLE WAVELENGTH			2.1-2.3 μm	9.1-10.3 μm
		MRI Nephelometer	18.3 m Trans.	2.7 m Trans.	18.3 m IR Trans.	18.3 m IR Trans.
1800	Stop Fi ..ion	1.4				
1802		1.4				
1804	600/cc; 77%	1.4				
1806		1.4				
1808		1.4				
1810	Start Filtration	1.4				
1812		1.2				
1814		1.0				
1816	Change Scale on Nephelometer	0.85				
1818		0.70				
1820	3,000/cc; 74% RH	0.61				
1822		0.50				
1824		0.44				
1826		0.36				
1828		0.32				
1830	<200/cc; end of test	0.27				

TEST 11

FOG; AMBIENT NUCLEI

TIME	COMMENT	EXTINCTION COEFFICIENT (km^{-1}) @ λ =				
		VISIBLE WAVELENGTH			2.1-2.3 μm	9.1-10.3 μm
		MRI Nephelometer	18.3 m Trans.	2.7 m Trans.	18.3 m IR Trans.	18.3 m IR Trans.
6 MAY 82						
1022	Start Pressurization; 14,000/cc					
1030	End Pressurization					
1040	Begin Expansion					
1041						
1042						
1043			51		41	
1044			69		64	
1045			79		75	
1046			85		82	
1047			90		81	
1048			92			29
1049			92		83	
1050			90		84	
1051			89		80	
1052			88		79	
1053			83			28
1054			81		71	
1055			79		66	
1056			74		67	
1057			68		52	
1058			53		40	
1059			40		29	

TEST 11 (Continued)

TIME	COMMENT	EXTINCTION COEFFICIENT (km^{-1}) @ λ =				
		VISIBLE WAVELENGTH			2.1-2.3 μm	9.1-10.3 μm
		MRI Nephelometer	18.3 m Trans.	2.7 m Trans.	18.3 m IR Trans.	18.3 m IR Trans.
1100			26		16	
1101			14		(8)	
1102	End Expansion		10		(6)	

TEST 12

FOG; CIGAR SMOKE NUCLEI

TIME	COMMENT	EXTINCTION COEFFICIENT (km^{-1}) @ λ =				
		VISIBLE WAVELENGTH			2.1-2.3 μm	9.1-10.3 μm
		MRI Nephelometer	18.3 m Trans.	2.7 m Trans.	18.3 m IR Trans.	18.3 m IR Trans.
6 MAY 82						
1209	Start Pressurization; 66,000/cc					
1217	End Pressurization					
1227	Begin Expansion					
1228						
1229						
1230			64			
1231			76		56	
1232			88		70	
1233			96		80	
1234			106		90	
1235			106		96	
1236			107			28
1237			104		96	
1238			98		89	
1239			90		82	
1240			79		68	
1241			60		49	
1242			46		33	
1243			24		17	
1244			14		(8)	
1245			10		(5)	
1246	End Expansion		6			

TEST 13

HAZE; MIXED SALT AEROSOL @ HIGH HUMIDITY

TIME	COMMENT	EXTINCTION COEFFICIENT (km^{-1}) @ λ =				
		VISIBLE WAVELENGTH			2.1-2.3 μm	9.1-10.3 μm
		MRI Nephelometer	18.3 m Trans.	2.7 m Trans.	18.3 m IR Trans.	18.3 m IR Trans.
6 MAY 82						
1450	Pre Test; 85% RH					
1456	Burn 2 g pyrotechnic					
1459	27,000/cc		30	26	(1.6)	(0.1)
1501	Burn 3 g pyrotechnic					
1504	58,000/cc; 85% RH		61	53	(3.0)	(0.2)
1506	Burn 5 g pyrotechnic					
1509	96,000/cc		108	95	5.4	(0.2)
1511	Burn 10 g pyrotechnic					
1514	150,000/cc		193	180	8.5	(0.3)
1516	Burn 20 g pyrotechnic					
1519	85% RH			367	23	(0.5)
1522	Burn 10 g pyrotechnic					
1525	85% RH			448	32	(0.8)
1530	Start Filtration					
1540	Stop Filtration					
1543	90,000/cc; 82% RH		Window Contaminated	172	(13)	(0.5)
1545	Start Filtration					
1555	Stop Filtration					
1558	37,000/cc; 81% RH			(70)	(7.4)	(0.4)
1600	Start Filtration					
1610	Stop Filtration					
1613	13,000/cc			(25)		
1615	Start Filtration					

TEST 13 (Continued)

TIME	COMMENT	EXTINCTION COEFFICIENT (km^{-1}) @ λ =				
		VISIBLE WAVELENGTH			2.1-2.3 μm	9.1-10.3 μm
		MRI Nephelometer	18.3 m Trans.	2.7 m Trans.	18.3 m IR Trans.	18.3 m IR Trans.
1625	Stop Filtration					
1632	6,000/cc; 81% RH			(10)		
1633	Start Filtration					
1640	Stop Filtration					
1643	3,000/cc					
1645	Start Filtration					
1655	Stop Filtration					
1658	1,500/cc	4.9				
1705	Start Filtration	4.9				
1706		4.4				
1708		3.7				
1710		3.1				
1712		2.6				
1714		2.3				
1715	Stop Filtration	2.1				
1716		2.0				
1718	700/cc; 77% RH	2.0				
1720		2.0				
1722		2.0				
1723	Start Filtration	2.0				
1724		1.8				
1726		1.5				
1728		1.3				

TEST 13 (Continued)

TIME	COMMENT	EXTINCTION COEFFICIENT (km^{-1}) @ λ =				
		VISIBLE WAVELENGTH			2.1-2.3 μm	9.1-10.3 μm
		MRI Nephelometer	18.3 m Trans.	2.7 m Trans.	18.3 m IR Trans.	18.3 m IR Trans.
1730		1.0				
1732		0.9				
1733	Stop Filtration	0.8				
1734	400/cc	0.8				
1736	Change Scale on Nephelometer	0.87				
1738	Start Filtration	0.87				
1740		0.75				
1742		0.61				
1744		0.55				
1746		0.44				
1748		0.36				
1750		0.34				
1752		0.29				
1754		0.24				
1756		0.21				
1758		0.19				
1800	End of Test	0.17				

TEST 14

HAZE; WHITE PHOSPHORUS @ LOW HUMIDITY

TIME	COMMENT	EXTINCTION COEFFICIENT (km^{-1}) @ λ =				
		VISIBLE WAVELENGTH			2.1-2.3 μm	9.1-10.3 μm
		MRI Nephelometer	18.3 m Trans.	2.7 m Trans.	18.3 m IR Trans.	18.3 m IR Trans.
7 MAY 82						
0932	Burn 1 g WP					
0935	75,000/cc; 33% $H		26	24	(0.3)	
0939	Burn 1 g WP					
0945			62	50	(0.5)	(0.4)
0950	Burn 3 g WP					
0956			156	131	(2.1)	(1.4)
1003	Burn 5 g WP					
1006				265	7.1	8.6
1009	Burn 10 g WP					
1013				525	17	31
1016	Burn 10 g WP					
1022				774	31	60
1025	Start Filtration					
1030	Stop Filtration		Window Contaminated			
1033				487	21	31
1035	Start Filtration					
1045	Stop Filtration					
1048	100,000/cc; 37% RH	Nephelometer out of Calib.		189	(7.5)	(3.5)
1050	Start Filtration					
1100	Stop Filtration					
1104	36,000/cc			76	(0.9)	(0.8)
1106	Start Filtration					
1115	Stop Filtration					

TEST 14 (Continued)

TIME	COMMENT	EXTINCTION COEFFICIENT (km^{-1}) @ λ =				
		VISIBLE WAVELENGTH			2.1-2.3 μm	9.1-10.3 μm
		MRI Nephelometer	18.3 m Trans.	2.7 m Trans.	18.3 m IR Trans.	18.3 m IR Trans.
1118	15,000/cc; 38% RH			33		
1120	Start Filtration					
1135	Stop Filtration					
1138	4,800/cc			(10)		
1140	Start Filtration					
1155	Stop Filtration					
1158	End of Test			(3)		

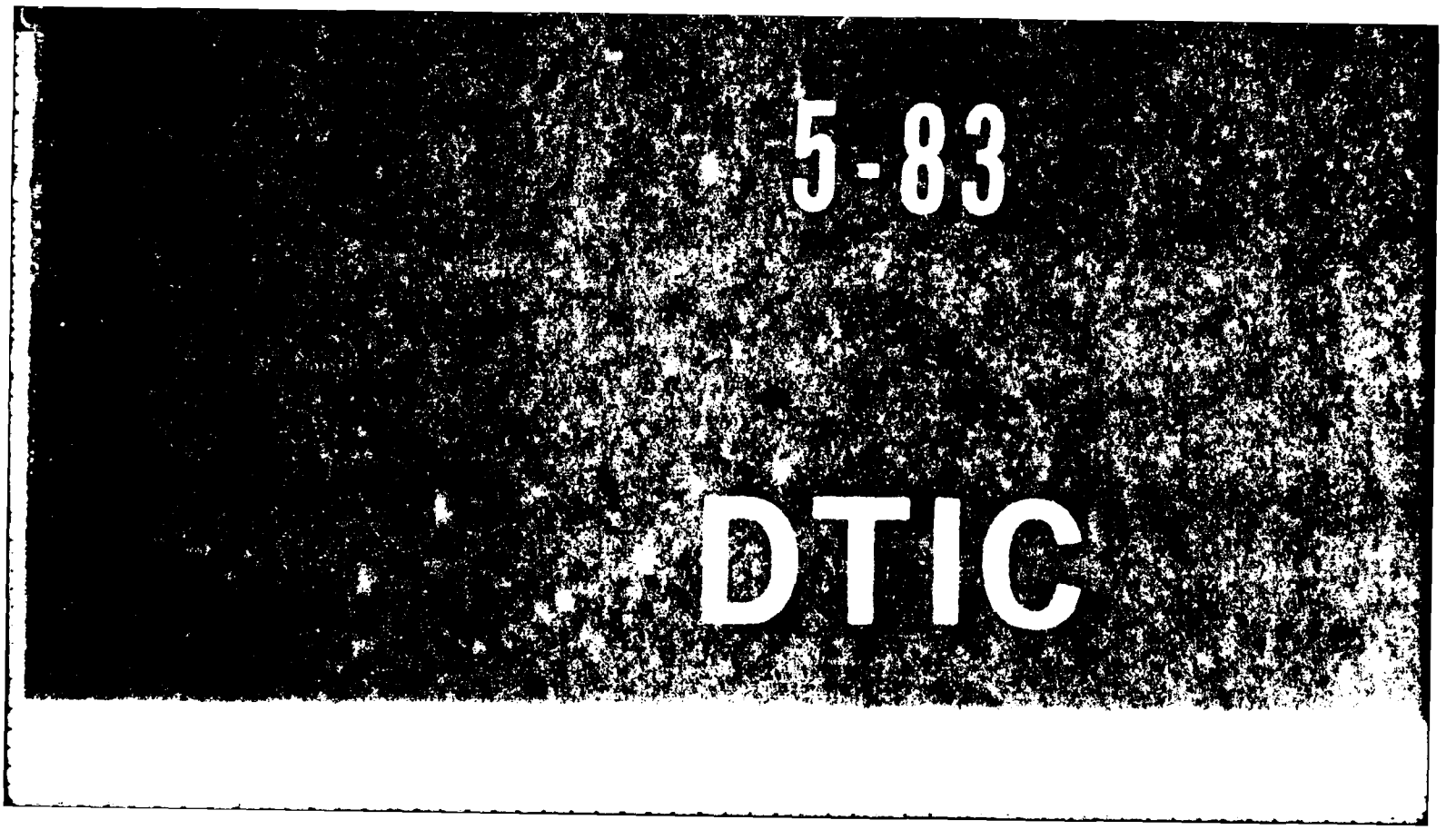
5-83
DTIC